University of Alberta

ULF WAVES IN THE MAGNETOSPHERE AND THEIR ASSOCIATION WITH MAGNETOPAUSE INSTABILITIES AND OSCILLATIONS

by

Abiyu Zerfu Nedie

A thesis submitted to the Faculty of Graduate Studies and Research
in partial fulfillment of the requirements for the degree of

Doctor of Philosophy

Department of Physics

Fall 2012

Edmonton, Alberta

To my lovely daughter

Marina

Abstract

This thesis addresses the question of excitation of ULF waves by magnetopause instabilities and oscillations. Given proper spacecraft orientations and near magnetopause encounters, the CLUSTER spacecraft mission is used to resolve the space-time ambiguity inherent in a single spacecraft measurements.

A case study is presented where a driver ULF wave is identified in the solar wind and on open field lines in association with a Field Line Resonance (FLR). This is one of the rare examples where a solar wind source has been unambiguously identified and causally linked with excitation of a FLR at the same frequency. It adds to a database of observations that can be used to determine the statistical relationship between various sources of ULF plasma waves and FLRs. It is also one of the few observations of a driver wave on open field lines by SuperDARN, and encourages further use of SuperDARN in that regard.

In the second case study, a ULF wave signature at 1.7 mHz is observed just outside the magnetopause using CLUSTER and compared with fluctuations at ionospheric altitudes and on the ground. It is shown that ULF fluctuations at the magnetopause coincide with discrete frequency oscillations in HF radars, magnetometers and spacecraft inside the magnetosphere. The Poynting vector and phase propagation outward from the magnetopause, and the absence of a source in the solar wind, suggest a KHI generated surface mode as a source mechanism.

A third case study presents a magnetopause oscillation resulting from a direct solar wind driver that transfers energy from the solar wind into FLRs. We observe a quasi-monochromatic 2.5 mHz discrete wave oscillation in IMF By. The dusk signature of the wave shows magnetic field and plasma flow oscillations at the magnetopause at the same discrete frequency. The SuperDARN Saskatoon radar in the pre-dawn sector reveals the footprint of an FLR structure with anti-sunward phase propagation that is linked to the solar wind driven magnetopause oscillation. This is the first work using SuperDARN that relates a solar wind driven magnetopause oscillation with a discrete frequency FLR in the magnetosphere.

The thesis concludes by presenting results from a 2D ideal MHD wave model that is successful in qualitatively reproducing observed structure of FLRs for both KHI-like drivers and solar wind-driven magnetopause oscillations.

Acknowledgements

The completion of this dissertation has been one of the most significant academic challenges I have had to face. Without the guidance, support and patience of the following people, this study would not have been completed.

First and foremost, my utmost heartfelt gratitude to my supervisors Dr. Frances Fenrich and Dr. Robert Rankin for offering me the opportunity to study in the Space Physics Group. Not only have they provided me an interesting and challenging doctoral problem, they gave me the freedom to work in my own way and time and provided me a break for as much as I wanted when I was unable to continue due to a family problem. On top of that, I am very much grateful to them for they fully funded my financial expenses to make my attendance possible at several international conferences and meetings.

Dr. Fenrich, I owe you my special thanks for your unique science perspective, for being a constant oasis of ideas and passions in science and for your constructive feedback. I benefited greatly from your expertise in time series and mining SuperDARN data. Throughout the program, no matter how many times I stepped into your office without appointment, I cannot remember a day when you said, "I am busy" and never did you hesitate to discuss my questions with me. You had so much to offer both professionally and personally.

Dr. Rankin and your wife, Sandy, never will I forget how hard you pushed to connect me to your family doctor when I had a difficult medical problem because of the hostile weather in my early days in Edmonton. Sandy, I am more than thankful for the winter rides to and from the medical centre and for your hospitality at home.

I would like to extend my thanks to members of my supervisory committee Dr. Richard Sydora and Dr. Ying Tsui and as well as my external examiner Dr. Sasha Koustov. I must also thank Dr. Jonathan Rae for all the invaluable discussions and fruitful insights on a whole range of topics, in particular ULF waves and field aligned coordinate systems. Also to Dr. Alex Degeling who overwhelmed me with his amazing programming knowledge and who was keen to share his perspective and work on the 2D MHD model for ULF waves.

Next comes Mark Gordon, systems analyst, who in one way or another was of huge assistance, especially when 'Scorvio' broke down several times during it's course of usage. Mark, also many many thanks for teaching me numerous English idiomatic expressions.

I also benefited from the outstanding lectures of Dr. Ian Mann on "Special Topics in Physics - Introduction to Space Weather & Space Environment". Many thanks go to him for allowing me to audit his course and for sharing his various thoughts and insights throughout our science discussions.

I would like to thank my friend and colleague in the Space Physics Group, Jan Paral, who has an amazing knowledge of debugging software, who also is very keen to help. Also to my long time friend, Mohammed Kedir, from graduate school at AAU to here in Canada, for your exceptionally cheerful friendship over the years. My friend Hava Turkakin has been exemplary and set the bar so high for how strong a student mother of four can be. Mauricio Blanco has been very cheerful over the years both in office and at the soccer field.

It is a pleasure to pay tribute also to all my Ethiopian friends in Edmonton and back home for your friendship and all-around amusement on a whole range of levels. To "the Friday Yekurt-Ken Group", who gave me a much needed escape from the world of space plasma physics.

I am much indebted to Emmanuel, for his amazing friendship and for nursing me during those painstakingly difficult days of my life. I totally regret for not having the chance to know him a bit earlier.

I owe sincere and earnest thankfulness to my friends and colleagues Mesay, Kebede, Yihunie, Teddy, Misrak, Yemisrach, Amare, Mulugeta, Fantahun, Fasil and Gashaw for your unwavering friendship over the years. I cherish the time spent with you all. I hope our lives will cross again.

This dissertation would not have been possible without the assistance and moral encouragement of my family members who in one way or another contributed and extended their valuable assistance through out this study. My father Zerfu, my sister Mistre, my brother Yonas, Abebe and Yeshiwas were my constant sources of inspiration and whose sincerity and encouragement I will never forget. Zerfu, your unparalleled support and unwavering encouragement over the years were sources of my strength. My mother, Yeshi, who so lovingly and unselfishly cared for my daughter Marina, and who gave me her unequivocal love and support throughout, as always, for which my mere expression of thanks likewise does not suffice. Nothing will ever repay my debt to you, Yeshi.

My lovely daughter Marina, who was born before this doctoral study was started and who spent five years with relatives to allow me to focus, I am deeply sorry for the time we spent apart. As time will make apparent as you

grow up, that was the only choice I had left to me. It's not hard to imagine how bad you felt to have passed five Christmases and birthdays without me. Not a day went by without my thinking of you, knowing how much you missed me every single day. Who else would understand what you and I have been through those years? Mari, words cannot express the profound love and care that I have for you. You have been my inspiration as I hurdled all the obstacles throughout the completion of this work. Though this day appeared a world away, it finally has come. This is your day; this is your moment - Mari.

Thanks also to my best friend Astatke Belay and his all time welcoming family and Drs. Kenneth and Mika who had kind concern and consideration regarding my academic achievement and the well-being of my family.

I gratefully acknowledge the Space Science Enhancement Program of the Canadian Space Agency (CSA) and the Department of Physics at the University of Alberta for funding my research project.

Last, by no means least, my best friend and cousin Esete, thank you very much for your love and support over the years.

Above all, my greatest thanks goes to the omnipresent God, for answering my prayers when I was broken, for giving me the perseverance to get back from the brink despite the few wanting me to give up and be thrown into the ditch, thank you so much Dear Lord.

Table of Contents

List of Figures

List of Symbols

Chapter 1

Introduction

1.A Preliminary Remarks

This thesis focuses on the characterization of magnetopause boundary instabilities and oscillations and Ultra-Low-Frequency (ULF) waves in the magnetosphere. It has the ultimate goal of elucidating the causal relationship between the two. This specific problem is categorized under the broad area of solar-terrestrial physics and is one of the subjects of interest, yet unsettled to date within the space physics community. The Earth sits protected from a relentlessly expanding solar atmosphere, known as the solar wind, inside the magnetic cavity called the magnetosphere. Most of the geomagnetic field lines forming this protective cavity are closed. That means both ends of field lines are anchored to the poles of the Earth. Surrounding each pole is a region of open field lines. These so called open field lines have one end anchored to the pole and the other end extending into the interplanetary space mapping all the way to the Sun. The region poleward of the last closed field lines containing all the open field lines is called the polar cap. The equatorward edge of the

polar cap forms the open closed field line boundary.

The interaction between the Sun and the Earth has been a subject of much interest and intense study since the launch of the first unmanned satellite in 1957. Magneto-Hydro-Dynamic (MHD) waves occur within the region of the Earth's magnetosphere and are believed to be generated by interactions of different plasma regimes of solar and terrestrial origin. As a result of the solar-terrestrial interaction, the magnetopause is subject to a variety of instabilities and wave processes. This thesis principally addresses the important scientific question of excitation of ULF waves by magnetopause instabilities and oscillations. Central to this project is clarifying and extending our understanding of the ULF wave source mechanism, and the propagation and coupling of ULF waves in the terrestrial magnetosphere. Thus, this project aims at providing an improved understanding of ULF wave processes in the terrestrial magnetosphere, their associated excitation mechanisms, and the physical interrelationships between them.

Once generated, the signatures of fundamental wave processes are observed in the near Earth environment in the form of spectacular observations such as FLRs. The basis for FLRs is the fact the propagation direction of MHD waves is field aligned (the Alfvén mode). The inhomogeneity in the plasma density and/or the non-uniformity in the geomagnetic field allows energy to couple from the other mode (the fast mode) into a narrow region of field lines when the frequency of the two modes exactly match.

Following on, the ultimate goals of this thesis work are 1) to address the

ULF source mechanism by providing experimental observations of magnetopause instabilities and/or oscillations and by investigating how they propagate and couple within the terrestrial magnetosphere 2) to present a numerical model (based on a pre-existing MHD model) which qualitatively reproduces and successfully explains the experimental observations to be presented. The model is a 2D ideal MHD model for ULF wave source mechanisms constrained in a compressed model magnetic field.

The principal data sets to be used include ground-based (Super Dual Auroral Radar Network) SuperDARN HF radar data from the Canadian Space Agency's (CSA) Canadian Geo-space Monitoring program. These radars measure the position and velocity of plasma particles in the Earth's ionosphere, the highest layer of the Earth's atmosphere. In addition, a variety of in-situ satellite-born instrumentation that includes the (CLUSTER, Advanced Composition Explorer (ACE), GEOTAIL and POLAR) along with ground-based magnetometer data, depending on their availability, are used.

ACE orbits the L1 libration point and primarily provides near-real-time continuous coverage of solar wind parameters, and interplanetary magnetic field and energetic particles accelerated by the Sun. The primary purpose of the GEOTAIL mission is to study the structure and dynamics of the magnetotail. For this reason, the orbit is designed to spatially cover the magnetotail over a wide range of distances ranging from $8R_e$ to $210R_e$ as measured from the Earth. This mission also provides an opportunity to study the boundary region of the magnetosphere as it skims the magnetopause at perigees. The POLAR spacecraft is a NASA science spacecraft designed to study the polar

magnetosphere and aurora. POLAR launched into orbit in February 1996 and remains in orbit, though it is now inactive.

The CLUSTER multi-satellite mission will also be used in this study. This mission provides by far a much better and reliable means of characterizing the spatio-temporal evolution of ULF waves at the magnetopause boundary, offering an ideal arena to prove or disprove pre-existing theories such as the Kelvin-Helmholtz-Instability (KHI) as the ULF wave source mechanisms.

The thesis contains five chapters. The remainder of this chapter describes the large-scale solar-terrestrial environment and the background of the theoretical constructs under which ULF MHD wave theory is operative. The first ground-based detection of a direct solar wind driven FLR event, where the source signature in crossing the magnetopause boundary is traced using SuperDARN, is presented in Chapter 2. A coordinated ground- and CLUSTER multi-satellite mission based observational study, including data from the POLAR spacecraft, which supports a KH source mechanism, is presented in Chapter 3. Chapter 4 presents observations of a solar wind driven magnetopause oscillation that excites a FLR observed by the SuperDARN HF radars and the CLUSTER multi-satellite mission. Then follows a 2D MHD global ULF wave model to reproduce the spatio-temporal observational results obtained in Chapters 3 and 4. Finally, conclusions of the thesis are drawn with comments of what needs to be done as a continuation of this work towards a full understanding of ULF wave energy transport processes, and in particular, excitation mechanisms, propagation and coupling in the terrestrial magnetosphere.

1.B The Solar-Terrestrial Environment

1.B.1 The Solar Wind and the Solar Environment

In astronomical terms, the Sun is an ordinary magnetic star of age 4.6 billion years. Its life expectancy is approximated to be an additional 5 billion years. It has an intermediate size and temperature with an absolute magnitude of 4.8. Although its size in astronomical scales is intermediate, it is 109 times larger than that of our Earth. It is also so massive that its mass is 333,000 times greater than the Earth [*Priest*, 1995]. The Sun is composed of 90% of hydrogen, 10% of helium and an admixture of 0.1% of heavier atoms. These solar materials are ionized because of the extremely high temperature ($\sim 10^7$ K) that results from the nuclear reaction occurring at the highly compressed core of the sun. This huge temperature subsequently provides electrons at the solar corona a thermal energy that exceeds the binding energy of atoms, leading to an escape mechanism. Because of the large electric field created between the excessive protons and electrons, which have managed to escape, the protons will be accelerated outwards [*Parks*, 2004]. The continuous streaming away of protons and electrons results in the supersonic expansion (300-800 km/s) of the solar corona into interplanetary space. This supersonic coronal streaming away, or outflow, is called solar wind and is a unique mechanism of the Sun to maintain its charge neutrality. The existence of the continuous coronal outflow was first predicted by *Parker* [1958].

Recent theories of the solar wind invoke a fluid description of solar wind generation in coronal holes [*Hollweg and Isenberg*, 2002]. According to this new theory, coronal holes have been very useful in determining the overall

heating requirements for the fast solar wind. A significant amount of heating above the sonic critical point is required to yield a fast speed. The heat energy required to power the heating is thought to be associated with large-amplitude chromospheric Alfvén waves, propagating outward into the corona from below and dissipating in the collisionless region. The existence of these waves has been confirmed by observation, where their energy is found to be sufficient to produce the required heating at corona [*De Pontieu et al.*, 2007].

The Sun has an internal magnetic field and thus interplanetary space is pervaded by a magnetic field of solar origin, also called the Interplanetary Magnetic Field (IMF). Because of its large conductivity, the solar wind is often assumed to be an ideal MHD fluid. An ideal MHD fluid treatment assumes the IMF is frozen in the solar wind and transported out with it into interplanetary space [*Gurnett and Bhattachajee* , 2005]. To first approximation, when the solar wind hits the Earths dipolar magnetic field, it cannot simply connect or make its way through but rather is slowed down and, to a large extent, flows around it. The Earth's magnetic field presents an obstacle to the solar wind flow [*Chapman and Ferraro*, 1931] and creates a cavity due to the fact that the terrestrial magnetic field excludes the ionized plasma of the solar wind. This means the two plasma environments get restricted to two separate plasma regimes: the magnetospheric cavity and the magnetosheath.

1.B.2 The Magnetosheath

The relatively well-defined boundary separating the magnetosphere from the solar wind is called the magnetopause. The shape and location of the mag-

netopause is determined by a balance between the dynamic pressure of the supersonic solar wind flow and the magnetic field pressure inside the magnetosphere. A bow shock wave is generated upstream of the magnetopause where the plasma is slowed down and a significant fraction of the solar wind's kinetic energy is converted into thermal energy. The thermalized region of space between the magnetopause and the bow shock is called the magnetosheath. The magnetosheath contains a warm and dense plasma population and is distinctly separated from the cold high-speed solar wind by the bow shock.

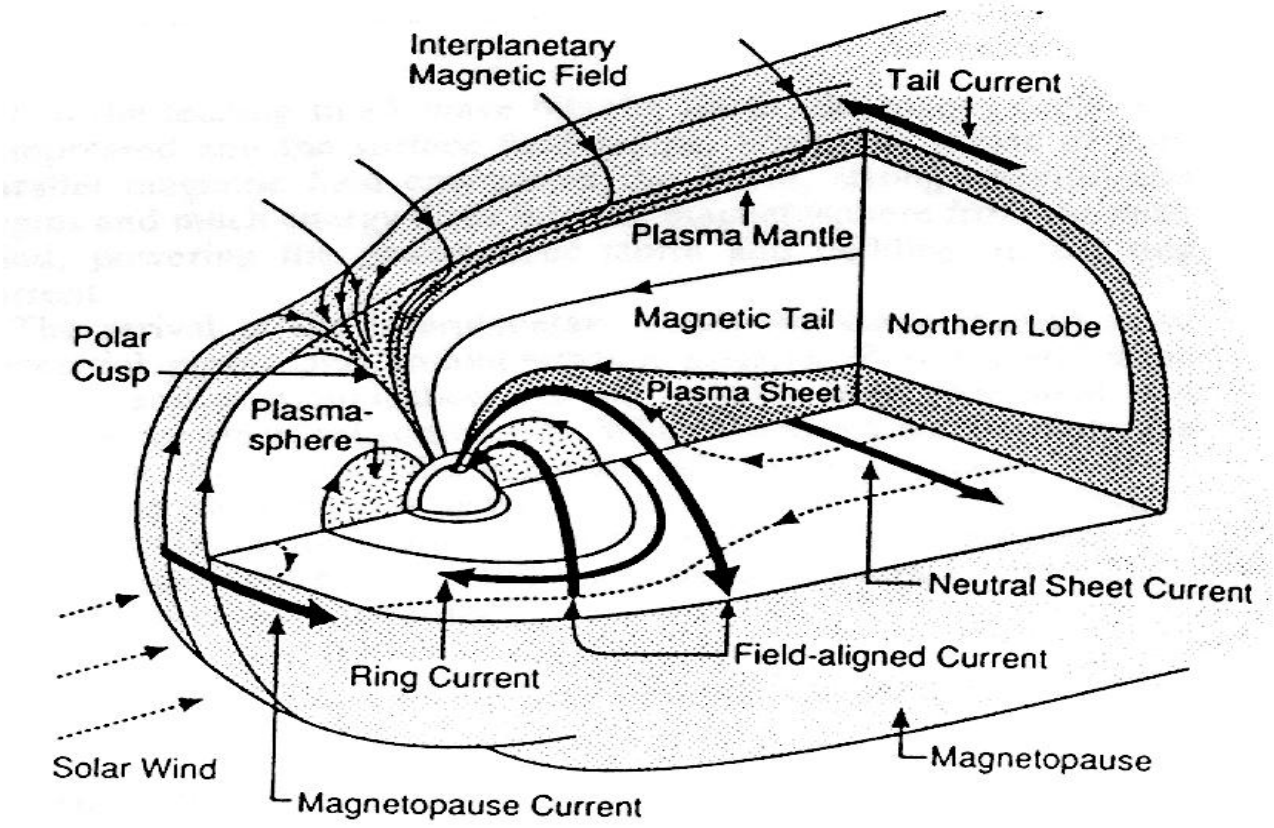

Figure 1.1: Cut away drawing of the Earth's magnetosphere showing the major plasma regimes, current systems and flows. Adopted from *Kivelson and Russel* [1995].

1.B.3 The Terrestrial Magnetosphere

The shape and size of the magnetosphere is controlled by the balance of the streaming solar wind dynamic pressure and magnetic pressure of Earth's dipolar field. The magnetosphere is compressed on the dayside and stretched into a magnetic tail-like structure on the night side of the Earth due to the solar wind dynamic pressure [*Walker and Russell*, 1985]. On the dayside, the equatorial pressure standoff distance has a typical value of $9-11$ R_e from the center of the Earth [*Roelof and Sibeck*, 1993]. The magnetotail is observed to extend beyond 1000 R_e down-stream of the Earth [*Villante*, 1975]. The magnetospheric plasma is composed mainly of protons and electrons. In addition, heavier ions such as He^+ and O^+ of ionospheric origin and He^{2+} and O^{2+} of solar wind origin are found. Depending on the plasma density, magnetic field and temperature, the magnetosphere is structured into various regions. Figure 1.1 depicts the schematic of the magnetospheric topography of some of these regions.

The plasmasphere is the region of the magnetosphere whose radial distance varies from $2.5-7.0$ R_e depending on the geomagnetic activity [*Moldwin et al.*, 2002]. The plasmasphere corrotates with the neutral atmosphere of the Earth and reaches its outer boundary, the plasmapause. The Van Allen radiation belt is collocated with the plasmasphere. This is the region consisting of trapped high-energy ion and relativistic electron plasma populations extending to $2-6$ R_e. The region that extends from the plasmapause to 10 R_e, where most of the magnetotail plasma is concentrated, is called the plasmasheet. The plasmasheet can extend well beyond 10 R_e, particularly on the night-side.

The magnetotail lobe is the furthest out region of the magnetosphere, with a highly tenuous plasma population neighbouring the magnetosheath.

1.B.4 The Terrestrial Ionosphere

In addition to the solar wind, the ionosphere is known to be the second most important source of magnetospheric plasma. This is the outer region of the Earth's atmosphere beginning at around 60 km and extending farther out into the magnetosphere. The solar ultraviolet radiation impinging on the neutral atmosphere plays a vital role in ionizing this portion of the atmosphere. Due to the slow recombination rate, the ionosphere is permanently ionized for altitudes above 80 km. Precipitation of energetic particles from the magnetosphere is another source of the ionospheric plasma population.

The ionosphere is traditionally designated into three distinct layers (D, E, and F) based on height and plasma density. The D-region is the lowest level that extends from 60 to 90 km with an electron density as low as $\sim 500\ cm^{-3}$. UV radiation from the Sun ionizes the D region. X-rays during active Sun can enhance the ionization. It is very weakly ionized and because of high collision frequencies (high recombination rate). It is dominated by the dynamics of the neutral atmosphere, and is known to absorb short wave radio frequencies during the daytime. The E-region is the region immediately above the D-region extending between 90 and 130 km. It has a plasma density of $\sim 10^5\ cm^{-3}$ and therefore it is relatively highly conducting. The UV radiation is responsible for its ionization. The degree of ionization actually depends on the intensity of the radiation (like the D-region) and with altitude and time of day. The upper

ionosphere (above 130 km) is referred as the F-region and has a maximum plasma density reaching $\sim 10^6\ cm^{-3}$. This layer has a high ionization gradient and is present both in the daytime and nighttime. Since air density is low at F-region altitudes, the free ions and electrons (due to the action of UV radiation from the Sun) can not recombine readily and subsequently store energy received from the Sun for many hours; this is the main reason the refractive property of this layer changes only slightly from day to night. It is this layer of the ionosphere that is very important in long distance HF radio communications, including the SuperDARN HF radars, because the enhanced electron densities refract and reflect HF radio signals.

1.B.5 Plasmas in Space

There are certain conditions that a system of charged particles needs to satisfy to be classified as plasma. Externally, a plasma needs to be electrically quasi-neutral. Quasi-neutrality is the direct result of cancellation of the randomly oriented electric fields generated by each individual charged particle in a large system. Quasi-neutrality is basically a statement of the first plasma criterion for defining a plasma.

For a low density plasma, direct collisions are negligible. In such a plasma, long-range electromagnetic (Coulomb) interactions are dominant. The condition that a plasma needs to contain a large number of particles introduces the concept of collective interaction and provides a very useful means to describe the plasma (as in MHD fluid theory). The impact of the force range of a charged particle over which its Coulomb effect is felt by others is defined by a

characteristic scale length, λ_D, called the Debye length

$$\lambda_D = \left(\frac{K_B T \varepsilon_o}{n_e e^2} \right)^{1/2}, \tag{1.1}$$

where K_B is the Boltzmann constant, ε_o is the dielectric constant of free space, and e, n_e, and T are charge, electron number density and temperature, respectively, of the electron species. For distances $r > \lambda_D$, the potential around a point charge is effectively shielded or screened out by particles of opposite charge in its neighbourhood. The characteristic scale variations of macroscopic parameters (e.g., density and temperature), L, need to be significantly larger than the Debye length, λ_D

$$L >> \lambda_D, \tag{1.2}$$

without which the condition for a collective shielding effect won't be satisfied, as there is no sufficient space to define the physical dimension of the plasma. Failure to satisfy equation (1.2) leads to an ordinary ionized gas.

As discussed above, the collective interaction is the very cause of Debye shielding. Therefore, the description of collective interaction is meaningful only when a sufficient number of particles are present in the system of charged particles. The number of particles, N_D, present in a Debye sphere is

$$N_D = \frac{4\pi}{3} n_e \lambda_D^3. \tag{1.3}$$

The plasma parameter, g, is defined by

$$g = \frac{1}{N_D}. \tag{1.4}$$

Equation (1.4) sets the second criterion for defining a system of charged particles as a plasma. A system of charged particles is considered as a plasma only when g is significantly smaller than 1 ($g << 1$). The third and the last criterion is related to the frequency of short-range collisions between the individual charged particles constituting the ionized medium. The condition $g << 1$ can be used to define the third criterion. The third criterion is best represented by the statement that the electron plasma frequency is much greater than the electron-neutral collision frequency. Combining equations (1.1), (1.3) and (1.4) yields

$$g \sim \sqrt{\frac{n_e}{T^3}} \tag{1.5}$$

Equations (1.4) and (1.5) show that short-range binary collisions decrease with decreasing density and increasing temperature. This is basically equivalent to the following statement: if the system of charged particles is disturbed by an external influence, the electrons being lighter and mobile tend to neutralize the medium of ionized gas. This subsequently results in the medium behaving as a plasma. Except in the terrestrial ionosphere, where density is higher and temperature is lower, the vast region of the solar terrestrial medium is pervaded by a system of charged particles where the density is low and the temperature is high and the medium can effectively be considered as collisionless.

1.C Theoretical Approaches

The purpose of this section is to describe the theoretical approaches that are used to describe plasmas in space. In general, the dynamics of a system of plasma can be described using four different approaches. The first and the easiest approach is the single particle picture. This approach is useful in describing the dynamics of a single plasma particle in complex electromagnetic fields. Although it is very useful to understand the dynamics of a single particle, this approximation is inadequate because the solution of the equation of motion does not take into account the internal fields generated by every other charged particle in motion. However, it is useful in getting insight into the dynamics of very low density plasma such as ring current particles.

The second approach is the one-fluid magnetohydrodynamic (MHD) approach where the individual particle aspects are neglected and instead the collective and macroscopic behaviour of the system of plasma is considered. In this picture, the plasma is assumed as a conducting fluid immersed in a magnetic field. Unlike the single particle approach, this picture takes into account electromagnetic effects that result from the motion of charged particles subject to the external magnetic field. This approach is of paramount importance in studying ultra-low-frequency waves in highly conducting fluids in the presence of a magnetic field. The third approach is called the multi-fluid MHD approach. In this case, different particle species are treated separately as a single fluid. This approach is useful in studying the effects of heavier species over the lighter ones while studying the composite effect of a multi-particle species. The fourth and the last approach is kinetic theory. Kinetic theory

is by far the most advanced theory. Kinetic theory studies the evolution of the plasma distribution function in phase space for a system of plasma particles. Next, we turn our focus to MHD theory, what MHD can and cannot do, followed by its applications to ULF waves.

1.C.1 MHD Theory

Because of their extremely low density and large scales, space plasmas are collisionless and quasi-neutral. Electromagnetic fields are necessary for the completeness of the system of plasmas under study. This is because the magnetic field arising from the fluid in motion extensively modifies the background magnetic field and consequently the original motion and state of the system of plasma particles gets altered. The motion of plasma across magnetic fields induces electric fields. MHD theory is a combination of the theory of fluid dynamics and electromagnetic theory. It is applicable when the scale size of the system is larger than the ion gyro-radius and the frequencies are much smaller than any of the natural plasma frequencies. Thus MHD has been successful in describing large scale structures such as coronal out flow, sun spots and magnetic fields in stars, and is sufficient for the study of ULF waves in the magnetosphere.

1.C.2 Introduction to MHD Waves

MHD theory has some limitations when applied to collisionless space plasmas. This is because of the fact that we do not have a good model of conductivity to describe collisionless plasmas. Therefore, a complete understanding of

space plasma needs concepts beyond what the fluid theory of MHD can do. However, the theory of MHD can still be used to successfully understand and interpret large-scale space observations as mentioned above under the assumption of near infinite plasma conductivity. This type of MHD treatment of a magnetized plasma as a highly conducting fluid is called ideal MHD.

The constitutive equations of MHD theory are expressions for Newton's laws of motion, the continuity equation, and the famous Maxwell equations in electrodynamics. In the treatment of ideal MHD, the displacement current in Maxwell equations is neglected, because of a low frequency approximation, as discussed above. With these assumptions in mind, the set of equations governing infinite conductivity, uniform, magnetized and cold MHD fluid are:

Continuity equation:

$$\frac{\partial \rho}{\partial t} + \nabla \bullet \rho \vec{V} = 0 \tag{1.6}$$

Equation of motion:

$$\rho \frac{d\vec{V}}{dt} = \vec{J} \times \vec{B} \tag{1.7}$$

Simplified Ohm's law:

$$\vec{E} = -\vec{V} \times \vec{B} \tag{1.8}$$

Maxwell's equations:

$$\nabla \times \vec{E} = -\frac{\partial \vec{B}}{\partial t} \tag{1.9}$$

$$\nabla \times \vec{B} = \mu_o \vec{J} \tag{1.10}$$

where μ_o is the permeability of free space, ρ is plasma mass density, $\vec{J}$ is current density, $\vec{E}$ is electric field, $\vec{V}$ is fluid velocity and $\vec{B}$ is magnetic induction.

For perpendicular ($\perp$) and parallel ($\|$) components, equation (1.8) reads

$$\vec{E_\perp} = -\vec{V} \times \vec{B} \tag{1.11}$$

$$\vec{E_\|} = 0. \tag{1.12}$$

Equation (1.8) is derived from $\vec{J} = \sigma(\vec{E} + \vec{V} \times \vec{B})$. For infinite conductivity (σ), $\vec{E} + \vec{V} \times \vec{B}$ must be equal to zero to avoid $\vec{J}$ from becoming infinite. Equation (1.8) also implies that, for a plasma of infinite conductivity in a frame where $\vec{E'} = 0$, $\vec{E_\perp} = -\vec{V} \times \vec{B}$. This is because electric fields are consequences of a Lorentz transformation into a moving system. Equation (1.11) is also called the "frozen-in" condition. In other words the field lines are frozen into the plasma and thus move with the plasma.

To describe the fundamental concepts of MHD wave theory, the simplest one can do is to assume an ideal, cold plasma subject to a uniform straight magnetic field. Another assumption is to assume the plasma is initially at

rest (no flow, no electric field). Assume also that no currents are flowing. Introducing small perturbations: $\vec{E}$, $\vec{b}$, $\vec{j}$ and $\vec{V}$, where $\vec{b}$ and $\vec{j}$ respectively are small perturbations in magnetic field and current density, respectively. To first order, Maxwell's equations (1.9) and (1.10) would then reduce to

$$\nabla \times \vec{E} = -\frac{\partial \vec{b}}{\partial t} \tag{1.13}$$

$$\nabla \times \vec{b} = \mu_o \vec{j}. \tag{1.14}$$

Because of equation (1.12), $\vec{E}_{\parallel} = 0$, and the electric field in equation (1.13) represents $\vec{E}_{\perp}$. The equation of motion in equation (1.7) also reads

$$\rho_o \frac{\partial \vec{V}}{\partial t} = \vec{j} \times \vec{B}_o. \tag{1.15}$$

where ρ_o and $\vec{B}_o$ are the background plasma mass density and magnetic field, respectively.

Combining equations (1.11), (1.13), (1.14) and (1.15) yields

$$\frac{\partial^2 \vec{E}}{\partial t^2} + V_A^2 \nabla \times (\nabla \times \vec{E}) = 0 \tag{1.16}$$

where

$$V_A = B_o/(\mu_o \rho_o)^{1/2} \tag{1.17}$$

is the Alfvén speed and is defined as the fundamental speed at which magnetic signals in a plasma can be transported by waves.

For the sake of simplicity, one can consider a background magnetic field

$\vec{B_o} = B_o\hat{z}$. Introducing a Cartesian coordinate system turns equation (1.16) into

$$(\frac{1}{V_A^2}\frac{\partial^2}{\partial t^2} - \frac{\partial^2}{\partial y^2} - \frac{\partial^2}{\partial z^2})E_x = \frac{\partial^2 E_y}{\partial x \partial y} \tag{1.18}$$

$$(\frac{1}{V_A^2}\frac{\partial^2}{\partial t^2} - \frac{\partial^2}{\partial x^2} - \frac{\partial^2}{\partial z^2})E_y = \frac{\partial^2 E_x}{\partial x \partial y}. \tag{1.19}$$

Now, consider a plane wave propagating in the yz plane with solution of the form $e^{-i(\omega t - k_y y - k_z z)}$ where ω represents wave frequency. In this system of coordinate, an assumption of $\partial/\partial x = 0$ reduces equations (1.18) and (1.19) into two familiar MHD equations:

$$V_A^2 = \omega^2/k_z^2, \tag{1.20}$$

$$V_A^2 = \omega^2/k^2, \tag{1.21}$$

where $k = \sqrt{(k_y^2 + k_z^2)}$ is the wave number. Equation (1.20) is the dispersion relation for the class of MHD wave called the shear Alfven wave, which propagates in plasma with a group velocity of $\vec{V_g} = d\omega/d\vec{k} = \pm V_A\hat{z}$. It is also a purely transverse wave with flow perturbations perpendicular to both the group velocity and the background magnetic field, $\vec{B_o}$. Because the energy flow is guided only along the background magnetic field $\vec{B_o}$, this mode has no magnetic field compression. This mode is therefore analogous to a wave on a non-uniform string. Figure 1.2 shows a schematic of the wave perturbations and polarizations associated with this mode in a cold plasma.

Equation (1.21) is the dispersion relation for another class of MHD wave

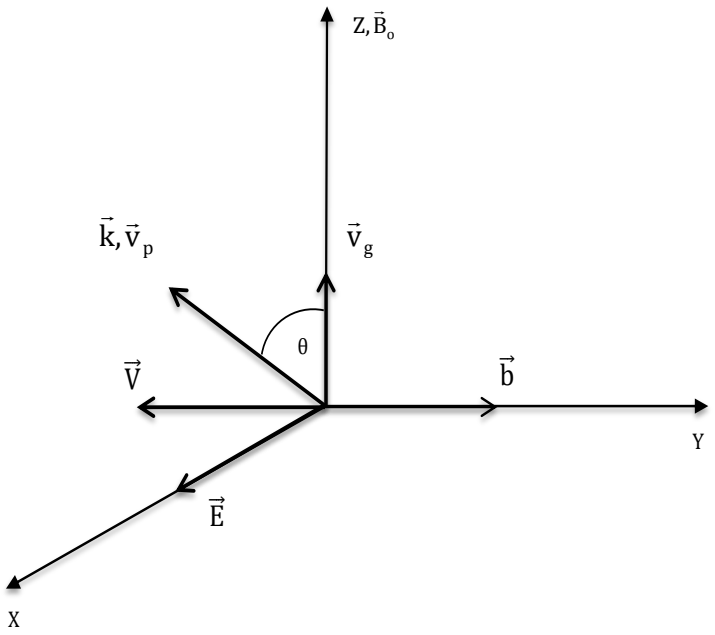

Figure 1.2: Schematic of Shear Alfv́en wave mode in a cold plasma [from *Fenrich* [1997]]. Here, $\vec{V}_p$ and $\vec{V}_g$ represent phase and group velocities respectively.

called a fast Alfvén mode. For this class of wave, the phase speed is still V_A, however, the group velocity is $\vec{V}_g = d\omega/d\vec{k} = \pm V_A \hat{k}$, where $\hat{k}$ is a unit vector defined along the direction of the wave vector $\vec{k}$ and $\vec{V}_g$ specify the direction of energy flow of the wave. In cold plasma, the energy and the phase of the fast mode propagate with speed V_A along the direction of the wave vector. This mode propagates across the background $\vec{B}_o$ and forces compression of the magnetic field. Because of this reason, this mode is also called compressional. This mode is therefore analogous to a sound wave and

transports energy and information isotropically. Figure 1.3 shows a schematic of the wave perturbations and polarizations associated with this mode in a cold plasma. Important to note is that, equations (1.20) and (1.21) impose relationships between wave number and frequency for the existence of an MHD wave in a cold plasma.

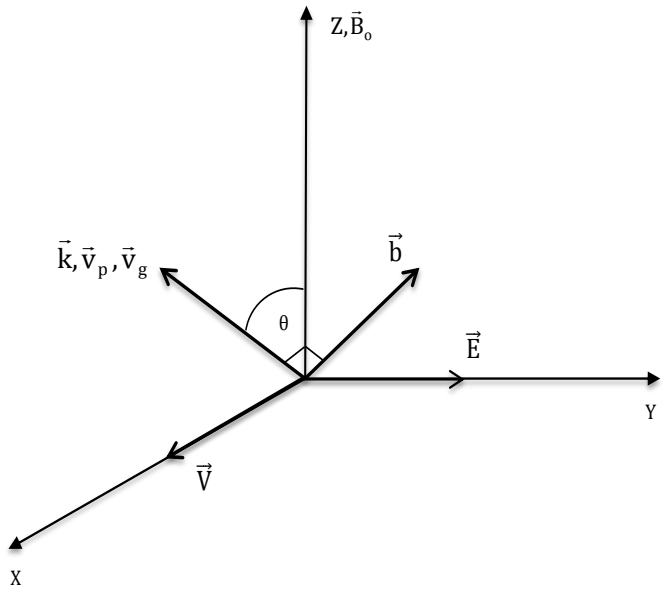

Figure 1.3: Schematic of fast compressional wave mode in a cold plasma [from *Fenrich* [1997]]. Here, $\vec{V}_p$ and $\vec{V}_g$ represent phase and group velocities respectively.

Thus far, the plasma treatment was for a cold, ideal MHD plasma subject to a straight homogeneous background magnetic field $\vec{B}_o$. Often we assume

the magnetosphere to be a cold plasma because the cold plasma approximation gives useful insights into the plasma environment in this limit. Introducing a finite temperature into our ideal MHD system mimics a realistic plasma environment, and is equivalent to introducing a finite equilibrium pressure, p_o. The introduction of a finite pressure, p_o modifies the dispersion relation for the fast wave mode equation (1.21) into

$$\omega^2/k^2 = \frac{1}{2}[V_A^2 + C_s^2 \pm \left\{(V_A^2 + C_s^2)^2 - 4C_s^2 V_A^2 \cos^2\theta\right\}^{1/2}], \tag{1.22}$$

where θ is the angle between $\vec{B}_o$ and $\vec{k}$, $C_s = (\gamma p_o/\rho_o)^{1/2}$ is the speed of sound in plasma, and γ is the ratio of the specific heats. For an example of the derivation see *Parks* [2004] and *Kivelson and Russel* [1995]. Equation (1.22) is the dispersion relation defining the magnetoacoustic wave modes. For propagation at an angle to the magnetic field, the plus and the minus signs give two hybrid modes, respectively, called the fast and slow magnetoacoustic modes. Equation (1.22) also states that in a plasma of finite temperature, the cold plasma MHD modes are coupled to a sound wave. Later on, in this chapter, an interesting class of coupling between the fast compressional and the shear Alfvén modes called Field line resonances (FLRs) will be discussed.

For a completely cold plasma, $C_s = 0$ and the dispersion relation of the fast magnetoacoustic mode in equation (1.22) reduces to

$$V_A^2 = \omega^2/k^2, \tag{1.23}$$

as expected, where as the dispersion relation of the slow magnetoacoustic mode

in equation (1.22) reduces to

$$\omega^2/k^2 = 0, \tag{1.24}$$

implying the slow mode can not propagate in cold plasma.

1.C.3 Impact of Magnetospheric Structure on MHD Waves

In the previous section, our discussion was based on an infinite uniform magnetized plasma. Unfortunately, no such plasma of infinite extent exists in nature. If so, how would our infinite plasma approximation of an MHD fluid address physical problems within the magnetospheric context (of finite scale size), which are the very focus of this thesis work? As long as the scale size of the plasma under consideration is much larger than the wavelength of MHD waves, boundary effects can be neglected and an infinite plasma approximation is justified to describe realistic problems of finite scale size. In the terrestrial magnetosphere, using a typical MHD wave frequency of 5 mHz, with a typical Alfvén speed in the day side of order 300 km/s, results in a wavelength of order 10 R_e. Noting that the typical distance of the dayside magnetospheric standoff distance from the center of the Earth is of order 10 R_e, we are led to the conclusion that boundary effects for waves in the mHz range (ULF waves) can not be neglected.

The coupled equations between compressional and shear waves in the magnetospheric context were developed by various authors [e.g., *Tamao*, 1966; *Southwood*, 1974; *Chen and Hasegawa*, 1974]. For simplicity, assume $\vec{B}_o = B_o\hat{z}$. Introducing an x-variation to the magnetic field $\vec{B}$ or mass density ρ_o,

results in the variation of the Alfvén speed across the magnetic field. How does this then affect the physics of MHD Alfvén waves in cold plasma described by equations (1.20) and (1.21)? First of all, the fact that we have introduced an x-variation on the Alfvén speed makes k_x a function of x. Assuming an electric field variation of the form

$$E_x(x, y, z, t) = E_x(x)e^{-i(\omega t - k_y y - k_z z)}, \tag{1.25}$$

$$E_y(x, y, z, t) = E_y(x)e^{-i(\omega t - k_y y - k_z z)}, \tag{1.26}$$

and using equations (1.25) and (1.26) in equations (1.18) and (1.19), results in

$$\left[k_y^2 - k_z^2 - \omega^2/V_A^2(x)\right] E_x = -ik_y(dE_y/dx) \tag{1.27}$$

$$\left[k_z^2 - \omega^2/V_A^2(x)\right] E_y = -ik_y(dE_x/dx) + (d^2E_y/dx^2). \tag{1.28}$$

Because of the mutual existence of variables E_x and E_y in equations (1.27) and (1.28), these equations are coupled and one can not be solved independently without use of the other.

For the more complex, yet interesting case where k_y is non zero ($k_y \neq 0$), the coupled equations (1.27) and (1.28) can be rewritten in a more compact way as

$$d^2E_y/dx^2 - C(dE_y/dx) + [K^2(x) - k_y^2 - k_z^2]E_y = 0, \tag{1.29}$$

where

$$C = k_y^2(dK^2/dx)/[(K^2 - k_y^2 - k_z^2)(K^2 - k_z^2)], \tag{1.30}$$

and

$$K^2(x) = \omega^2/V_A^2(x). \tag{1.31}$$

Equation (1.29) has a turning point x_t at a point where the coefficient $[K^2 - k_y^2 - k_z^2]$ vanishes. The location of this point is different from the location of the zero of $(K^2 - k_z^2)$, which we will consider next (when $k_y = 0$). Defining the vanishing point of $(K^2 - k_z^2)$ to be at x_r, one can see that for a monotonically increasing $K^2(x)$, such as the magnetosphere, a wave propagating from a region of large x (towards the Earth, in Cartesian geometry) meets the turning point x_t followed by x_r. That means the point x_r is located within the spatially evanescent region of the wave.

From equation (1.30), one can see that C has singular points at x_r and x_t, which have physically very interesting interpretations. The singularities cause problems in finding a mathematical solution to equation (1.29). From a series of rigorous solutions, one can show that the solution of equation (1.29) at x_t is finite. However, the singularity at x_r is unavoidable and turns the solution to infinity. The point x_r is called a resonance point. Physically, the resonance point is where the fast mode frequency matches the shear Alfvén mode and coupling between the two modes occur by way of transferring energy into the shear Alfvén mode. Therefore, for a wave propagating from a region of large x (say the magnetopause, as in the case of an external driver) towards the

Earth ($x = 0$), the incident wave gets reflected at the turning point, x_t, by the increase in the Alfvén speed gradient. Beyond this point, the evanescent wave drives a (Field Line Resonance) FLR. The FLRs will be discussed in depth in the next sections.

Choosing the simplest case where $k_y = 0$ reduces equations (1.27) and (1.28) into two decoupled equations,

$$\left[k_z^2 - \omega^2/V_A^2(x)\right] E_x = 0, \tag{1.32}$$

$$\left[k_z^2 - \omega^2/V_A^2(x)\right] E_y = d^2E_y/dx^2. \tag{1.33}$$

For a function E_x not everywhere zero, equation (1.32) yields

$$\omega^2 = \omega_A^2(x) = k_z^2 V_A^2(x), \tag{1.34}$$

where $\omega_A(x)$ represents the Alfvén frequency. Assuming $K^2(x) = \omega^2/V_A^2(x)$ to be a monotonically increasing function of x, one can rewrite equation (1.33) as

$$d^2E_y/dx^2 + \left[K^2(x) - k_z^2\right] E_y = 0. \tag{1.35}$$

Once again, from equation (1.35), it can be seen that a radial position x_t exists for which the coefficient of E_y vanishes. In the Earth's magnetosphere, as one travels in the direction of increasing x away from Earth (i.e., $x > x_t$), $V_A(x)$ decreases, turning $K^2(x) - k_z^2 > 0$ and $K^2(x) - k_z^2 < 0$ for $x < x_t$. Hence, the behaviour of the solution of equation (1.35) changes sign from be-

ing spatially oscillatory ($x > x_t$) to evanescent ($x < x_t$) in space. Physically, the point x_t is a reflection point where the wave stops travelling towards the Earth and turns around at this point. That is, at the point x_t the refractive index of the medium vanishes.

Before closing this section, one thing that warrants discussion is how the singularity at the resonance position can be handled mathematically. In general, assuming a small time dependent energy sink in the system (for example introducing Joule dissipation in the ionosphere) will help to avoid the singularity in equation (1.29). Doing so is physically justifiable, since the ionosphere is not a perfect reflector, thereby it damps the energy of the coupled system and provides a finite and justifiable solution to the physical problem. Field-Aligned-Currents (FACs) associated with FLRs are responsible for dissipating their energy at the ionospheric foot prints in the form of Pedersen current [e.g., *Allan and Knox*, 1978; *Newton et al.*, 1979].

1.C.4 Field Line Resonances

The application of the theory on how waves originating from outside the magnetosphere couple compressional waves in the outer magnetosphere to the FLR is understood from the discussion of the above section. We also understand how FLRs transfer that energy to the ionosphere. What is not known is the source of the discrete FLR frequencies, i.e., where do the compressional waves in the outer magnetosphere come from and how do they evolve spatially and temporally? Why should we care about FLRs anyway? FLRs can be used to infer equatorial plasma densities along a magnetic field line using the funda-

mental eigen-frequencies of guided toroidal Alfvén waves [*Waters et al.*, 1996]. FLRs also play a role in auroral arc generation and substorm onset [e.g., *Samson et al.*, 1996; *Rankin et al.*, 1999]. They are found to provide sufficient energy to drive discrete auroral arcs [*Samson et al.*, 1991].

FLRs are standing MHD Alfvén waves on closed geomagnetic field lines [e.g., *Tamao*, 1966; *Dungey*, 1967; *Radoski*, 1967; *Southwood*, 1974]. The simplest possibility for a standing wave to exist in a cold plasma is the shear Alfvén mode. In the simplest magnetospheric model, one can envisage a box model where the field lines are straight and of length l with infinitely conducting (reflecting) ionospheres. This will help to illustrate the basic characteristic features of FLR coupling. Choosing an average Alfvén velocity $\langle V_A \rangle$ along a field line, it can be easily shown that the condition for the existence of a standing shear Alfvén wave is $\lambda_n = 2l/n$. That is the length of the field line l should be an integral multiple of half the wavelength, where $n = 1, 2, 3, ...$ The possible oscillation frequencies, also called resonant frequencies, ω_n of this mode can be calculated using the dispersion relation of this mode from equation (1.20)

$$\omega_n = n\pi \langle V_A \rangle / l \tag{1.36}$$

Equation (1.36) shows the dependence of ω_n on the field line length l. Hence, for a more realistic geometry, where the length of the field line increases with latitude, the oscillation frequency decreases. That means field lines at larger x (near the magnetopause) have lower frequencies than those at smaller x (closer to the Earth). As we already discussed in equation (1.29), the

coupling between the fast mode and shear Alfvén mode occurs when $k_y \neq 0$, and when the frequency of the two modes match. In this picture, the result is that the coupling between the two modes exhibits an amplitude maximum at some radial distance corresponding to the resonant field line and exhibits a characteristic feature of a 180^o phase shift across the resonance. The phase shift is due to the continuum in the local Alfvén frequency gradient. This is the characteristic signature of a classical field line resonance.

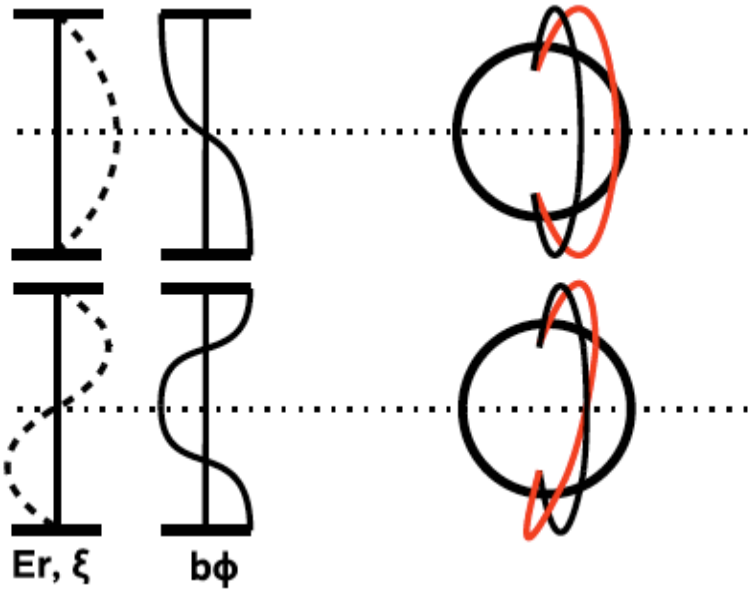

Figure 1.4: Left: Field line structure of a first harmonic (top) and a second harmonic (bottom) toroidal oscillation, where E_r is the radial component of the electric field, ξ the displacement vector, and b_ϕ the azimuthal component of the magnetic field disturbance. Right: Sketch of the azimuthal field line oscillation, where the red line marks the disturbed field line. Adopted from *Schafer* [2008].

FLRs can in general be classified into toroidal and poloidal modes of oscil-

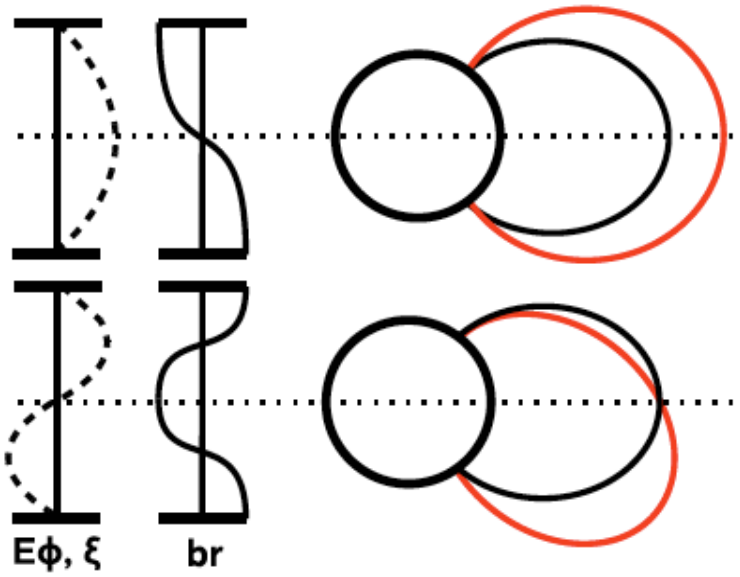

Figure 1.5: Left: Field line structure of a first harmonic (top) and a second harmonic (bottom) poloidal oscillation, where E_ϕ is the azimuthal component of the electric field, ξ the displacement vector, and b_r the radial component of the magnetic field disturbance. Right: Sketch of the azimuthal field line oscillation, where the red line marks the disturbed field line. Adopted from *Schafer* [2008].

lations. The excitation mechanisms, as well as the wave characteristics such as the field line displacement and the plasma bulk flow distinguishing these waves are different. The toroidal FLR has a characteristic feature of displacement and magnetic field perturbations along the azimuthal direction and an electric field perturbation in the radial direction. This class of FLR is therefore analogous to a wobbling oscillation of a field line. The field line structure for the fundamental and second order harmonics of a toroidal mode are shown in Figure 1.4. For reasons of large conductivity of the ionospheres, displacement and electric field are zero at the foot point of the field line. In contrast, the

magnetic field exhibits an amplitude maximum at the ionospheric foot point. A toroidal mode FLR exhibits a 180^o phase shift across the resonance and is associated with small k_y values. All of the FLRs presented in this thesis have relatively small k_y values. Although the FLRs considered in this thesis correspon to positive IMF B_z, FLRs are known to occur in both positive and negative IMF B_z conditions.

The second class of FLR, the poloidal field line oscillation, is characterized by displacement and magnetic field perturbations in the radial direction. Because of its field line oscillation structure, this class of FLR is also referred to as a breathing oscillation of a field line. The field line structure for the fundamental and second order harmonics of a poloidal oscillation are shown in Figure 1.5. This class of wave is associated with large k_y values and the phase shift may exceed 180^o depending on the strength of the driver and how large k_y is [*Fenrich and Samson*, 1997].

1.C.5 Previous Work on FLR Coupling

Establishing the mechanisms by which fast compressional waves enter the terrestrial magnetosphere is an important objective in space physics, as they are believed to be ultimately related to space weather phenomena [*Hasegawa et al.*, 2004]. The most common observables of space weather phenomena include magnetic storms, aurorae, energized radiation belt particles and FLRs. The knowledge of the existence of FLRs dates back to the late 1960s [e.g., *Dungey*, 1967; *Radoski*, 1967]. ULF waves which play a major role in driving FLRs are believed to be significantly involved with energization of radiation

belt electrons and their dynamics, such as transport and diffusion [e.g., *Rostoker et al.*, 1998; *Elkington*, 2006; *Degeling et al.*, 2008]. They also provide the free energy required to accelerate electrons to relativistic energies [*Liu et al.*, 1999; *Elkington et al.*, 1999] and form auroral arcs [*Samson et al.*, 1996; *Lotko et al.*, 1998; *Rankin et al.*, 1999; *Rae et al.*, 2007], that may be associated with an explosive plasma instability in geomagnetic storms during their expansion phase [*Dobias et al.*, 2004], main phase [*Baker et al.*, 1998] and magnetotail dynamics [*Sanchez et al.*, 1997].

FLRs are known to occur at specific discrete, stable, and sharply peaked ULF frequencies and are observed in ground based HF radar and magnetometer data [e.g., *Fenrich et al.*, 1995; *Samson et al.*, 1992; *Kivelson and Southwood*, 1985; *Mann et al.*, 2002]. *Rankin et al.* [1993] has done interesting work on the nonlinear evolution of field line resonances in the Earth's magnetosphere. Although it has been identified that there is a direct link between solar wind and FLR wave activities, the source of the discrete FLR frequencies is still unresolved, although the Sun is the ultimate source of all the energy in the solar wind and sources driving FLRs.

One can associate FLRs with FACs [e.g., *Allan and Knox*, 1978; *Newton et al.*, 1979], which are a specific class of currents flowing along geomagnetic field line connecting the Earths magnetosphere to the high latitude ionosphere. Upward FACs are believed to be somehow related to the downward acceleration of electrons producing the optical aurora at the high latitude ionosphere [e.g., *Dungey*, 1967; *Radoski*, 1967; *Rae et al.*, 2005].

1.C.6 FLR Excitation Mechanisms and Motivation

Toroidal mode FLRs are believed to be driven by sources external to the magnetosphere. Potential driving mechanisms include: Kelvin Helmholtz (KH) surface waves on the magnetopause [*Hughes*, 1994] and [*Walker*, 1981]; magnetospheric waveguide/cavity modes driven by a continuum of wave energy or a pressure pulse in the solar wind [*Kivelson and Southwood*, 1985], [*Samson et al.*, 1992], and direct driving via entry of solar wind MHD waves across the magnetopause and into the magnetosphere, [e.g., *Stephenson and Walker*, 2002; *Walker*, 2002; *Fenrich and Waters*, 2008; *Kepko et al.*, 2002].

Recent work carried out using WIND in the solar wind and GOES-10 at geosynchronous orbit [*Kepko et al.*, 2002] has shown that ULF waves in the solar wind at least in some cases are direct sources for discrete ULF pulsations. In Chapter 2, a rare SuperDARN observation of a ULF wave in the solar wind that crossed Earth's bow-shock and excited a FLR will be presented [*Nedie et al.*, 2012]. Several studies have shown that discrete, stable and sharply peaked field line resonance (FLR) structures are excited inside the Earth's magnetosphere in response to fast mode ULF pulsations. There have been reports of ground-based and space-based ULF discrete field line resonances (FLRs) in the range of mHz frequencies in the terrestrial magnetosphere since the late 1960s. Although, the nature of the source of oscillation for the discrete FLR frequencies is still unsettled, recent observations have shown that simultaneous occurrence of discrete fluctuations in the upstream solar wind and in the magnetosphere suggest that the solar wind may be a direct source for the observed discrete FLRs at least in some cases.

There is observational evidence in support of the hypothesis that both pressure pulses in the solar wind and direct entry of MHD waves across the magnetopause drive FLRs. However, to date no concrete observational evidence has been presented to prove or disprove KHI generated surface waves and/or magnetopause oscillations as drivers of FLRs. The work of *Rae et al.* [2005] presents the evolution of an extremely long lasting narrow band Pc5 pulsation of 1.5 mHz during a high solar wind speed and northward IMF interval using data from multiple instrumentation. Without a detailed analysis on features such as: radial Poynting flux structures, propagation time delay on the wave phase, observed growth time of the driver wave and whether the condition for the most unstable mode is met, the authors hypothesized KHI as a potential source mechanism. Thus, a work with this type of detailed analysis is required and is the motivation behind this project. Chapter 3 presents a new result using the suggested detailed analysis.

As opposed to the toroidal modes, the generation mechanisms associated with poloidal mode FLRs are believed to be sources from within the magnetosphere [*Fenrich and Samson*, 1997]. Potential sources are drift mirror instability [*Hasegawa*, 1969] and bounce instability [*Southwood et al.*, 1969].

Since MHD ULF waves can be used as diagnostics of certain properties of the magnetospheric system, the global time dependent behaviour of the magnetosphere can be described in terms of ULF waves. Since ULF waves are also important in substorm dynamics and in energizing radiation belt electrons and ions, understanding their origin is important in space weather research where

forecasting the effect of solar storms on satellites technology is paramount.

1.D Theory and background on magnetopause instabilities and oscillations

In situ measurements of the flanks magnetospheric boundary (magnetopause and low latitude boundary layer) sometimes show the presence of periodic surface waves [e.g., *Couzens et al.*, 1985; *De Keyser and Roth*, 2003]. The existence of surface waves has been proposed to explain multiple crossing of the magnetopause past satellites [*Ledley*, 1971]. If not always, at least sometimes, this periodic oscillation of the boundary is due to the motion of the boundary in attempting to establish pressure balance on either side of the boundary [*Sibeck et al.*, 1991]. That is, the boundary of the magnetosphere oscillates in response to changes in solar wind pressure. Multiple magnetopause crossings by ISEE 1 and 2 satellites showed that magnetopause oscillations can occur because of solar wind pressure fluctuations [*Song et al.*, 1988]. The magnetopause moves inward when the solar wind dynamic pressure increases and outwards when it decreases. The solar wind dynamic pressure is the most important factor that controls the position of the subsolar point [*Martyn*, 1951] and influences the shape of the magnetosphere [*Ferraro*, 1960]. *De Keyser et al.* [2002] showed that it actually takes a small percent of the total pressure change to move the boundary in- or outward over a 1000 km. The boundary can also move in- and out in response to surface instabilities [e.g., *Sckopke et al.*, 1981; *Kivelson and Chen*, 1995]. Boundary motion of the magnetopause generates magnetopause oscillations which propagate downtail with the anti-sunward motion

of the plasma [*De Keyser and Roth*, 2003].

The KH instability is one major candidate that is thought to be responsible for launching compressional surface waves. The generation of surface waves at the inner boundary through KHI has been predicted by *Lee et al.* [1981]. These KH instability driven surface waves can tunnel deep into the inner magnetosphere, [e.g., *Farrugia et al.*, 2000; *Otto and Fairfield*, 2000]. The early evidence for this dates back to *Dungey* [1954], followed by detailed theoretical attempts to describe it [e.g., *Sen*, 1963; *Fejer*, 1964; *Southwood*, 1968; *Pu and Kivelson*, 1983; *Miura and Prichett*, 1982; *Miura*, 1990; *Walker*, 1981]. The KH instability at the boundary is fed continuously by the free energy source that is available in the shear flow of the magnetosheath. The shear flow along the boundary is highest at the flanks of the magnetosphere, and this makes this region of the magnetospheric boundary significantly more vulnerable to trigger the instability, where the shocked solar wind is flowing fast relative to the stagnant magnetospheric plasma, [e.g., *Hasegawa et al.*, 2004]. A KH instability at the flank magnetopause is more complicated than a simple case of fluid shear because of a stabilizing effect of field line bending.

The early theoretical works of linear MHD assumed the boundary between the magnetospheric and magnetosheath plasmas to be a tangential discontinuity. These works resulted in the KH instability condition at the magnetopause for an incompressible plasma [*Hasegawa*, 1975], expressible in terms of plasma

and field parameters as:

$$(\vec{k}\cdot\vec{v})^2 > \frac{1}{\mu_o m_i}\left(\frac{1}{n_1}+\frac{1}{n_2}\right)\left[(\vec{k}.\vec{B}_1)^2+(\vec{k}.\vec{B}_2)^2\right], \tag{1.37}$$

where in equation (1.37) $\vec{k}$ is the wavenumber, $\vec{v}$ is the relative velocity shear on both sides of the boundary, μ_o is the permeability of the free space, m_i is mass of proton, and (n_1, n_2 and $\vec{B}_1$, $\vec{B}_2$) are the proton densities and magnetic fields on both sides of the boundary (subscripts 1 and 2 refer to inside and outside the boundary, respectively).

While theoretical work [e.g., *Sen*, 1963; *Fejer*, 1964; *Southwood*, 1968] assumed tangential discontinuity, satellite observations revealed the existence of a low latitude boundary layer [e.g., *Hones et al.*, 1972; *Eastman et al.*, 1976]. The existence of such a boundary implicates that modelling the interface by a tangential discontinuity is unrealistic. Furthermore, the growth rate of such a KH unstable interface can be estimated by left-hand side (LHS)−right-hand side (RHS) of equation (1.37). The LHS−RHS is an increasing function of the wave number, $\vec{k}$, and this model predicts that a whole spectrum of wavelengths will be excited. This is inconsistent with observations of magnetopause crossings where monochromatic waves with well defined frequencies are identified [*Claudepierre et al.*, 2008].

A KH unstable surface wave is distinguished by a wavelength of 0.5 to 25 Re (which is the scale size of dayside flank magnetosphere) [*De Keyser and Roth*, 2003]. Such a wave is evanescent on either side of the boundary according to $exp(-k_y s)$, where s is distance measured inward from the magnetopause

[*Walker*, 1981] and [*Allan and Poulter*, 1992]. According to the early linear theoretical works, as the wave occurs on the magnetopause, large k_y is expected. Linear theory predicts the larger the k_y, the more unstable the KH wave becomes and the more rapidly it evanesces. This leads to a negligible amplitude of the wave in the magnetosphere and raises controversy on how deep the wave can penetrate into the magnetosphere to excite the observed FLRs [*Allan and Poulter*, 1992].

A more realistic KH theory constraining finite thickness and compressible plasma developed by *Walker* [1981] showed that when the thickness of the boundary, Δ, is comparable with the wavelength of the disturbance tangent to the boundary, k_y (i.e., $k_y\Delta \sim 0.6 - 0.8$), the instability criteria is effectively met. The condition $k_y\Delta$ at which the instability is satisfied corresponds to a maximum in the curve representing the growth rate as a function of k_y. The author suggested that the instability occurs in the low latitude boundary layer just inside the magnetopause. This implies that the velocity shear is spread over the low latitude boundary layer of thickness Δ. The repercussion of this new theory is that a particularly defined wavelength corresponds to the fastest growing mode. This essentially means a single frequency ($f = V_\phi/\lambda$) for the fastest growing mode. According to the new formalism, the wave number of maximum growth corresponds to $k_y \sim 0.6/\Delta$ (if one takes the lower limit for the fastest growing mode). On the magnetospheric flanks, Δ varies roughly between 2 R_e and 4 R_e [*Miura and Prichett*, 1982]. The inward amplitude fall-off thus becomes considerably less rapid [*Allan and Poulter*, 1992] and this results in an e-folding distance of many Earth radii [*Walker et al.*, 1992]. Consequently, the wave can penetrate deep into the magnetosphere and

this leads to a resolution to the evanescence controversy. The inclusion of a boundary of finite thickness and compressibility in the new theory successfully explains the observation of a single resonant frequency in the Pc4-Pc5 range [*Walker*, 1981] and [*Allan and Poulter*, 1992].

A numerical simulation by *Claudepierre et al.* [2008] has actually shown that a flank fast compressional wave mode associated with a KH instability in its linear phase and *Miura* [1990] and *Hasegawa et al.* [2004] in its non-linear phase can propagate deep into the interior of the magnetosphere. The work of *Pu and Kivelson* [1983] and *Michael et al.* [2011] further supports this claim that KHI driven compressional waves at the boundary can trigger a significant energy flux to mode-couple into transverse magnetic standing waves on closed magnetic field lines and cause the observed FLRs.

1.E Methodology and Data Acquisition

In order to achieve the goals of this research, a case study approach is employed using the various ground and space instruments listed in section 1.A. In principle, a statistical analysis of events can be used to characterize the different types of magnetopause instabilities and oscillations based on upstream solar wind conditions. However, if not impossible, it is very hard to find a database of such events with simultaneous occurrence of the wave signatures at the boundary and inside the magnetosphere.Yet, individual case studies are of paramount importance in providing detailed information and new insights to improve our understanding of ULF waves in the terrestrial magnetosphere and associated excitation mechanisms. Detailed individual case studies

have proven to be incisive in enhancing our understanding of magnetospheric physics and complementing results from large statistical databases. In this thesis, three individual case studies were studied in a more detailed way using a variety of ground and space based instrumentation in characterizing rarely reported events. For the latter two a 2D ideal MHD model for ULF waves in a compressed model magnetic field will be used to explain the observations.

In order to examine potential source mechanisms such as magnetopause instabilities and oscillations, several instrumentation were considered. The first event was found initially with SuperDARN and later observed on GEOTAIL. The other two case studies which are on the same day were observed first on SuperDARN and were found to have reasonably good data. In the later two, CLUSTER was at the boundary observing lots of wave activity. POLAR also observed a strong and clear wave activity in both magnetic and electric field data of the second case study.

It is very important to check if the spacecraft are at the right position and right time. The reason for doing so is because wave activity generated by the KHI are preferentially located at the magnetopause boundary. Events such as those with strong northward IMF and very high solar wind speed were of top priority, because these conditions favour KH instabilities at the magnetopause. Also considered is the presence/absence of a source mechanism such as dynamic pressure pulses or MHD waves located inside the solar wind.

Characterizing magnetopause instabilities and oscillations as a source mechanism using a single spacecraft is a complicated and often gives an ambiguous

result. The CLUSTER multi-satellite mission offers a unique opportunity to observe wave processes at the magnetopause boundary. Having traced a possible source mechanism at the magnetopause boundary or within the upstream solar wind region, it is important to investigate wave processes inside the magnetosphere and study their association with the sources already identified. To do so, we need the availability of ground-based and satellite borne-instrumentation inside the magnetosphere. While data from spacecrafts, magnetometers and HF radars were used in this thesis, SuperDARN is used substantially in all the events considered.

1.E.1 Principles of Coherent Scatter Radar Techniques

Coherent scatter radars such as SuperDARN operate on a mechanism of volume scattering whereby the radar detects a backscattered signal from within a medium. The basis of coherent HF radar scattering is non-thermal, but enhanced plasma density irregularities due to gradient-drift instabilities. The scattered signal is coherent because half the radar wavelength matches the size of the irregularity structures. A good description of an early SuperDARN HF radar work that discusses the instabilities producing the irregularities, as well as reports that show irregularities drifting with the bulk plasma, can be found in *Greenwald et al.* [1995], *Greenwald et al.* [1985] and references therein.

Research has shown that much of the ionospheric irregularity structure is the result of a plasma instability processes (e.g. review by *Fejer and Kelley* [1980]). In the E-region, plasma streaming instabilities, particularly the crossed-field two stream [e.g., *Buneman*, 1963; *Farley*, 1963] and the gradient

drift [e.g., *Knox*, 1964; *Reid*, 1968], are dominant. Electrostatic ion cyclotron instability [*Fejer et al.*, 1984] is proposed and thought to be operative in the E-region plasma. The most prominent plasma instability in the F-region is the gradient drift instability [*Simon*, 1963]. In addition, Rayleigh-Taylor [*Dungey*, 1956] and Kelvin-Helmholtz [*Keskinen et al.*, 1988] instabilities are believed to be fairly operative.

For good coherent radar backscatter, the transmitted signal must have a frequency above the E and F region plasma frequency. The necessary condition for HF radar backscatter is the availability of ionospheric irregularities, and the transmitted signal must be orthogonal to the field aligned irregularities.

Employing the principle of conservation of momentum and energy to coherent HF radar systems *Fejer and Kelley* [1980], one finds

$$\hbar\vec{k_t} = \hbar\vec{k_b} + \hbar\vec{k_i}, \tag{1.38}$$

$$\hbar\omega_t = \hbar\omega_b + \hbar\omega_i, \tag{1.39}$$

where in equations 1.38 and 1.39, $\hbar$ is Planck's constant, $\vec{k}$ is the wave vector, ω is angular frequency in rad/sec and t, b, and, i are subscripts that represent the transmitted, backscattered, and irregularity respectively. For good radar backscatter where the transmitted signals are orthogonal to the field aligned irregularities, $\vec{k_t} = -\vec{k_b}$. Then, from equation 1.38 follows, the relation between the scale size of the the irregularity and the radar operating wavelength. That is, for a radar backscatter, the scale size of the irregularity (spatial resolution)

must have a size of half the radar operating wavelength to reinforce constructive interference in the direction of the radar. This is referred to as the Bragg condition. Also from equation 1.39 follows the difference in the transmitted and backscatter frequency, which provides information on the radar's line of sight Doppler frequency shift as a measurement of the irregularity. These are primarily used to extract information on the target's line of sight Doppler velocity, backscattered power, and spectral width measurements in coherent radar experiments such as SuperDARN.

HF radars also receive backscattered signal from ground or sea. These backscatters have a typical characteristic feature of relatively low Doppler velocity and spectral width [*Menk et al.*, 2003]. These features provide a very convenient tool to exclude ground (sea) backscatter from ionospheric backscatter during the process of data analysis.

1.E.2 The Super Dual Auroral Radar Network

The data used in this study is collected mostly by northern hemisphere HF radars of the international Super Dual Auroral Radar Network (SuperDARN) [*Greenwald et al.*, 1995]. SuperDARN is a global network of radars operated by a consortium of 9 nations with 26 identical radars over the Arctic and Antarctica for studying the mid- and high- latitude ionospheric convection. Eighteen of the HF radars are deployed in the northern hemisphere whereas the remaining eight are in the south. The fields of view of the northern hemisphere radars are shown in Figure 1.6. Each of the radars use a multi-pulse technique and operate in the High Frequency (HF) band between 8 and 22 MHz. In their

standard operating mode, each radar is electronically steered into 16 beams separated by 3.24^o in azimuth with a total scan time of 1 min for the entire field of view. Each beam is divided into 75 range gates of 45 km extent, so in each full scan each radar covers 52^o in azimuth and over 3000 km in range, an area of over 50,000 km^2. In this thesis, we will use the radar back-scattered Doppler velocities which give the component of the ionospheric plasma convection along the beam line-of-sight (l-o-s). These l-o-s Doppler velocities can be used to measure ULF oscillations in F-region plasma flows associated with field line resonances [*Fenrich et al.*, 1995].

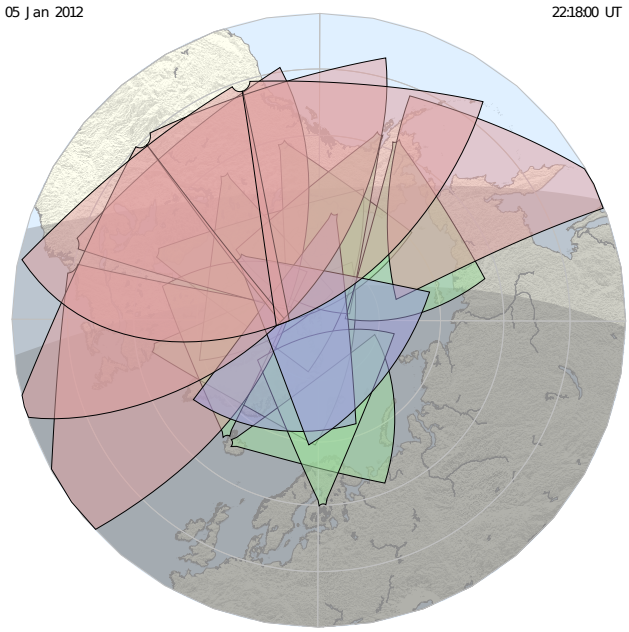

Figure 1.6: Field of view of the Super Dual Auroral Radar Network (SuperDARN) radars from all of the northern hemisphere HF radars in AACGM in 2012. This is the most recent coverage including the mid-latitudes in addition to the high latitudes [superdarn.jhuapl.edu].

Measurements of ionospheric $\vec{E} \times \vec{B}$ plasma drifts obtained from SuperDARN HF radars show signatures of ULF FLRs. For reasons explicable in terms of electric and magnetic field perturbations resulting from ULF wave

oscillations in the ionosphere, periodic oscillations in the $\vec{E} \times \vec{B}$ drift are expected. The shift in Doppler frequency, Δf of the radar back-scatter associated with the motion of the ionospheric irregularities is detected by HF radars. The line-of-sight (l-o-s) Doppler velocity plasma drift V_D of the irregularity is estimated by using the measured Δf through, $V_D \simeq \Delta f \lambda_r/2$. Where, λ_r is the operating radar wavelength. Merging the l-o-s Doppler velocities from beams of overlapping HF radar pairs (common-volume areas) yields the velocity of the plasma drift in 2D. Global scale convection velocities are derived by repeating this procedure for all overlapping field of views in the ionosphere. It was with this intent and purpose of studying the large-scale ionospheric convection that the international collaborative project of SuperDARN network of radars was primarily developed [*Greenwald et al.*, 1995].

Sometimes, data from overlapping field of views are not available for different reasons. In regions where there is little or no data, a very powerful technique called Map Potential [*Ruohoniemi and Baker*, 1998] is used to fit the observed l-o-s Doppler velocities to a series of spherical harmonic functions based on the prevailing upstream IMF conditions. This essentially means that in regions of little or no data, a statistical model constrains the global electrostatic potential. The global distribution of the electrostatic potential derived on the basis of $\vec{E} = -\nabla\Phi$ is capable of providing information on the current state and dynamics of the ionosphere.

The success of this technique is contingent on the number of observed l-o-s Doppler velocities that contribute to the solution. In general, the more radars that are used, the more the ionospheric back-scatter will be, resulting in a

more reliable global convection pattern. As discussed above, the data obtained from HF radars can therefore be used to remotely monitor the dynamics of the magnetosphere and the ionosphere and provide a convenient tool to study solar wind-magnetosphere-ionosphere coupling. A global convection pattern will be used in the next chapter to help us understand a magnetospheric FLR wave process driven by a direct solar wind driver. The l-o-s Doppler velocities will also be extensively used in the analysis of the FLRs.

1.E.3 The CLUSTER Multi-Spacecraft Mission

In the past, satellite-borne and ground based instrumentation rarely seem to be in the appropriate position, at the right time, under the right conditions, and most importantly in an operational state. The kind of events that are of interest to this thesis are those that would help to characterize magnetopause boundary instability/oscillations and ULF wave activity inside the magnetosphere. Particular focus is on the ultimate goal of elucidating the causal relationship between the two. The simultaneous presence of data from multi-satellite- borne instrumentation, near the magnetopause, is therefore ideal for identifying a plausible source mechanism at the magnetopause boundary. The CLUSTER multi-satellite mission along with data from Geotail, ACE, OMNI database, and magnetometers is ideal to address the objectives of this thesis.

CLUSTER, launched into their final orbits on August 14, 2000, constitutes four identical spacecraft that fly in a tetrahedron constellation [*Kronberg et al.*, 2011]. Eleven scientific instruments are deployed on each CLUSTER spacecraft. These instruments are designed to measure space weather inside

and outside the magnetosphere. In this thesis, measurements particularly from FGM, EDI, CIS and PEACE instruments will be used [*Kronberg et al.*, 2011]. The Fluxgate Magnetometer (FGM) instrument measures magnetic field in high resolution, with up to 67 samples per second along the orbit of the spacecraft. Electron Drift Instrument (EDI) fires beams of electrons and the returning electrons which are affected by the electric field in space are used to measure the strength of the electric field. The Cluster Ion Spectrometry experiment (CIS) is designed to diagnose the composition, mass and distribution functions of ions in the magnetosphere and solar wind during each four second spin of the spacecraft. Plasma Electron And Current Experiment (PEACE) measures the incoming electrons direction of travel and speed. Chapters 3 and 4 will make use of the CLUSTER mission to characterize two different ULF wave events produced by a KH boundary instability at the magnetopause and a ULF wave event triggered by a solar wind driven magnetopause oscillation, with simultaneous data from ground- and space-based instrumentation.

Chapter 2

SuperDARN observations of the driver wave associated with FLRs

[1]

Ultra-low frequency (ULF) field line resonances (FLRs) cause oscillations in F-region plasma flows and can be detected in SuperDARN measured line-of-sight (l-o-s) Doppler velocities. In this chapter, a ULF wave event is characterized with coordinated use of SuperDARN HF radars, optical instrumentation, ground based magnetometers, and spacecraft observations. The SuperDARN Pykkvibaer radar observes first and second order FLR harmonic signatures at 0.8 mHz, while the Kodiak and Hankasalmi radars simultaneously observe the driver wave on open field lines at exactly the same 0.8 mHz frequency. These observations show that SuperDARN can provide a diagnostic of MHD wave

[1] A version of this chapter has been published. A. Z. Nedie, R. Rankin, and F. R. Fenrich, SuperDARN observations of the driver wave associated with FLRs, *J. Geophys. Res.,* 117, A06232, doi:10.1029/2011JA017387, 2012.

propagation on open field lines and potentially be used to monitor MHD wave transmission across the magnetopause, and through the outer regions of the magnetosphere. During the time interval of interest, Geotail was in the solar wind just outside the dawn flank region and observed clear oscillations in the IMF Bz component at 0.8 mHz. A high coherence between the Geotail Bz oscillations and the radar Doppler velocities at 0.8 mHz is shown, confirming that the 0.8 mHz FLR harmonic and the associated wave on open field lines is directly driven by the 0.8 mHz oscillation in the solar wind. The observation of first and second order harmonic FLRs in SuperDARN data supports the theoretical body of work on expected behaviour of FLRs (higher harmonic orders maps to higher latitudes), and their potential use in estimating magnetospheric properties such as density and magnetic topology.

2.A Introduction

Magnetospheric ULF event, where an FLR is directly driven by an MHD wave in the solar wind is presented. Measurements from multiple SuperDARN HF radars in the morning, midnight, and afternoon sectors, show harmonic FLR wave signatures on closed field lines simultaneous with coherent wave signatures on open field lines at a frequency of 0.8 mHz. The ground based observation of coherent wave signatures on open field lines associated with FLRs is presented as one of a few observations of a driver wave on open field lines [e.g., *Prikryl et al.*, 1998, 2005, 1998b]. In addition, the 0.8 mHz waves observed by the radars are found to correlate well with Geotail spacecraft IMF Bz measurements in the solar wind, suggesting that the observed 0.8 mHz waves in the magnetosphere are directly driven by MHD waves in the solar

wind. This type of observation adds to a growing database of observations that suggest the same conclusion.

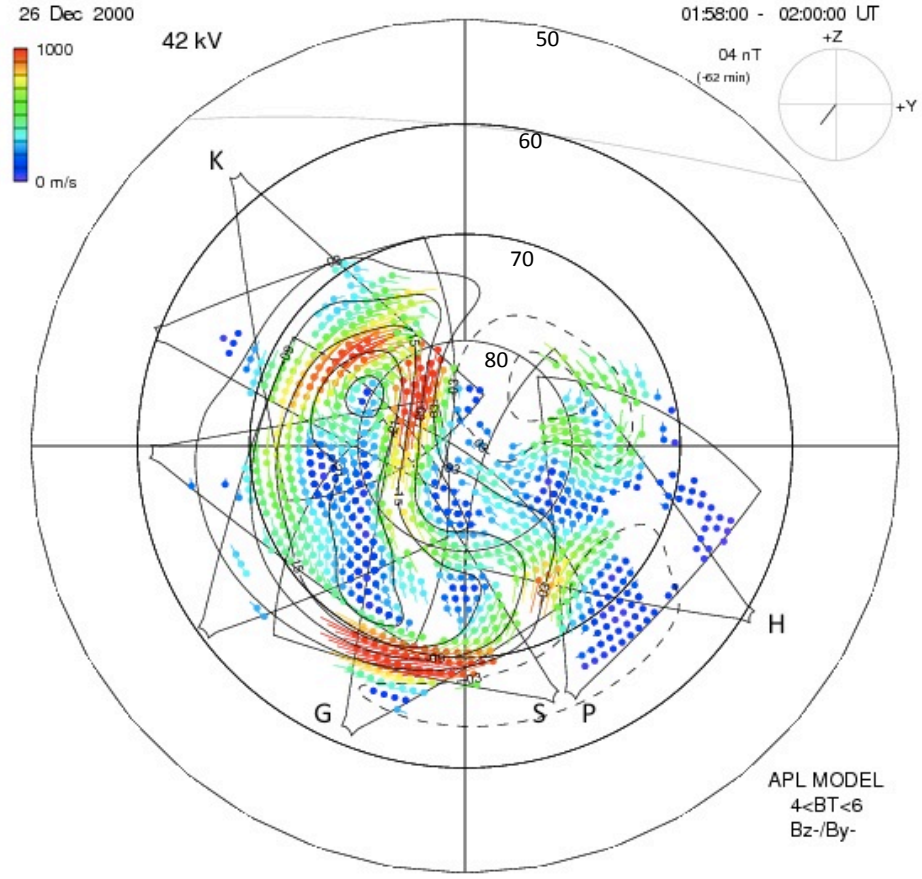

Figure 2.1: SuperDARN convection map showing convection flow velocity and convection cells in the dawn and dusk sectors in the time interval 01:58-02:00 UT on December 26, 2000. Here K, G, S, P and H respectively stand for Kodiak, Goose Bay, Stokkseyri, Pykkvibaer and Hanksalami.

2.B Instrumentation and Observations

The SuperDARN observation reported here focuses on the time interval 0000-0400 UT on December 26, 2000. We use data from the Pykkvibaer and Hankasalmi radar pair, which has a common field of view in the morning sector.

We also use the Kodiak radar in the afternoon sector, and the Goose Bay and Stokkseyri radars in the midnight sector. Figure 2.1 shows the SuperDARN convection map at 01:58-02:00 UT on this day, with the Pykkvibaer, Hankasalmi, Stokkseyri, Goose Bay, and Kodiak radars identified. The Hankasalmi and Kodiak radars observe good scatter in the higher latitude regions of their fields of view, while Pykkvibaer, Stokkseyri and Goose Bay observe good scatter in the lower latitude region of their fields of view. In this time interval, both the ACE and WIND spacecraft detect a solar wind speed close to 415 km/s on average, a dynamic pressure of 3.5 nPa and a Dst value close to 8 nT (ground based magnetometers are used for Dst estimation). The magnetosphere is relatively quiet, implying that any field line resonances occurring during this interval are most likely independent of a particle driven drift mirror instability.

For analysis, the ionospheric back-scatter data for a given beam and gate are selected and interpolated to fill small data gaps. This interpolated data is then detrended (a continuous, piecewise single linear trend over the chosen time interval is removed) to remove low frequency trends. An example of the detrended l-o-s Doppler velocities for selected beams and gates is shown in Figure 2.2. Included are Hankasalmi (beam 12, range gate 47), Kodiak (beam 6 and range gate 49), Pykkvibaer (beam 3 and range gate 17) and Pykkvibaer (beam 13 and range gate 16). Also shown here are the magnetic field GSE Bz component from the Geotail spacecraft, which is situated upstream of the bow shock just outside the dawnside magnetosheath at $[X_{GSE}, Y_{GSE}, Z_{GSE}] \approx [0.7, -29, 3.8]R_E$ at 01:10 UT, and the Hornsund (HOR) Z-component of the magnetic field from the IMAGE magnetometer network. Clear ULF wave oscillations are seen in the SuperDARN, Geotail

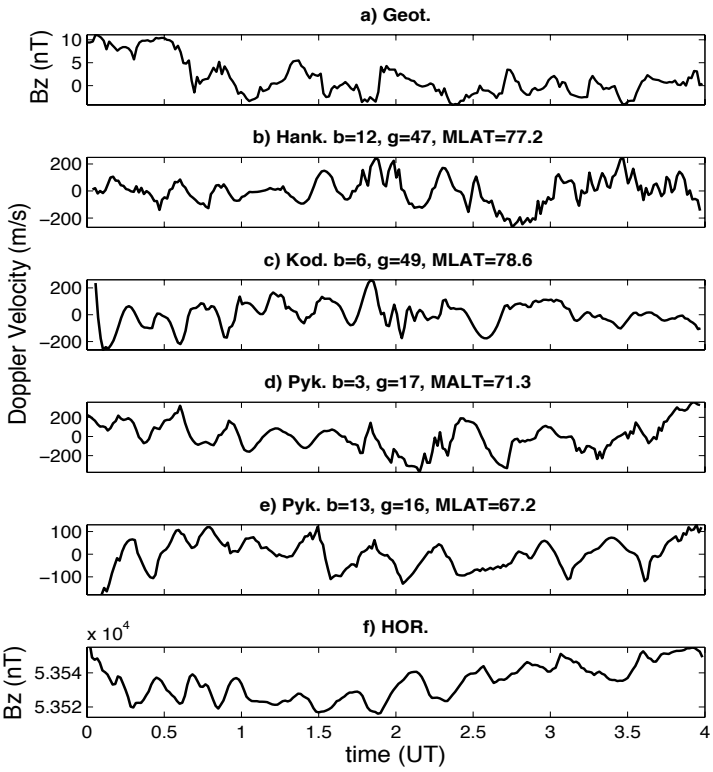

Figure 2.2: a) Geotail Bz, b) -e) de-trended radar Doppler l-o-s velocity and f) the Hornsund IMAGE magnetometer plots for the time interval 0000 - 0400 UT on December 26, 2000.

and the Hornsund data. Note that other high latitude stations from the IMAGE network, including BJN, HOP, LYR, and NAL, also observed similar ULF wave oscillations. To identify the spectral frequencies present, Figure 2.3 shows the Fast-Fourier-Transform (FFT) of the data in Figure 2.2 for the 00:10 -02:10 UT time interval. Figure 2.3 shows enhanced power around 0.8 mHz in both ionospheric radar, ground magnetometer, and Geotail solar wind data. Note that in Figures 2.2 and 2.3 we include only the Geotail Bz component because it has the largest oscillation at 0.8 mHz. However, signatures of the driver wave at 0.8 mHz are also present in Geotail Bx and By, and in

the solar wind magnetic field components measured by both ACE and WIND (data not shown). This suggests a well defined path of energy transfer from the solar wind into the inner magnetosphere, a point that will be discussed later in section 2.C.

In order to investigate the spatial variation in spectral power and phase at 0.8 mHz, FFTs of the 2 hour interval from 00:10-02:10 UT are calculated for all beams and gates for which good radar back-scatter is observed. Contour plots of the spectral power density and phase at 0.8 mHz are then plotted for a given radar as a function of Altitude Adjusted Corrected Geo-Magnetic (AACGM) coordinates (A brief description and application of AACGM can be found from *Baker and Wing* [1989] and *Hosokawa et al.* [2010]). Examples of these contour plots are presented and discussed in the following section, and will be used to identify FLR characteristics as well as other regions of wave phase coherence.

2.B.1 Field Line Resonance

For the event under investigation, the contour plot of the power spectral density and phase at 0.8 mHz, as seen by the Pykkvibaer HF radar, is shown in Figure 2.4 for the interval 00:10 -02:10 UT. In this figure, latitudinally localized enhancements in spectral power can be seen extended azimuthally along latitudinal contours close to the 67-68^o and 71-72^o AACGM latitudes. Note that these latitudinally localized enhancements in power have a nearly 2^o latitudinal extent, and are signatures of first and second order field line resonance harmonics at 0.8 mHz. Associated with the localized enhancements in power

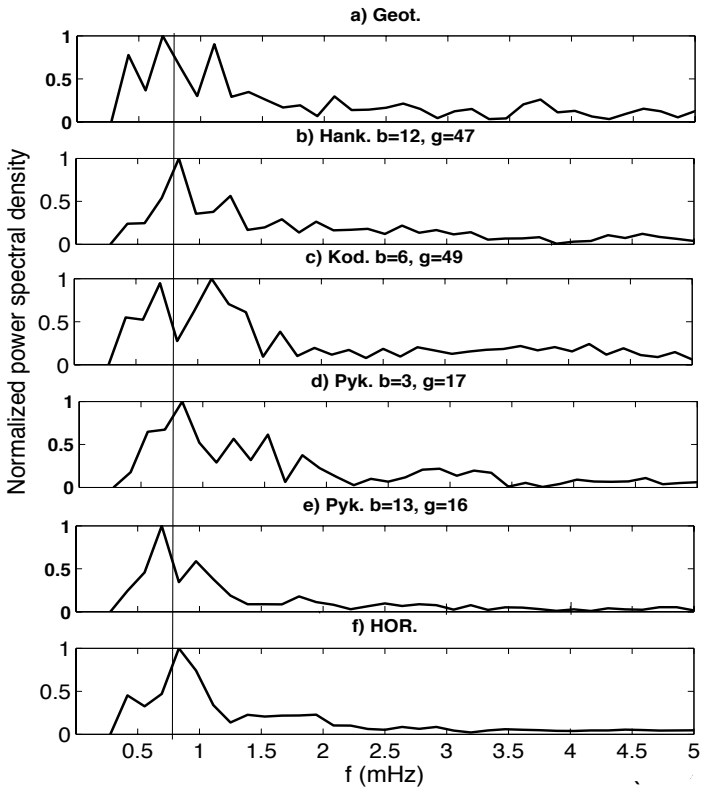

Figure 2.3: The FFT of a) Geotail Bz, b) -e) de-trended radar Doppler l-o-s velocity and f) the Hornsund IMAGE magnetometer plots for the time interval 00:10 -02:10 UT on December 26, 2000. The solid vertical line drawn at 0.8 mHz indicates a quasi-stable frequency around 0.8 mHz with in the range of the frequency of resolution, 0.14mHz.

are bands of constant phase seen in the phase contour plot around 67-68^o and 71-72^o.

To determine the overall spectral content in the Pykkvibaer data at this time, Figure 2.5 presents the contour plot of spectral power density as a function of frequency and latitude for the interval 00:10-02:10 UT. This plot is derived from range gate 17 data from all 16 beams of the Pykkvibaer radar, which corresponds to an approximate latitude profile. Spectral peaks at 0.8 mHz are clearly seen localized at $\sim$67-68^o and $\sim$71^o. To clearly identify the 0.8

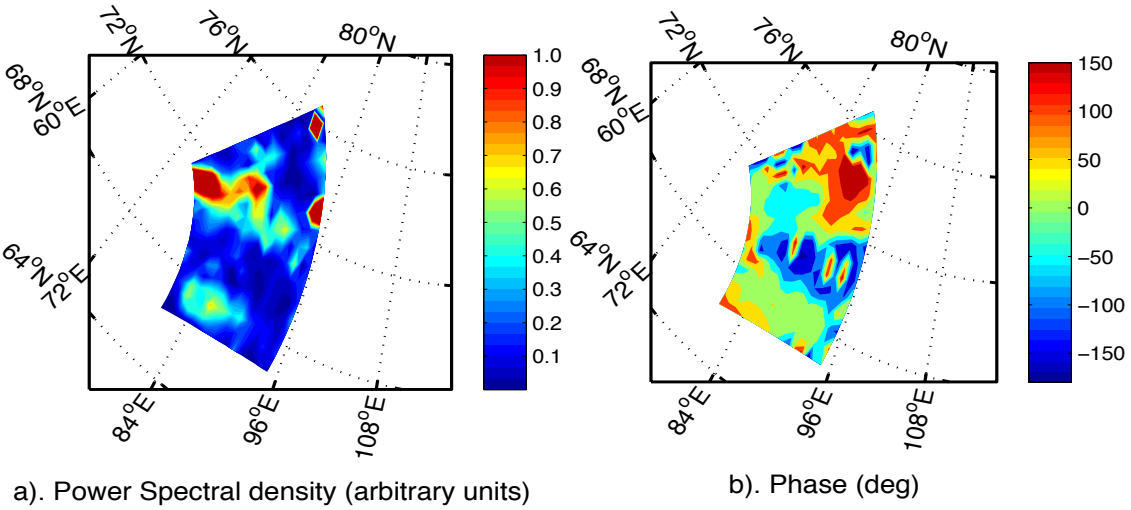

Figure 2.4: a) Contour plot of the spectral power and b) phase at 0.8 mHz from the Pykkvibaer HF radar in the time interval 0010-0210 UT on December 26, 2000. Note that beams 0-15 and range gates from 15-30 which have good radar echo were only used to make this 2-D contour plots. The latitudes and longitudes shown are AACGM coordinates.

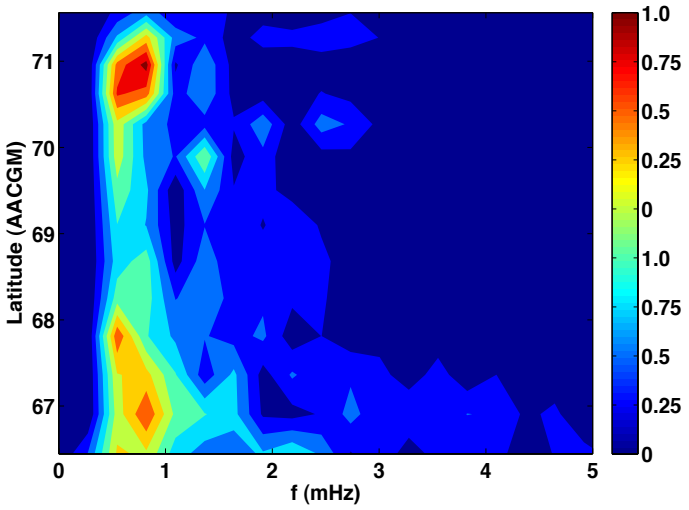

Figure 2.5: Contour plot of the power spectra as a function of frequency and latitude from the Pykkvibaer radar in the time interval 0010-0210 UT on December 26, 2000. All the 16 beams and range gate 17 are used here to give a profile along $\sim 84^o$ E longitude. Notable are the peaks representing the first and second order harmonics at 0.8 mHz.

mHz peak as a field line resonance, the latitude profile of amplitude and phase at 0.8 mHz is shown in Figure 2.6. Again, this plot is derived from range gate 17 data from all 16 beams of the Pykkvibaer radar. The peak in amplitude at 67 -68 degrees, and decrease in phase across this peak, are clear signatures of a 0.8 mHz FLR. The latitudinal phase decrease can be interpreted as a phase lag (lead) between the driver and the driven damped oscillation of the field lines that are slightly off-resonance [*Mager et al.*, 2009]. A decrease in phase with latitude is typical of low-m FLRs [*Fenrich et al.*, 1995].

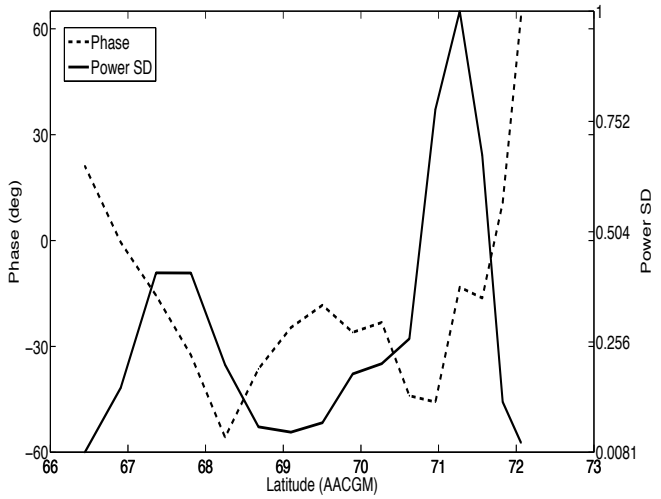

Figure 2.6: Plot of the spectral power and phase versus latitude for the 0.8 mHz resonance on December 26, 2000. The data plotted is along gate 17 and across all beams of Pykkvibaer for the interval 0010- 0210 UT. This profile helps to identify the 0.8 mHz peak as a field line resonance.

The second 0.8 mHz peak in amplitude at 71-72^o is interpreted as a second harmonic field line resonance. It is at a different latitude (different field line) than the first order FLR and it has to be noted that at 71-72^o the first order FLR should be around 0.4 mHz. For this peak, the phase variation is irregular with an initial decrease followed by an increase. We hypothesize that

this is because this structure is near the OCB boundary, and the dynamics of the boundary may have influenced the phase variation. Both the UVI image shown in Figure 2.7, and the SuperDARN spectral width plot in Figure 2.8, suggest the open closed boundary in the region of the Pykkvibaer field of view is near 71-72^o latitude, which is collocated with the higher latitude 0.8 mHz peak. Given that the OCB in Pykkvibaer's field of view is close to 71-72^o, one could also interpret the power enhancement around 71-72^o as the signature of the solar wind driver wave at the boundary which drives the FLR observed by Pykkvibaer near ∼67-68^o. Details on the use of UVI and SuperDARN widths for identifying the open-closed boundary are presented in the next section. The m-values of these FLRs are estimated to be 5 or 6 for the lower latitude first order FLR and 12 for the higher latitude second order FLR, both with westward or anti-sunward phase propagation, respectively. Note that anti-sunward phase propagation is consistent with a solar wind source.

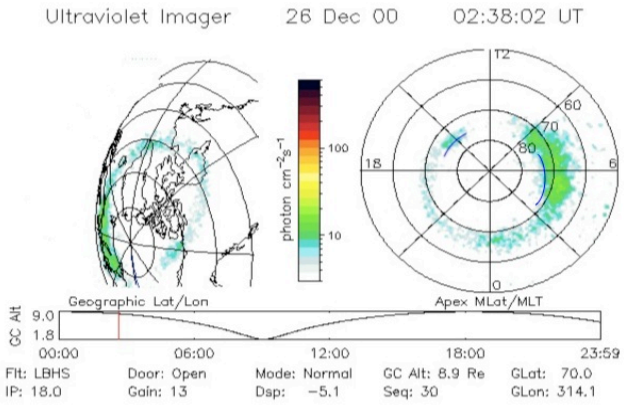

Figure 2.7: A plot of the Polar UVI image which can be used to estimate the OCB. It is given as a function of both geographic and geomagnetic latitudes at 02:38 UT on December 26, 2000. Here the blue lines in the geomagnetic plot depict the open closed boundary in the region of Kodiak's field of view in the afternoon sector and (Pykkvibaer's and Hankasalmi's) in the morning sector.

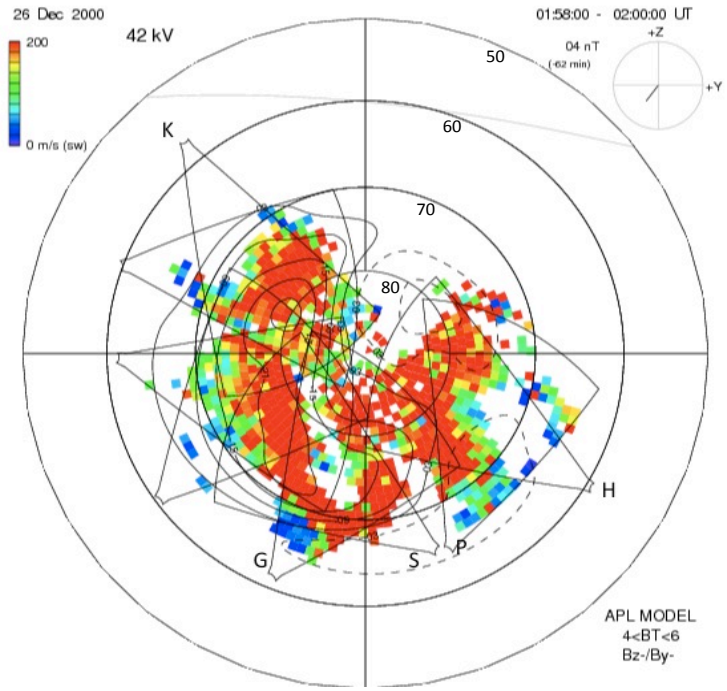

Figure 2.8: SuperDARNs spectral width estimate in AACGM coordinates in the time interval 01:58 - 02:00 UT on December 26, 2000. Transitions to widths $>$ 200 m/s may be used to indicate the OCB. Here K, G, S, P and H respectively stand for Kodiak, Goose Bay, Stokkseyri, Pykkvibaer and Hankasalmi.

The global nature of wave activity at 0.8 mHz is also observable simultaneously in the night sector by the overlapping Stokkseyri and Goose Bay HF radars. In the time period 00:10- 02:10 UT, high power and bands of constant phase structures that appear to be FLRs, are visible from Stokkseyri at 0.8 mHz. The power is localized in latitude from 71-72^o with an m-value that is estimated to around 6 (consistent with Pykkvibaer's lower latitude FLR observation), and with westward phase velocity. Although Goose Bay sees coherent phase at 0.8 mHz in the westward portion of it's field of view, the amplitude structure is less clear due to l-o-s effects. Data from the Kerguelen radar, which is in the Southern hemisphere and conjugate to Hankasalmi, has also

been examined. Although there is a sporadic presence of the 0.8 mHz wave at higher latitudes, the data is not as clear as in the Northern hemisphere radars. The 0.8 mHz wave is not observed on the other radars in the SuperDARN network due to an insufficient amount of ionospheric echoes to work with either because there was no backscatter at all or there was significant ground scatter contamination.

2.B.2 Observation of the driver wave on open field lines

Figures 2.9 and 2.10 show contour plots of power spectral density and phase at 0.8 mHz for Kodiak and Hankasalmi, respectively, for the time interval 00:10-02:10 UT. Although the amplitude structure is irregular, it shows bands of constant phase in the high latitude regions above 75^o latitude for both radars. In order to get insight into where the coherent phase regions are located relative to the open closed boundary, we use auroral emissions from the Polar Ultraviolet Imager to make an estimate of where the OCB is located [*Milan et al.*, 2003]. The poleward edge of the green-line auroral emissions from the Ultraviolet Imager is often used as the OCB proxy [e.g., *Boakes et al.*, 2008; *Milan et al.*, 2003]. The idea behind this estimate is that closed field lines are characterized by 557 nm green-line auroral emissions, relating to particle precipitation from the central plasma sheet. The UVI image at 02:38 UT is illustrated in Figure 2.7 in both geographic and geomagnetic coordinates. The OCB is estimated by eye from UVI in the regions of the 0.8 mHz wave on Kodiak and Hankasalmi to be close to 75^o and 73^o, respectively. SuperDARN's spectral width is also known to provide a good proxy for the OCB, [e.g., *Baker et al.*, 1995; *Milan et al.*, 2003; *Chisham and Freeman*, 2004]. In general, a

transition from low to high spectral widths can be used as an indicator of the OCB. The SuperDARN spectral widths at 01:58-02:00 UT are shown in Figure 2.8. The spectral width estimate of the OCB in the region of the 0.8 mHz wave on Kodiak and Hankasalmi places it close to 74 and 75 degrees, respectively.

One should note the differences in OCB estimates in different field of views (MLTs). The OCB via spectral widths in the region of the 0.8 mHz high-latitude FLR observed by Pykkvibaer agrees well with the UVI determined OCB near 71-72 degrees as discussed in Section 2.B.1. In the morning sector, east of Pykkvibaer (in Hankasalmi's field of view), the OCB estimate from both UVI and SuperDARN is in the range of 73^o to 75^o. Regarding Kodiak's field of view, both UVI and SuperDARN estimates show that the OCB falls with in the range of 74^o to 75^o.

A point that warrants comment is the discrepancy between the night side OCB (which is close to 65^o) with that of the UVI OCB proxy at around (70^o). There were reports of this discrepancy between ground and spacecraft data in *Woodfield et al.* [2002] and *Blanchard et al.* [1997]. A more precise determination of the OCB boundary is, however, provided by spacecraft data [e.g., *Blanchard et al.*, 1997; *Brittnacher et al.*, 1999; *Kauristie et al.*, 1999; *Boakes et al.*, 2008]. Based on the above estimates of the OCB, it appears that the coherent phase observations of 0.8 mHz at high latitudes observed on both Kodiak and Hankasalmi simultaneously, are outside the OCB on open field lines. This confirms the existence of ULF waves outside the magnetosphere and is consistent with a source in the solar wind at 0.8 mHz.

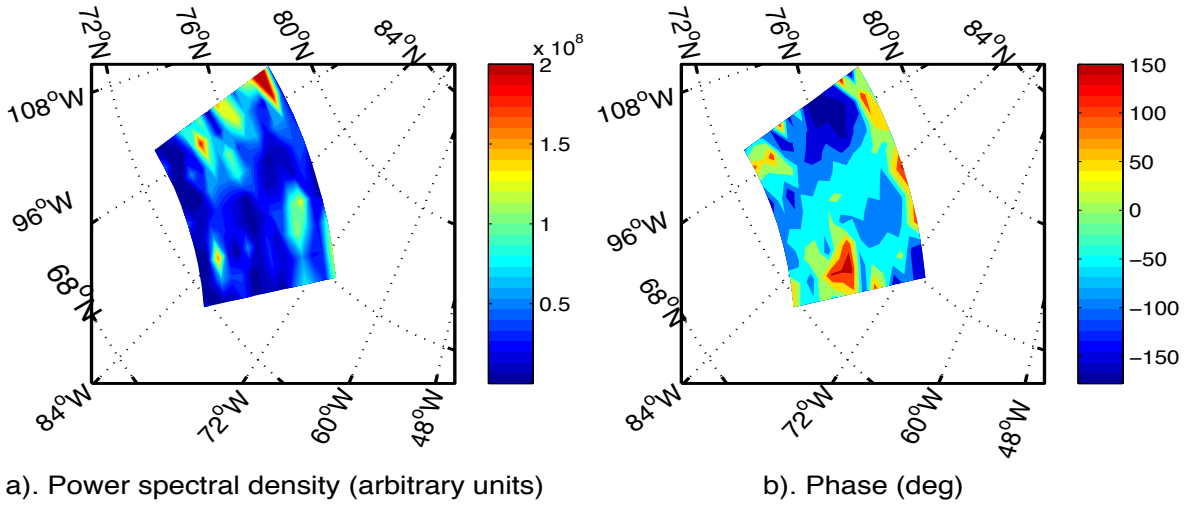

Figure 2.9: Contour plot of the coherent wave spectral a) power and b) phase at 0.8 mHz from the Kodiak HF radar in the time interval 0010 - 0210 UT on December 26, 2000. Note that beams 0 - 10 and range gates from 35-50 which have good radar back scatter were only used to make this 2-D contour plots. The latitudes and longitudes shown are AACGM coordinates.

2.B.3 Sources in the Solar Wind

Previous studies have shown that the wave packet structure from ground based measurements of FLRs is consistent with the wave packet structure of solar wind pressure oscillations [*Stephenson and Walker*, 2002]. A decade ago, *Walker* [2002] suggested that FLRs can be driven by MHD waves in the solar wind. The idea behind this hypothesis is that the compressional waves that are generated in the solar wind propagate through the bow shock and the magnetopause. *Kepko et al.* [2002] have presented observations relating ULF oscillations in the solar wind to ULF pulsations at geosynchronous orbit,

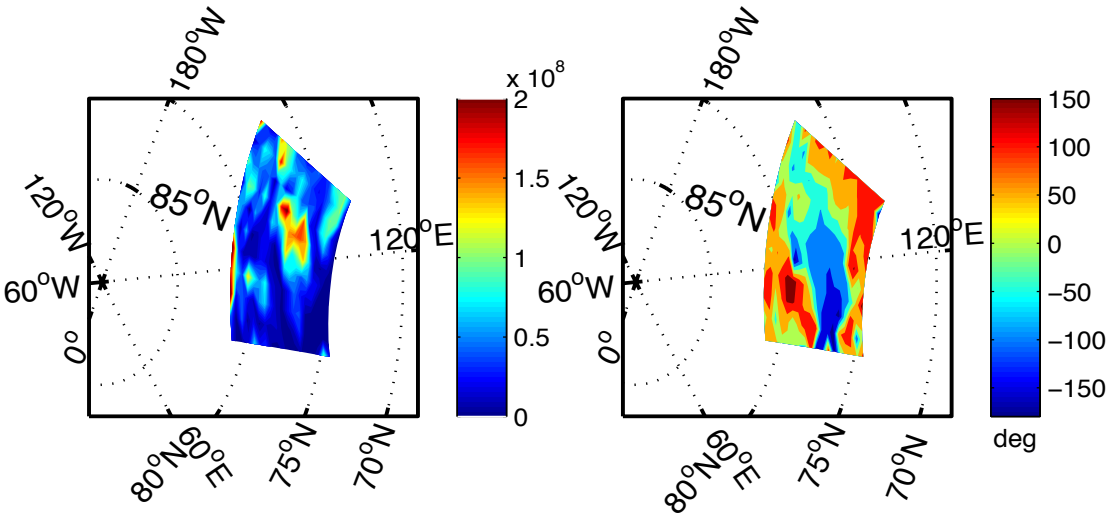

a). Power spectral density (arbitrary units) b). Phase (deg)

Figure 2.10: Contour plot of the spectral a) power and b) phase of the ULF wave at 0.8 mHz from the Hanksalami HF radar in the time interval 0010 -0210 UT on December 26, 2000. Note that beams 5-15 and range gates from 38-55 which have good radar echo were used to make this 2-D contour plots. The latitudes and longitudes shown are AACGM coordinates.

lending further support to a direct solar wind source of ULF waves.

Figure 2.11 shows an overlay between the Doppler l-o-s velocity of the Pykkvibaer radar and Geotail Bz. A time delay of ∼15 min for the Geotail data is employed here to take into account the propagation time from the dawn side flank solar wind through the magnetosheath and magnetosphere to the ionosphere. The corresponding cross power spectral density and coherence between the Pykkvibaer radar and Geotail data are shown in Figure 2.12. To facilitate the cross power and coherence analysis, the 60 second sampled radar data for beam 13 and range gate 16 of Pykkvibaer was linearly interpolated to the same 64 second time points as the Geotail data. As can be seen from Figures 2.11 and 2.12, the radar data and spacecraft data at 0.8 mHz are

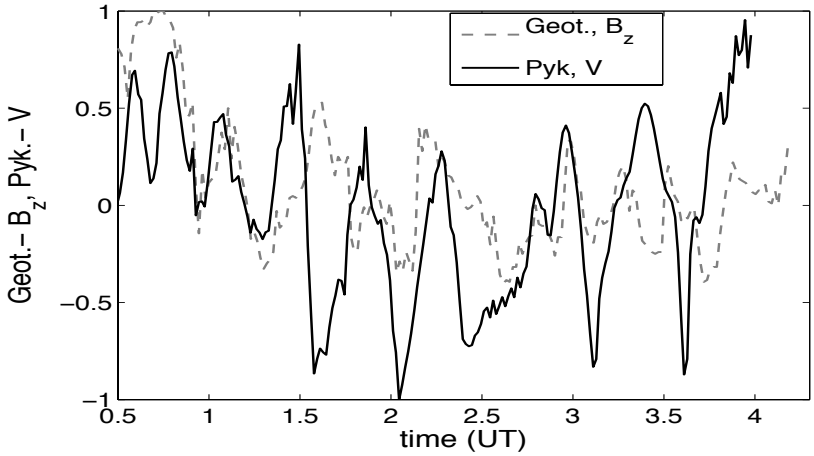

Figure 2.11: An overlay between Pykkvibaer HF radar Doppler l-o-s velocity plot of beam 13 and range gate 16 and Geotail Bz for the time interval 0030 - 0400 UT on December 26, 2000. The 0.8 mHz frequency ULF wave can be seen in both data sets.

correlated and coherent. The coherence between SuperDARN and Geotail data at 0.8 mHz is found to be close to 0.7, which is high and significant. The IMAGE magnetometer data are also found to show a similar cross-power spectral density and a coherence value close to 0.6 with the Geotail data at 0.8 mHz. This strongly suggests that the FLRs on closed geomagnetic field lines are directly driven by MHD waves in the solar wind. Radar data from Kodiak and Hankasalmi in the regions of the 0.8 mHz coherent phase show similar cross-power spectral density, and coherence with the Geotail data at 0.8 mHz, which is evidence of a well defined path of energy transfer from sources in the solar wind to the outer magnetosphere/magnetosheath region into the inner magnetosphere and ionosphere.

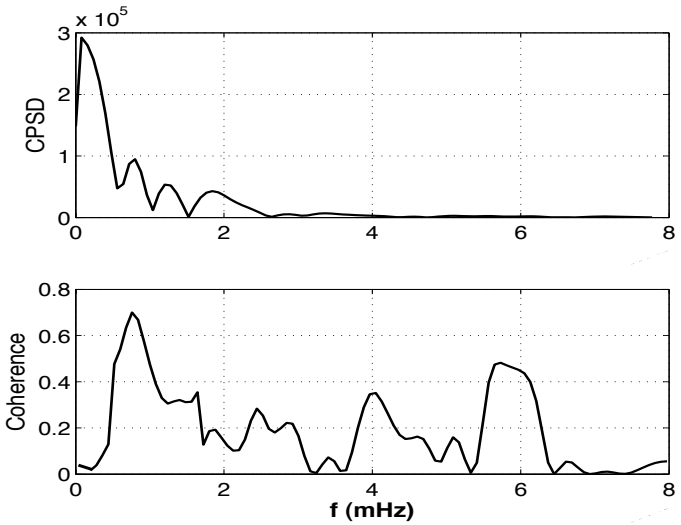

Figure 2.12: Plots of the cross power spectral density and and coherence of Pykkvibaer (beam 13 and range gate 16) HF radar and Geotail spacecraft Bz in the time interval 0100 - 0340 UT on December 26, 2000.

2.C Discussion

In this chapter, we have presented observations of first and second order FLR harmonics, which show evidence of a solar wind driver that excites global Pc5 oscillations propagating through the magnetosheath. Of particular interest in Figures 2.4, 2.5 and 2.6 is the somewhat unusual situation where the 0.8 mHz FLR extends all the way down to 67 -68^o AACGM latitudes, which maps out close to the geosynchronous region. In section 2.B.1, this FLR is referred to as the low latitude FLR to distinguish it from the second order harmonic, also referred to as the high latitude FLR. The typical latitude for localization of the first order 0.8 mHz FLR is reported to be around 70^o in *Walker et al.* [1992] and 72.5^o in *Fenrich et al.* [1995]. The observation of the first order 0.8 mHz oscillation at lower than typical latitudes can be explained in terms of mass loading as follows. The plasmasheet density observed by the Polar

spacecraft approximately 10 hours prior to the interval of interest was significantly enhanced at $\sim$ 7-10 cm^{-3} which implies a lower frequency oscillation on associated field lines. *Joseph et al.* [1997] have reported that two to three times per month the plasmasheet density is several times higher than its average value (0.5-1.2 cm^{-3}) at geosynchronous orbit, and lasts about 12-18 hours. Thus, higher than normal plasma sheet density is the most probable reason to account for this anomalous observation.

The observed phase coherence of the driver wave in the dusk (Kodiak) and dawn (Hankasalmi) sectors is illustrated in panel (b) of Figures 9 and 10, respectively. The variation of phase vs longitude in these plots can be used to determine the azimuthal phase velocity of the 0.8 mHz driver wave. Following *Oslon and Rostoker* [1978] the wave phase velocity is given by $V_\phi = 2\pi f R_e cos\lambda/m$, where f is the ULF wave frequency, λ is the latitude, R_e is Earth's radius and m is the azimuthal wave number, which is determined by the ratio of the change in phase to the change in longitude. The direction of the azimuthal phase velocity is observed to be from high to low phase. Using this relation, the phase velocity of the 0.8 mHz driver wave is 670 m/s and 1400 m/s on Kodiak and Hankasalmi, respectively. Both are directed westward, which is sunward for Kodiak and anti-sunward for Hankasalmi. Anti-sunward phase velocity is consistent with an external wave source in the solar wind. However, the sunward phase velocity observed by Kodiak does not exclude an external solar wind source. The sunward phase velocity might be explained by considering the background convection flow velocities. Referring to Kodiak's field of view in Figure 2.1, the background convection flow in the region of the observed 0.8 mHz wave is on the order of 1000 m/s in the sunward direction,

which is greater than the 670 m/s phase velocity. Thus it can have a significant effect on the observed phase velocity due to the fact that MHD waves are carried by the bulk plasma flow. Note that sunward convection flow on open field lines is known to occur during intervals of lobe convection [*Eriksson et al.*, 2005] and [*Marcucci et al.*, 2006]. For comparison, Hankasalmi's convection flow in the region of the 0.8 mHz wave is predominantly in the north-south direction, with a sunward component no greater than ∼700 m/s during the interval of interest, and thus not large enough to impact the anti-sunward direction of the wave phase velocity.

2.D Summary

The Geotail and SuperDARN radar observations presented in this chapter are evidence of a coherent 0.8 mHz MHD wave from the solar wind that propagates through the magnetosheath and outer magnetosphere into the inner magnetosphere, where it couples to FLRs. The Hankasalmi and Kodiak radar observations of coherent phase on open field lines corresponds to the ionospheric signature of the driver wave as it propagates in the magnetosheath and outer magnetosphere. MHD waves in the outer magnetosphere, which couple to FLRs, are seldom observed, and as far as we know this is the first report of a ground based observation of the driver wave using superDARN. It's occurrence in both the dawn and dusk sectors classify this as a global ULF wave event.

The observation of coherent phase on open field lines indicates that SuperDARN can provide a diagnostic on the transmission of solar wind MHD

waves across the magnetopause and through the outer regions of the magnetosphere. Diagnostics of transmission can be accomplished by continuously monitoring amplitude and phase structures of the wave across the boundary. Such transmission has not been measured with ground based instrumentation before, and provides new insight into MHD waves in the outer magnetosphere that are responsible for driving FLRs.

Chapter 3

A Magnetopause Surface Mode Excited During a High Solar Wind Speed and an Interval of Strong Northward IMF

Coordinated ground and space-based observations of ULF waves in the magnetosphere in the range of mHz frequencies are primarily used to enhance our understanding of MHD wave propagation and coupling in the Earth's magnetosphere. This chapter focuses on characterization of a KHI generated magnetopause boundary instability and it's association with ULF waves in the magnetosphere, with the ultimate goal of demonstrating how the global nature of MHD waves links them together. ULF wave event observational case study from coordinated measurements of HF radars, multi-satellite-borne instrumentation and ground-based magnetometers will be analyzed.

3.A Introduction

In-situ observations of the flanks of the magnetopause boundary (magnetopause and boundary layer) sometimes show periodic surface waves to be present [*Kivelson and Pu*, 1984]. A recent work by *Rae et al.* [2005] has shown that the observed surface perturbations are due to the boundary motion of the magnetosphere. These boundary motions produce surface waves that are convected tailward with the obvious anti-sunward magnetosheath plasma flow. *Rae et al.* [2005] present the evolution of an extremely long-lasting narrow band Pc5 pulsation of 1.5 mHz during a high solar wind speed interval using CANOPUS, CLUSTER, POLAR, GOES and HF radar data. The pulsations are observed in both electric and magnetic field data while CLUSTER is in the vicinity of flank magnetopause. In their study the POLAR spacecraft outside geosynchronous orbit observed significant electric and magnetic perturbations around a frequency of 1.5 mHz. Considering the strong field-aligned oscillations in the Poynting vector, the authors argued that this is the characteristic feature of standing Alfvén waves. The nonzero azimuthal component of the Poynting vector is interpreted to indicate a downtail energy propagation. In characterizing the source mechanism for this global Pc5 pulsation event, they used the following argument: Changes in the observed dynamic pressure of the solar wind is long known to cause boundary motion that would trigger periodic surface waves on the magnetopause boundary. However, in the absence of changes in the solar wind dynamic pressure, the observed discrete frequency pulsations in the magnetosphere could be excited via the the Kelvin-Helmholtz instability or via over-reflection at the flank magnetopause [*Mann et al.*, 2002].

We consider a magnetospheric ULF wave event 3 hours after the 25 November 2001 event of *Rae et al.* [2005]. We present a magnetospheric ULF event directly driven by a magnetopause surface mode under conditions of very high solar wind speed and strong northward IMF interval. We demonstrate conclusive proof that the FLRs and the global wave activity observed in our event are indeed driven by a KHI. Analysis shows that the radial Poynting flux structures, the propagation time delay, and the observed growth time of the surface wave are all consistent with KHI theory. Furthermore, the condition for the most unstable KH mode is met and the estimated magnetopause boundary thickness is within the range of those in the literature. This type of detailed analysis was not performed by *Rae et al.* [2005] in their event analysis and thus is presented here as a new result.

The event considered in this study uses measurements from two SuperDARN HF radars in both the dawn and dusk time sectors to show FLR structures on closed field lines at a frequency of 1.7 mHz that matches the enhanced wave activity at the flank magnetopause observed by CLUSTER. Furthermore, measurements from the combination of multi-spacecraft instrumentation (POLAR and GOES-8) and the IMAGE chain of magnetometers (Fennoscandia, Svalbard) and CANOPUS(DAWS) ensures an almost global coverage of observations in both time sectors and hemispheres. The observations provide evidence for strong coupling between a surface wave mode, fast compressional wave in the outer magnetosphere, and a shear Alfvén FLR.

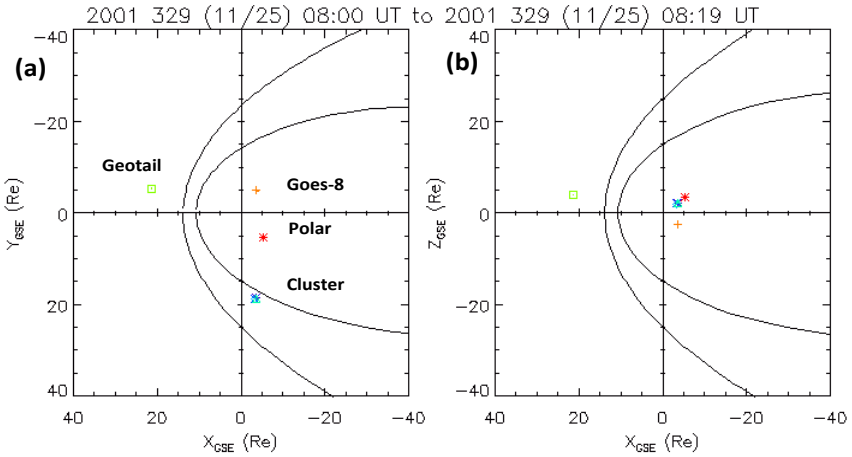

Figure 3.1: The position of some of the spacecrafts used in this study in geocentric solar ecliptic (GSE) (a) X-Y plane and (b) the X-Z plane between 0800UT to 0819UT for 25 November 2001. Also shown here are the paraboloic solid black lines representing the magnetopause and the bowshock for the relevant IMF and solar wind conditions. The satellite graphic locator in http://sscweb.gsfc.nasa.gov/cgi-bin/Locator˙graphics.cgi is used to generate this plot.

3.B Instrumentation and Observations

Satellite-borne and ground based instrumentation are rarely in the appropriate position at the right time under the right conditions and most importantly in an operational state. Luckily, we have no such constraint in this study as CLUSTER is very close to the dusk flank magnetopause, as shown in Figure 3.1. The data to be presented provide an observational link between wave activity at the magnetopause boundary (CLUSTER), in the magnetosphere (POLAR and GOES-8), in the ionosphere (SuperDARN) and in the IMAGE magnetometer network and CANOPUS(DAWS).

Cluster is a set of four identical spacecraft that fly in a tetrahedral con-

figuration [*Kronberg et al.*, 2011]. Eleven scientific instruments are deployed on each Cluster spacecraft. These instruments are designed to measure space weather inside and outside the magnetosphere. In this study, measurements from Fluxgate Magnetometer (FGM), Electron Drift Instrument (EDI), Cluster Ion Spectrometry experiment (CIS) and Plasma Electron And Current Experiment (PEACE) instruments will be used [*Kronberg et al.*, 2011]. On November 25, 2001 from 0600 - 1000 UT the CLUSTER spacecraft skimmed through the dusk flank magnetopause in its outbound pass throughout the interval. It was the motion of the magnetopause outward and then inward that caused the spacecraft to pass into the magnetosphere. Figure 3.1 shows the positions of some of the spacecraft used in this study in the GSE X-Y plane (Figure 3.1a) and X-Z plane (Figure 3.1b) from 0800UT to 0819UT.

3.C Observations

3.C.1 Upstream IMF conditions

Magnetic field, flow pressure (follows plasma density almost exactly) and solar wind flow data from the ACE spacecraft are shown in Figure 3.2. Upstream ACE magnetic field, ion plasma density, and solar wind velocity data in GSE coordinate for 25 November 2001 in the time interval from 0630 - 1000 UT were analyzed. A time delay of nearly 38 minutes is calculated between the ACE and CLUSTER spacecrafts. The wave that we focus on in the next section (1.7 mHz) can not be seen in the upstream plasma and magnetic field data. Geotail and Wind (Figures not shown), which were also in the upstream solar wind region, were not able to trace any signature of a wave of 1.7 mHz

frequency. The absence of this wave in the magnetic field, solar wind dynamic pressure variation and plasma velocity data in the solar wind is suggestive of the lack of a monochromatic source mechanism in the upstream solar wind region [*Rae et al.*, 2005]. From the upstream data, it can be seen that the IMF is dominantly northward as Bx varies from 5 to -5 nT and By from 2 to -8 nT and the plasma speed on average exceeds 640 km/s in this time interval. The considerable velocity shear at the magnetopause makes a KHI mechanism a possible candidate for driving ULF waves on the boundary of the magnetosphere. Throughout this event, we will comment on a KHI mechanism in driving ULF pulsations deep inside the terrestrial magnetosphere and at auroral altitudes when appropriate.

3.C.2 Dusk-Sector Magnetopause Measurements

The CLUSTER Spacecraft FluxGate Magnetometer provides three dimensional magnetic field measurements. Figure 3.3 is a plot of CLUSTER C1 FGM raw magnetic field and C1 PP CIS proton bulk velocity data in GSE coordinates for 25 November 2001 in the time interval from 0630-1000 UT. This interval corresponds to an outward and sunward motion of the CLUSTER spacecraft during which time the four spacecraft were totally outside the magnetopause from 0630-0830 UT. During the interval 0840-0910 UT the magnetosphere expands due to a decrease in the solar wind dynamic pressure from 3 nPa to 0.6 nPa as can be inferred from the ACE data of 0752-0822 UT. This caused the magnetopause to move outwards past the CLUSTER spacecraft leaving them inside the magnetopause. The interval from 0910-1000 UT is a period where the magnetopause has moved inward and the spacecraft are

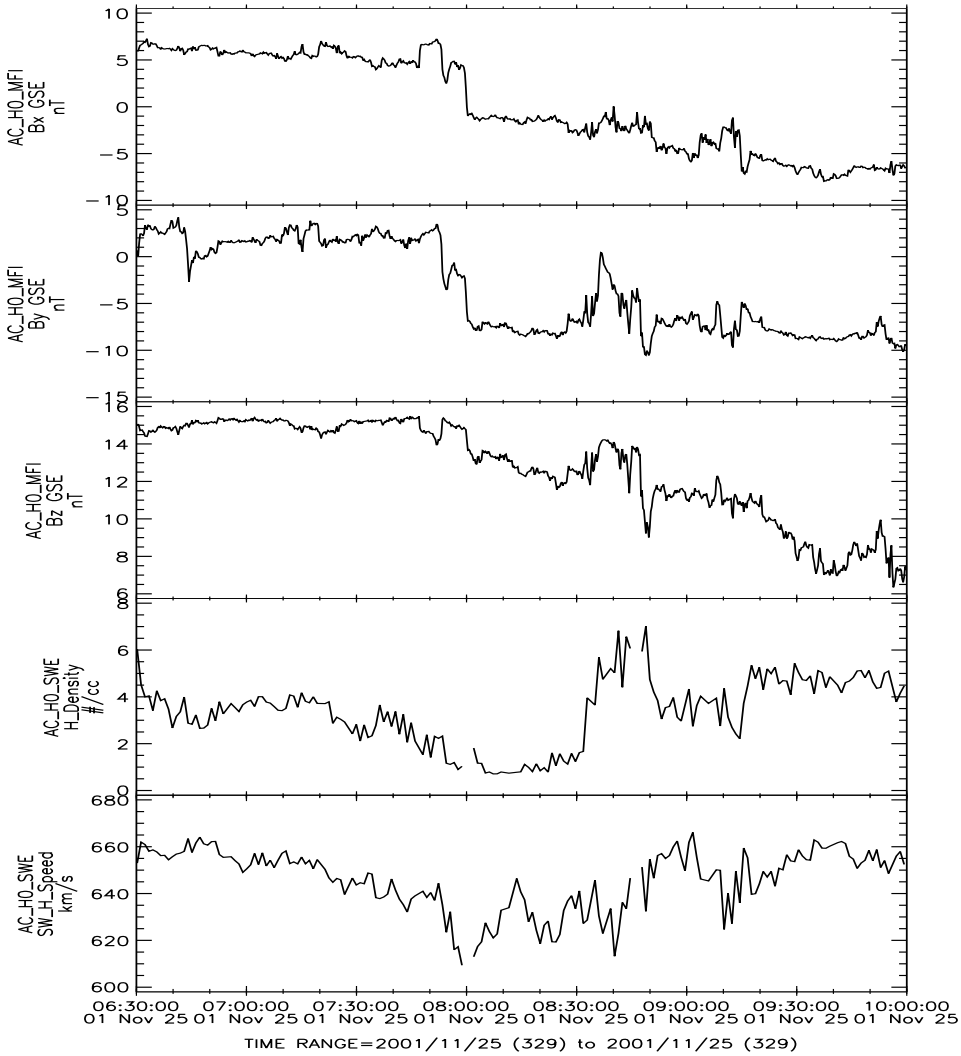

Figure 3.2: ACE raw magnetic field and solar wind proton number density data along with solar wind flow speed data in GSE for 25 November 2001 in the time interval from 0630-1000UT. It takes approximately 38 minutes of propagation time for this fluctuation to be felt at the magnetopause.

again outside the magnetopause, but inside the magnetosheath.

An FFT analysis of the magnetic field data in Field-Aligned-Coordinate system (FAC) in the time interval from 0630-0830 UT when the CLUSTER spacecraft are outside the magnetosphere is shown in Figure 3.4. A FAC coordinate system was set up on the basis of a moving average filter implemented

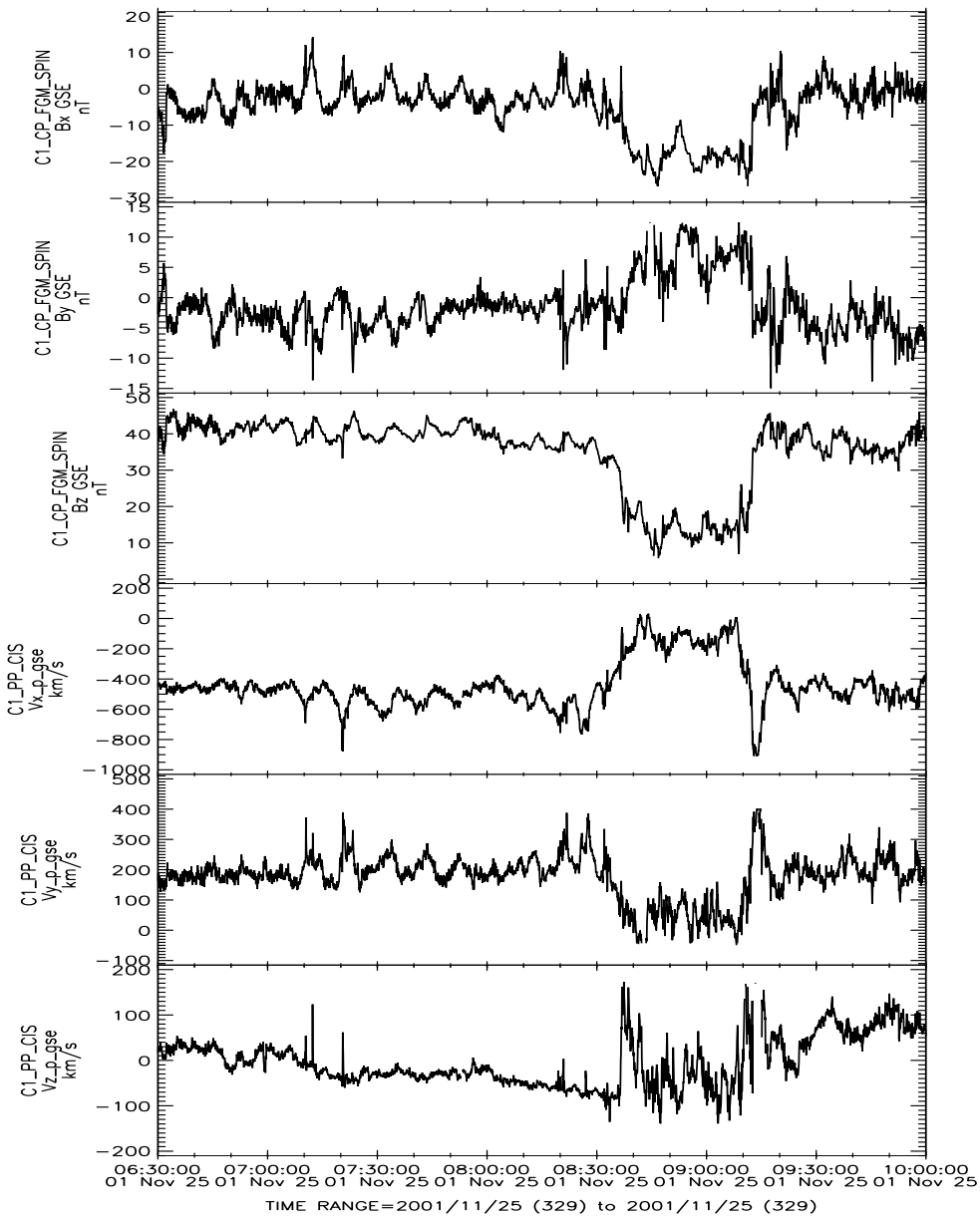

Figure 3.3: Cluster C1 FGM raw magnetic field and C1 PP CIS proton bulk velocity data plots in GSE for 25 November 2001 in the time interval from 0630-1000 UT.

in the magnetic field direction of 20 minute window. Employing a moving average filter helps to eliminate variations in the signal due to long period trends

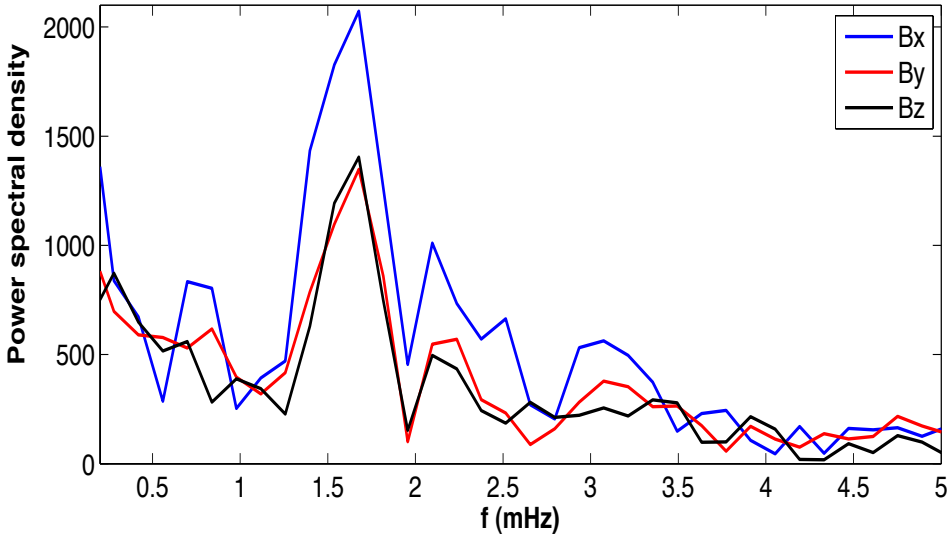

Figure 3.4: An FFT analysis of Cluster C1 FGM magnetic field perturbation plot in FAC for 25 November 2001 in the time interval from 0630-0830 UT.

and short period waves. In this system of coordinates, the direction of Z_{FAC} is defined to be the direction of the ambient magnetic field. The Y_{FAC} direction of the FAC is obtained by the vector product of the spacecrafts position vector (directed Earthward from the spacecraft) and Z_{FAC}. The X_{FAC} direction completes the orthogonal right-hand system and is directed away from Earth. Figures 3.3 and 3.4 clearly illustrate the presence of a quasi-stable, discrete and periodic ULF wave of 1.7 mHz both in time and frequency domain in all the three components of the magnetic field. Notable from Figure 3.4 is the dominance of the magnetic field wave in Bx. This interesting feature is also observed in magnetic field data of the remaining three CLUSTER spacecrafts C2, C3 and C4. Furthermore, this discrete 1.7 mHz wave is also observed in the plasma density (Figure 3.5), velocity (Figures 3.3), and electric field measurements (Figure 3.6) on each of the four Cluster spacecraft. The extremely

clear presence of this wave in the magnetic field, plasma density, plasma flow and electric field data, with the lack of such a wave in the upstream solar wind data, is suggestive of a coherent source mechanism at the location of the dusk flank magnetopause.

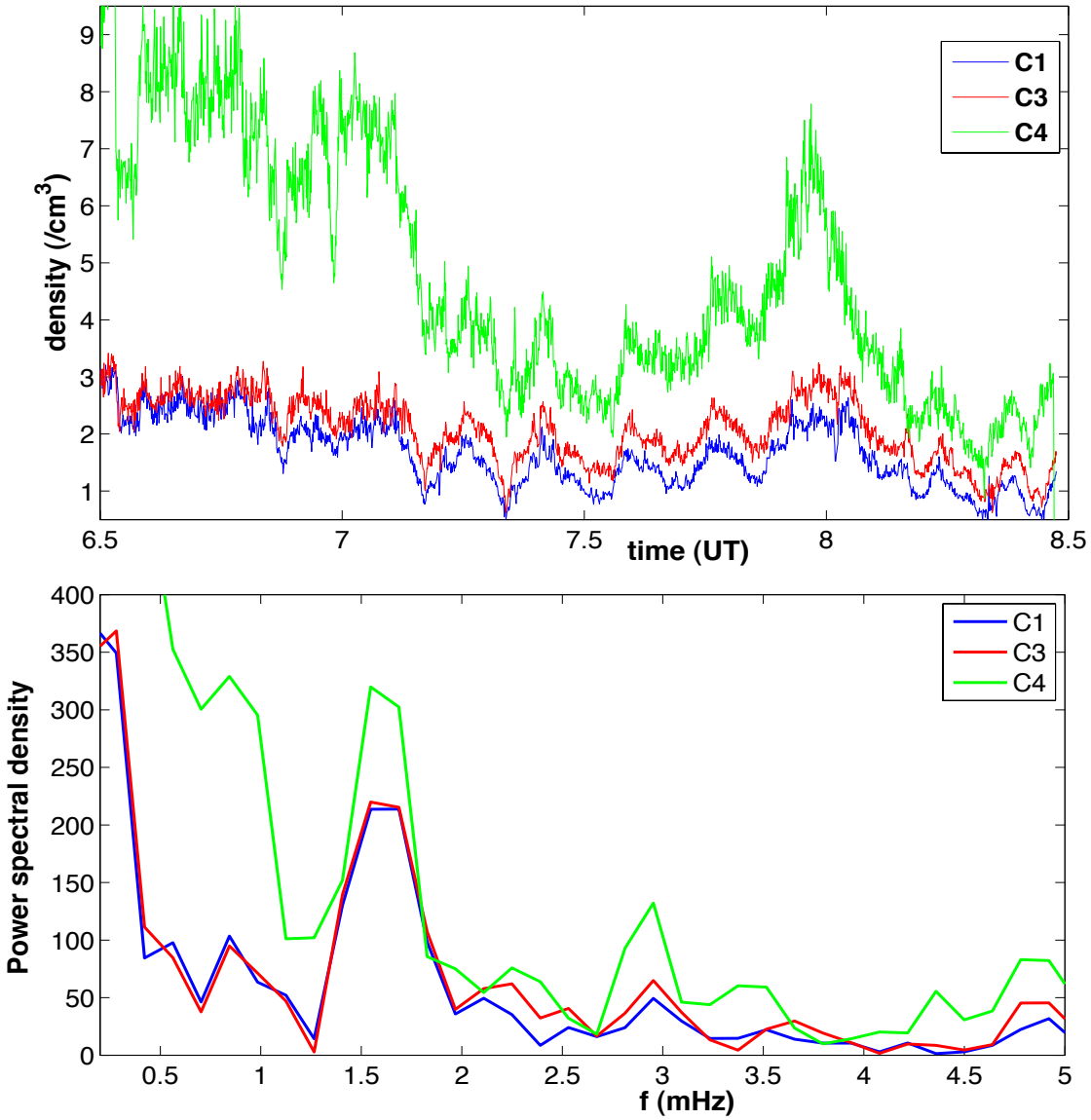

Figure 3.5: CLUSTER PP CIS Proton Density from each of the different CLUSTER (top panel) and their corresponding FFT (bottom panel) from each of the four CLUSTER spacecraft for 25 November 2001 in the time interval from 0630-0830 UT.

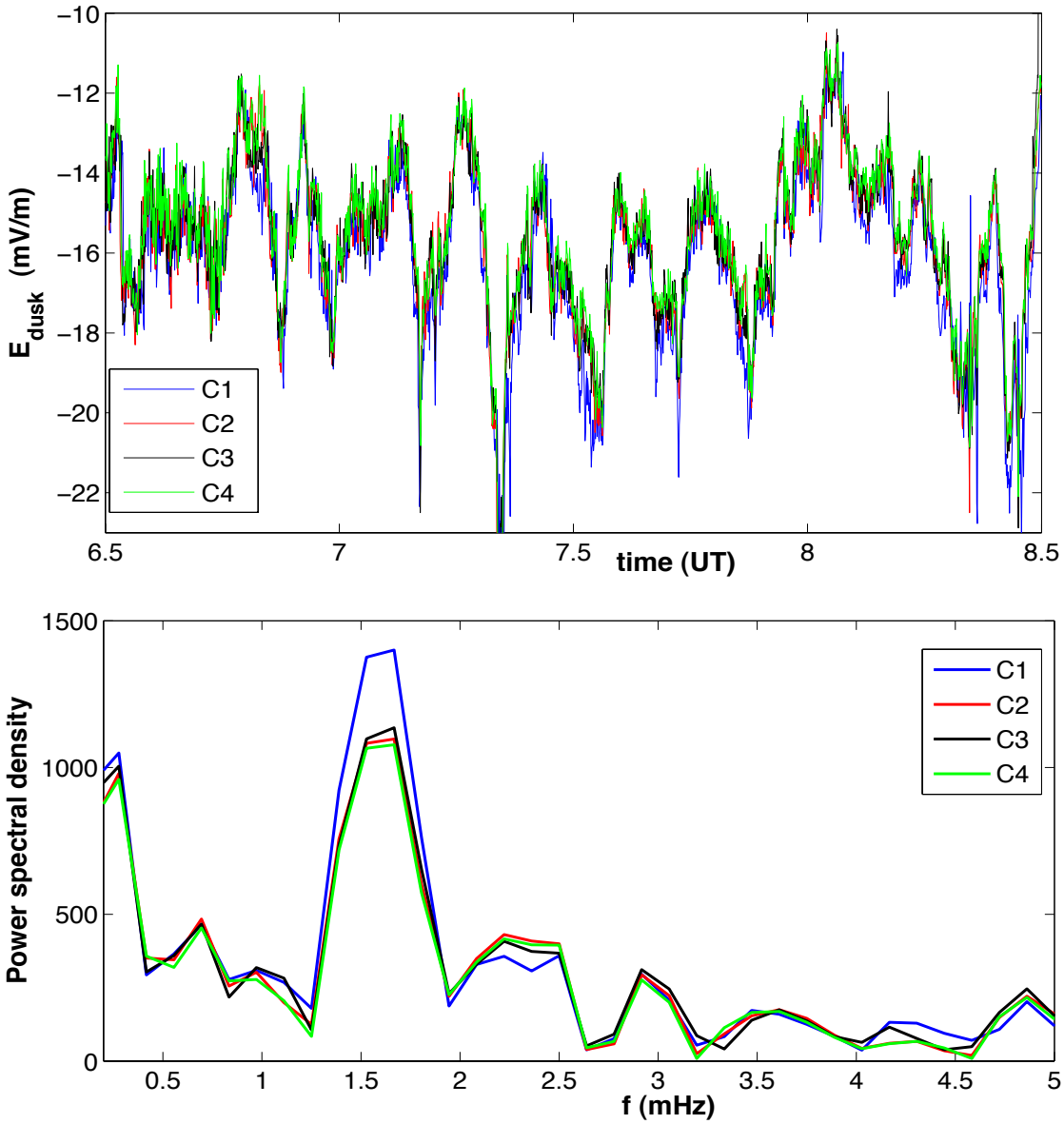

Figure 3.6: Magnitude of CLUSTER PP EFW duskward electric field (top panel) and their corresponding FFT (bottom panel) from each of the four CLUSTER spacecraft for 25 November 2001 in the time interval from 0630-0830 UT.

3.C.3 Space and Ground-Based Measurements

Comparison of ionospheric HF radar measurements with spacecraft measurements at the boundary will help us to fully characterize the driving mechanism

of the ULF wave at the magnetopause boundary. For analysis, a 1-D [Panels 2 and 3 of Figure 3.9] ionospheric back scatter data for a given beam and range gate are selected and interpolated to fill small data gaps. These interpolated data are then detrended (a continuous, piecewise single linear trend over the chosen time interval is removed) to remove low frequency trends.

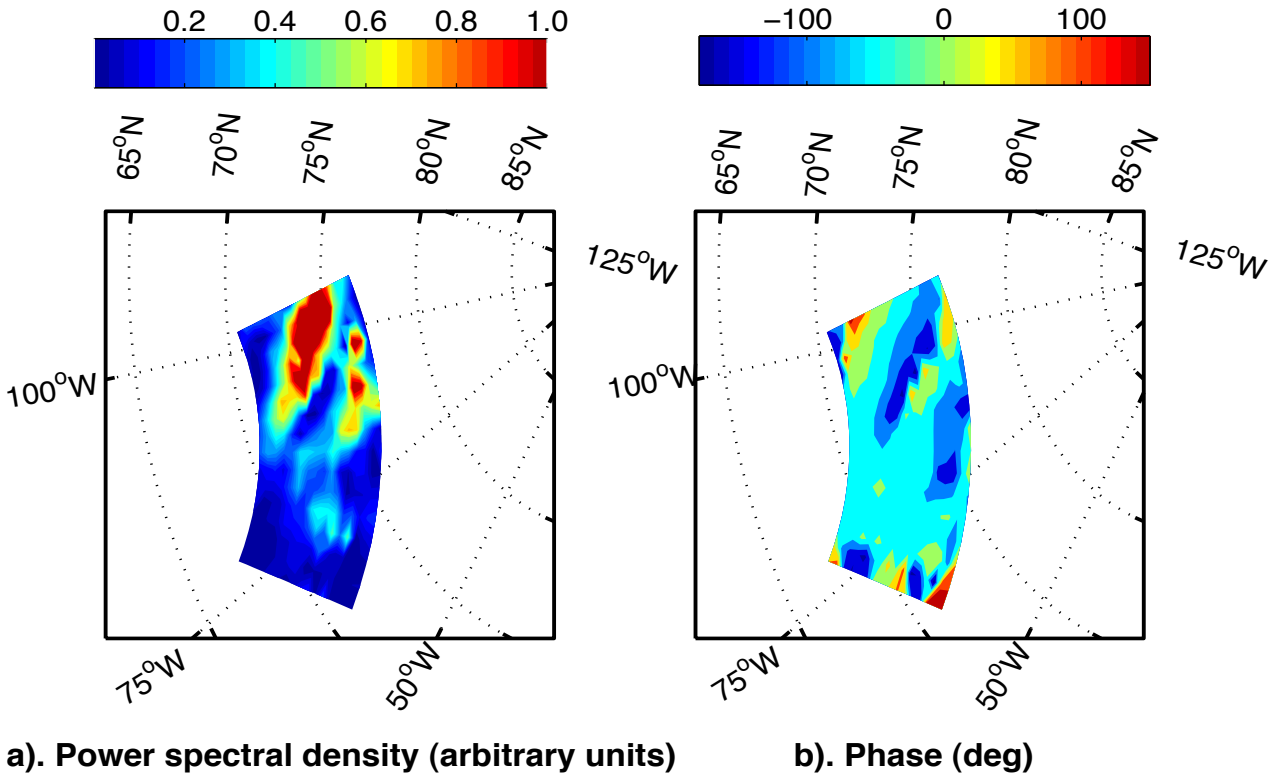

Figure 3.7: a) Contour plot of the spectral power and b) phase at 1.7 mHz from Kodiak radar on 25 November 2001 in the time interval from 0637-0837UT. Beams 0-15 and range gates 30-42 are used to generate this 2D plot. The latitudes and longitudes shown are AACGM coordinates.

In order to investigate the 2-D spatial variation in spectral power and phase of this wave activity, FFTs of the 2 hour interval for a given HF radar are calculated for all beams and gates for which good radar backscatter is

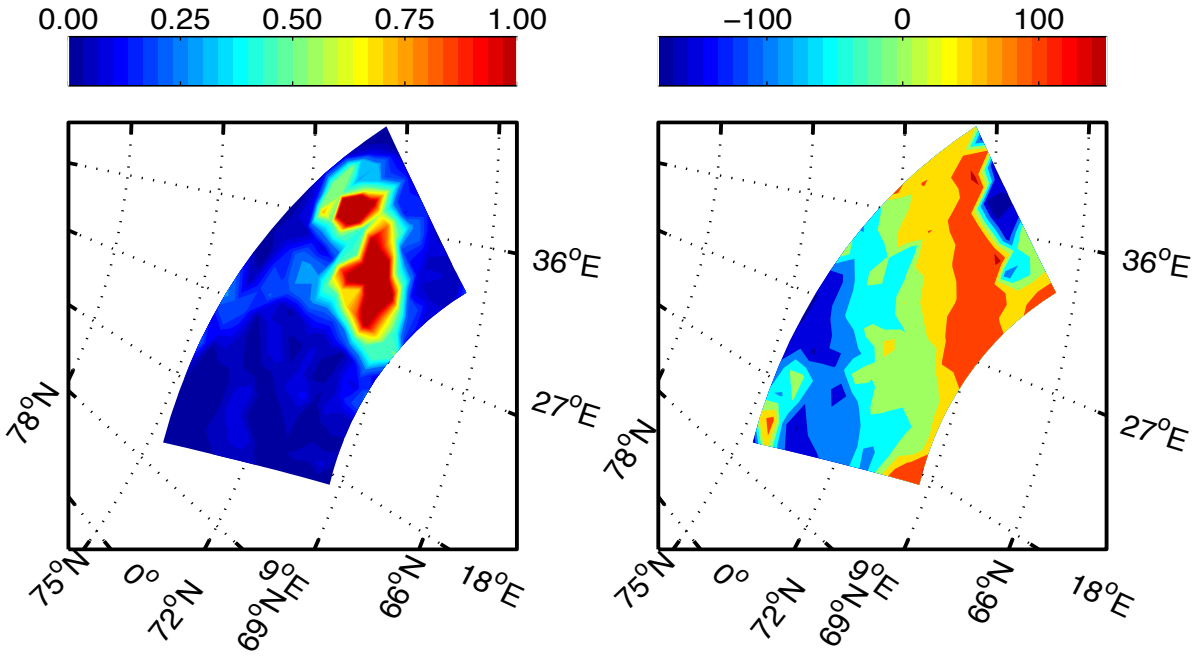

Figure 3.8: a) Contour plot of the spectral power and b) phase at 1.7 mHz from Goose Bay radar on 25 November 2001 in the time interval from 0637-0837UT. Beams 0-15 and range gates 17-30 are used to generate this 2D plot. The latitudes and longitudes shown are AACGM coordinates.

observed. Contour plots of the spectral power density and phase of the wave at 1.7 mHz [Figures 3.7 and 3.8] are then plotted for a given radar as a function of Altitude Adjusted Corrected Geo-Magnetic (AACGM) coordinates. A detailed note on the discussion and application of the revised AACGM can be found from *Gustafsson et al.* [1992] and *Baker and Wing* [1989].

An example of the use of auroral radars in the study of ULF waves is illustrated in Figure 3.7, which shows the 2-D spectral power density and phase of a 1.7 mHz field line resonance observed by the Kodiak HF radar, which is located between the dusk and mid-night time sectors. In this figure, Kodiak observes enhanced wave activity in it's field of view from 71 to 75^o latitudes in AACGM. The wave is found to have an m value of $m \sim 10$ with anti-sunward

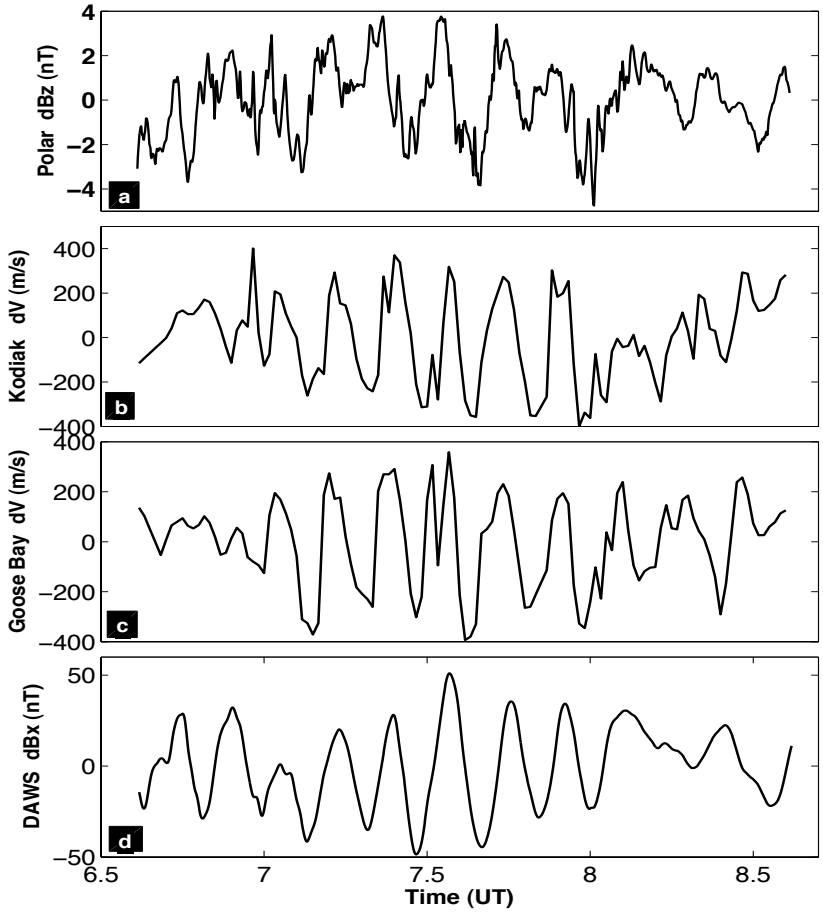

Figure 3.9: A panel showing the time series for a) the POLAR spacecraft B_z b) Kodiak HF radar Doppler line-of-sight velocity of beam 4 and range gate 37 c) Goose Bay HF radar Doppler line-of-sight velocity of beam 10 and range gate 21 d) DAWS/CANOPUS magnetometer B_x on 25 November 2001 in the time interval from 0637-0837UT.

and little poleward phase propagation. Also shown in Figure 3.8 is the spectral power density and phase of a 1.7 mHz FLR structure observed by the Goose Bay HF radar, which is located in the dawn time sector. In the field of view from 69 to 72^o latitudes in AACGM, the Goose Bay HF radar observes very clear bands of constant phase with strong latitudinally localized power enhancement. For the event at hand, Goose Bay is again found to have an observed m-value of $m \sim 10$ with anti-sunward phase propagation. Note that

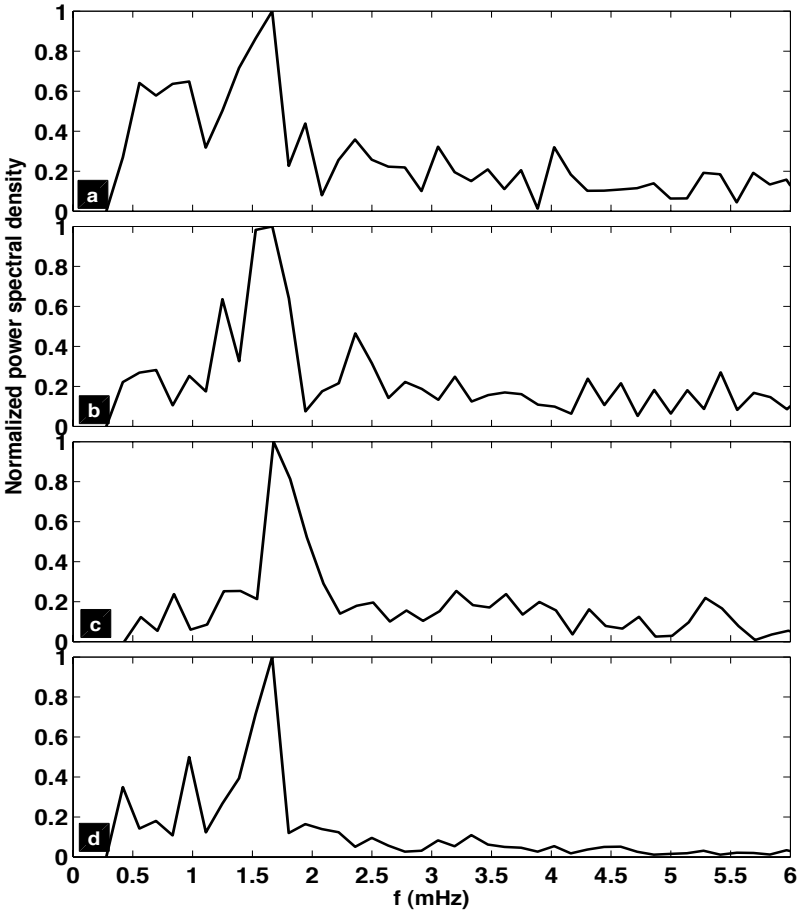

Figure 3.10: A panel showing the FFT for a) the POLAR spacecraft B_z b) Kodiak HF radar Doppler line-of-sight velocity of beam 4 and range gate 37 c) Goose Bay HF radar Doppler line-of-sight velocity of beam 10 and range gate 21 d) DAWS/CANOPUS magnetometer B_x on 25 November 2001 in the time interval from 0637-0837UT. Notable on each panel is a quasi-stable and sharply peaked 1.7 mHz wave presence from in-situ, ionospheric and ground-based measurements.

the radars observe this ULF wave in different MLT sectors (Kodiak at dawn and Goose Bay at dusk) in the northern hemisphere, which is strong evidence for the global nature of the wave.

Raw time series and the Fast Fourier Transform (FFT) corresponding to

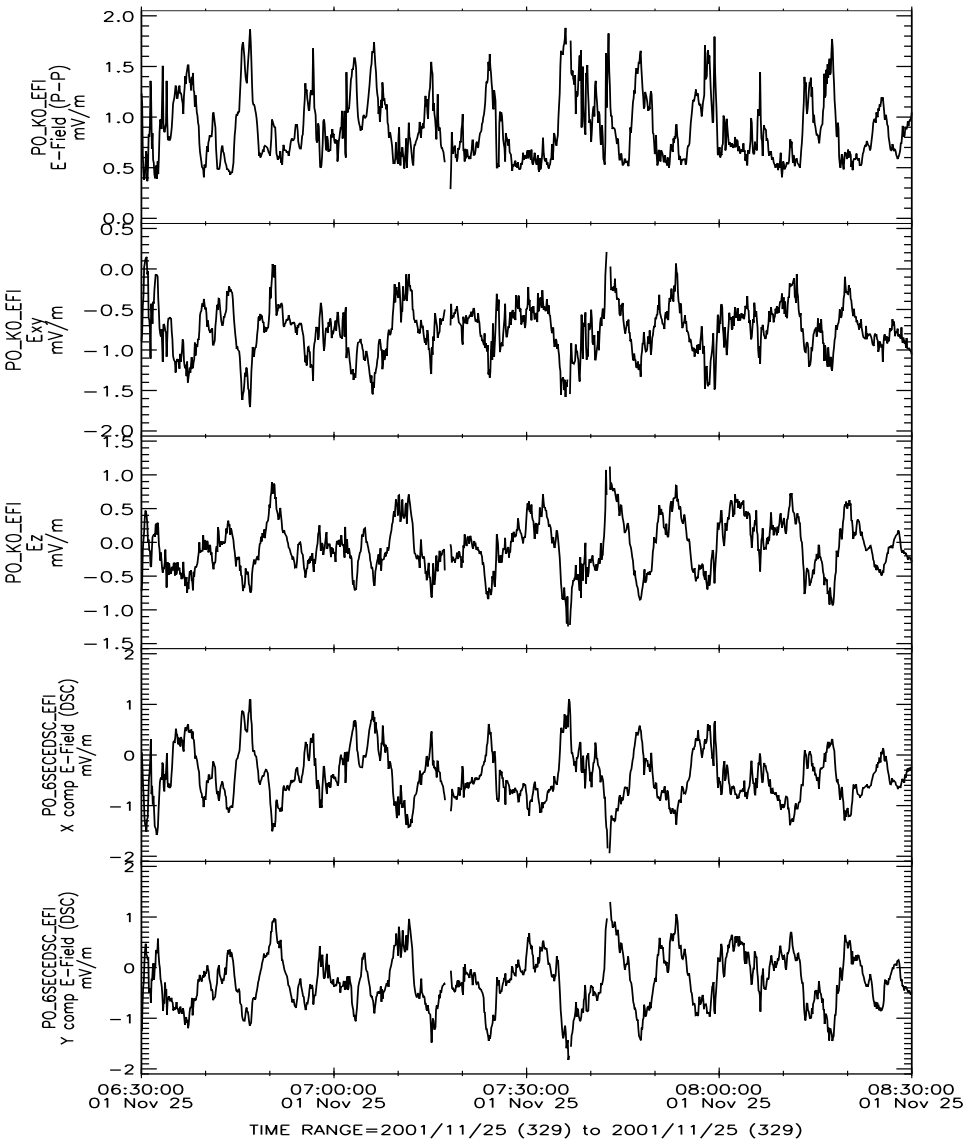

Figure 3.11: A panel showing the time series: for POLAR PO K0 EFI instrument a) E-field magnitude b) E_{xy}-field in xy plane c) E_z-field in z plane and: for POLAR PO 6SECEDSC EFI instrument d) X component of the electric field E_x e) d) Y component of the electric field E_y on 25 November 2001 in the time interval from 0630-0830 UT.

POLAR B_z, Kodiak HF radar of beam 4, and range gate 37, Goose Bay HF radar of beam 11 and range gate 21, and B_x of the DAWS/CANOPUS

magnetometer, are plotted in Figures 3.9 and 3.10. The z-component of the magnetic field on POLAR is dominant because the wave is compressional. The x-component of the magnetic field on DAWS (at a latitude of 65.90, but certainly within the field of view of Kodiak) is shown because it was found to be maximum, which implies a toroidal mode [*Kivelson and Southwood*, 1988]. The fact that the x-component is dominant over the y-component is due to the 90^o rotational effect of the ionosphere [*Hughes*, 1983]. This is a characteristic feature of toroidal mode FLRs with magnetic perturbations above the ionosphere in the azimuthal direction. Although there are other CANOPUS magnetometers that observed the wave, it is not as strong as in DAWS. This makes the magnetometer measurement consistent with the radar measurement. Figures 3.9 and 3.10 imply the ground-based fluctuations have the same period/frequency as the waves seen at CLUSTER.

Interestingly, measurements from POLAR's magnetic field from PO K0 MFE (Figure 3.9), POLAR's electric field from PO KO EFI, and PO 6SECEDSC EFI (Figure 3.11), and the G8 KO MAG magnetometer of Geostationary Operational Environmental Satellite (GOES-8) (Figure not shown because the wave is weak), magnetometers like DAWS/CANOPUS magnetometer, observed 1.7 mHz ULF wave inside the magnetosphere. During this time period, the DAWS magnetometer is located in the afternoon sector (65.90, 273.89) in CGM coordinates. We choose to show the plot from the DAWS magnetometer (DAWS falls within the field of view of Kodiak), which observed the wave in all the components of the magnetic field data very clearly. In this time period the POLAR trajectory is found to map from L $\sim$ 7.3 Re to L$\sim$4.5 Re in the equatorial plane (range of Z GSE values varies from $\sim$ 2.5 Re to L$\sim$3.5 Re)

in the afternoon sector, but on the northern hemisphere. GOES-8 is found to map from L ∼-2 Re to L∼-3 Re in the equatorial plane (range of Z GSE values varies from ∼ 2.5 Re to L∼3.5 Re) in the morning sector. The IMAGE chain of magnetometer (Fennoscandia, Svalbard) data (Figure not shown) are also found to have enhanced wave activity at the same frequency as that of the CLUSTER measurement at the magnetopause. These stations have a spatial coverage ranging from Kiruna (KIR) station of (64.69N, 102.64) to Ny Alesund (NAL) station of (75.25N, 112.08) in CGM coordinates. That is, the wave activity has a signature in the post-midnight sector where 2.5 hours $\leq$ MLT$\leq$ 5 hours. The fact that multiple instrumentation observed the same wave activity at different Magnetic Local Times (MLT) confirms that the wave has a global scale. Consequently, wave activity at the magnetopause boundary has an influence on coherent fluctuations in space, at auroral latitudes and on the ground.

3.D Discussion

If the signature of magnetopause disturbance is related to the F- region plasma oscillations in the ionosphere, then this implicates a well defined path of energy transport mechanism from the boundary to the ionospheric heights. This is consistent with the hypothesis that a localized monochromatic source at the magnetopause launches a fast wave mode into the magnetosphere that couples to a standing shear Alfvén wave on closed geomagnetic field lines. The Goose Bay HF radar observations of the wave in the morning section suggest this mechanism is operating on the dawn flank as well. The results above present an excellent conjuncture where CLUSTER and SuperDARN can be used to-

gether in witnessing the global nature of MHD waves.

This work has used measurements from several instruments to characterize a ULF wave at 1.7 mHz. The present observations show evidence that the source mechanism is consistent with a global wave mode. One piece of evidence supporting a global wave interpretation is found from the magnetic field measurement of POLAR and GOES-8 (weak, yet detectable from the magnitude of B) spacecrafts in different local times and hemispheres. Another piece of evidence to support this claim is again the clear presence of this ULF wave at Kodiak and Goose Bay HF radars in different MLTs, with anti-sunward phase propagation. The observations shown above indicate a global wave is present and thus the source mechanism must be consistent with a global wave mode.

In this study, in the time period 0600-0830 UT the multi-satellite CLUSTER mission were located in the dusk sector magnetosheath. Their radial location across magnetopause is found to be in the sequence C1, C3, C2, and C4 as one moves from the magnetopause radially out into the magnetosheath region. A schematic of their position in the equatorial plane can be seen from Figure 3.12.

Figure 3.13 shows a color coded overlay of the filtered B_z field component at 1.7 mHz of the CLUSTER measurement in the time period considered. The field components are band passed filtered in the 1.5-1.9 mHz band. A similar result is found for the electric field data (calculated from $\vec{E} = -\vec{v} \times \vec{B}$) during this period. From the color coded signals in Figure 3.13, it is evident that

the wave phase is seen by C1 earlier, followed by C3, C2 and finally by C4. This implies that there is a finite propagation time delay in seeing the wave among each of the different CLUSTER spacecraft. The propagation time delay of the wave phase as seen by each of the spacecraft is clearly related to the equatorial position of each spacecraft across the magnetopause (along positive X_{FAC}). Thus, the plot in Figure 3.13 clearly indicates that the wave phase is propagating outwards from the boundary. Also notable from Figure 3.13 is the decay in the amplitude of the wave as one traverses outwards from the boundary in the equatorial plane. The two main features that prevailed here are: the propagation time delay and decay in amplitude of the wave supports an interpretation of a source mechanism situated at the boundary.

Figure 3.14 shows the x-component of Poynting flux for C1, C3 and C4. The Poynting flux from C2 is not included here as there was no plasma data in this time period. The field components used to calculate the Poynting flux are again band passed filtered in the 1.5-1.9 mHz band. Calculation of electromagnetic Poynting vector $\vec{S}$ from CLUSTER electric and magnetic measurements is a significant aspect of this work to diagnose energy propagation across the magnetopause [*Walker et al.*, 1992]. The Poynting vector is calculated by the cross product of the two filtered fields,

$$\vec{S} = \delta\vec{E} \times \delta\vec{B}/\mu_o \tag{3.1}$$

The x-component of electromagnetic Poynting flux shown in Figure 3.14 oscillates with a frequency that is twice the 1.7 mHz frequency of the Alfvén wave as *Rae et al.* [2005]. Here, the x-component of electromagnetic Poynting flux is positive and this, according to our FAC system of coordinate, indicates

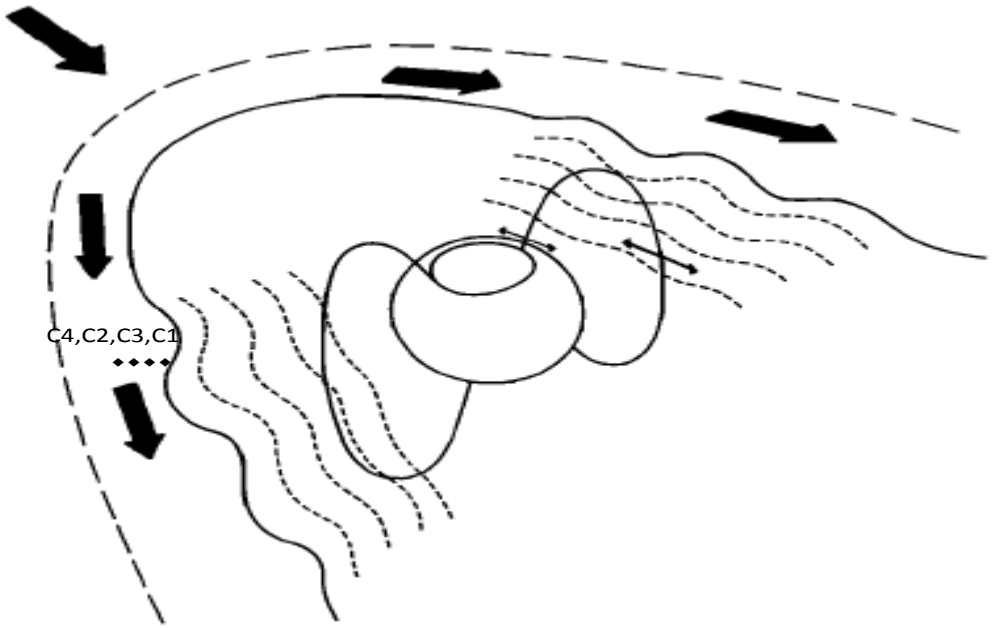

Figure 3.12: A schematic of X-position of CLUSTER in FAC (X_{FAC}) on November 25, 2001 between 0600-0830 UT. The dots are locations where the spacecraft are situated. The dots are locations where the spacecraft are situated. Positive X_{FAC} is directed radially away from the Earth and is perpendicular to the dusk flank magnetopause. Note: CLUSTER locations are not to scale. Adopted from *Poulter* [1982].

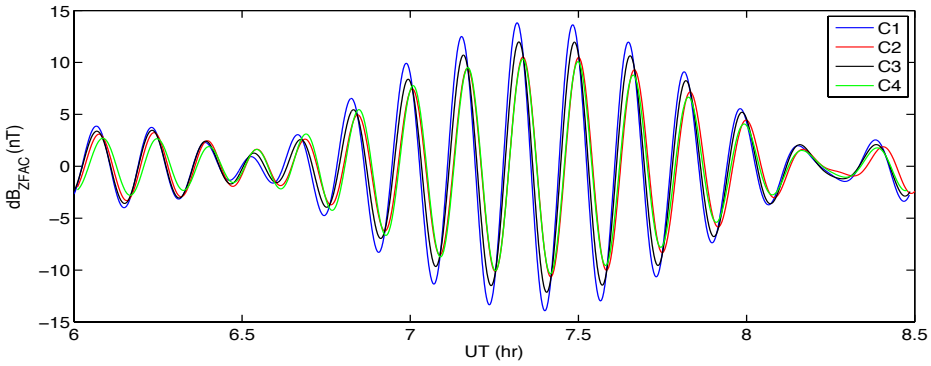

Figure 3.13: Band passed filtered z-component of the CLUSTER magnetic field data in FAC on November 2001 between 0600-0830 UT.

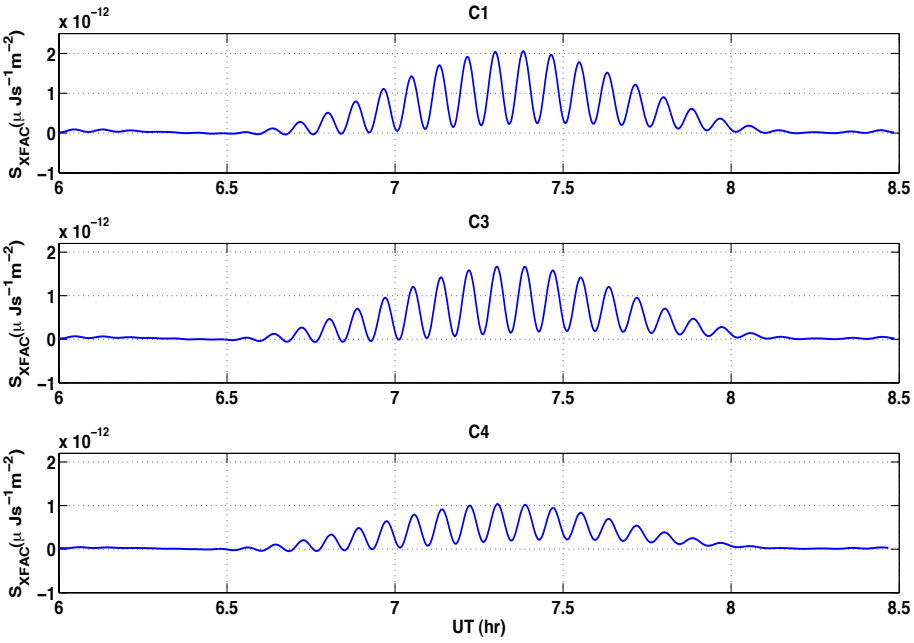

Figure 3.14: Band passed filtered X-component of the CLUSTER Poynting flux data in FAC on November 2001 between 0600-0830 UT.

an outward propagating Poynting flux away from the boundary. The wave is clearly evanescing radially away from the boundary, i.e. the amplitude is decreasing as one moves away from the magnetopause. This is a feature one would expect to see outside the boundary for a surface mode driver located on the magnetopause boundary that is possibly excited by a KH instability [e.g., *Pu and Kivelson*, 1983; *Miura*, 1990; *Walker et al.*, 1992; *Allan and Poulter*, 1992]. If the wave at the boundary is a surface mode, by the same token one would expect an Earthward penetration of the radial energy flux from the magnetopause flanks to drive FLRs in both time sectors such as those observed by the Kodiak and Goose Bay HF radars.

For the event at hand, the flank magnetosheath flow speed is on average

600 km/s and the ambient magnetic field is positive throughout the interval. According to *Mathie and Mann* [2000], there is a clear correlation between the existence of FLRs and the presence of fast magnetosheath flow speed $>$ 500 km/s. This is consistent with our observation of discrete frequency FLRs at ionospheric altitudes and ULF wave signatures from POLAR spacecraft inside the magnetosphere.

Inner mode KHI-driven waves, which are predicted to be unstable most of the time, have phase velocities roughly equal to half the plasma flow velocity in the magnetosheath ($\sim$ 620 km/s) [e.g., *Couzens et al.*, 1985; *Lee et al.*, 1981; *Walker*, 1981]. The wavelength λ_y of the wave can be estimated from the observed values by $\lambda_y = \frac{V_{sheath}/2}{f} \sim 28R_e$, where $f = 1.7$ mHz is used. The wavenumber along the boundary is $k_y = 2\pi/\lambda_y = 4 \times 10^{-8}\ /m$. Upon using $v_1 = 620$ km/s, $B_{1XGSE} = -5$ nT (estimated when the spacecraft are inside the magnetosheath from 0630-0830 UT) and $n_1 = 8\ /cm^3$ for the magnetosheath side of the boundary and $v_2 \sim 0$, $B_{2XGSE} = -23$ nT (estimated when the spacecraft appeared to have crossed the magnetopause from 0830-0910 UT) and $n_2 = 0.5/\ cm^3$ for the magnetospheric side of the boundary, the necessary condition for the onset of KHI, equation (1.37) reads $9\times10^{-4}/s^2 > 6\times10^{-4}/s^2$. Although the KHI onset criteria appears to be satisfied, LHS and RHS expressions are of same order. Given that this is the condition for a non-realistic magnetopause boundary (tangential discontinuity), much weight could not be given if this condition is not met satisfactorily.

The thickness of the boundary layer can be approximated by identifying a time interval when the magnetopause intercepts CLUSTER. This can be

achieved by noting an abrupt change in the orientation of the magnetic field [*Couzens et al.*, 1985], a condition when B_z drops from 40 nT to 20 nT. This condition happens for C2 at 08:37:09 UT and $Y_{gse} = 120,053$ km and for C3 at 08:37:00 UT and $Y_{gse} = 119,752$ km. The speed of the magnetopause in the Ygse direction is then $v_{my} = \Delta Y_{gse}/\Delta t \sim 120,400$ km/h. In this time interval Δt, the velocity of reference spacecraft C3 in GSE from CLUSTER Auxiliary Parameters(CL SP AUX) is $v_{C3} \sim 1440$ km/h. Considering the fact that both C3 and the magnetopause are moving in the same direction along positive $Ygse$, the relative speed is the difference between v_{my} and v_{C3}. The thickness of the magnetopause boundary can thus be estimated by $\Delta = (v_{my} - v_{C3})\frac{\Delta T}{2} \sim 4.67R_e$, where $\Delta T \sim 30$ min of two way back and forth travel time of the magnetopause is used here. The estimated thickness of the boundary layer of $\sim 4.67R_e \sim 29,785$ km is found to be close to the range of those reported for a KHI generated surface wave [*Miura and Prichett*, 1982], $2R_e - 4R_e$. The boundary layer estimate is very close to the $20,000 - 28,000$ km range reported in *Hasegawa et al.* [2004] for the most KH-unstable low-latitude regions based on numerical simulations.

The thickness of the boundary can be used together with k_y to determine if the KHI criteria for the fastest growing mode is met. According to the theory of KHI generated waves, the observed wave frequency at the boundary estimated the wavelength of the surface wave to be $\sim 28.5R_e$. The condition for the fastest growing mode then reads $k_y\Delta \sim 1.05$. This is in very good agreement with the theory of a KHI driven ULF wave frequencies [*Walker*, 1981] for which the occurrence of the fastest growing mode is reported to be $k_y\Delta \sim 0.5 - 0.8$ for several geometric configurations. Also, results from

similar studies by *Miura and Prichett* [1982] and *Claudepierre et al.* [2008] found the condition for the fastest growing mode to be $k_y\Delta \sim 0.5 - 1.0$ and $k_y\Delta \sim 0.6 - 1.0$, respectively.

3.E Summary

The data presented in this chapter provides evidence for an observational link between ULF wave activity at the magnetospheric boundary, in the magnetosphere, in the ionosphere at auroral altitudes and on the ground. In this study, the simultaneous presence of satellite-borne and ground based instrumentation offered a unique opportunity to diagnose the properties of the observed ULF waves in different parts of the magnetosphere and identify a plausible source mechanism at the boundary.

The decay in the electromagnetic Poynting vector and the propagation time delay in the phase of the ULF wave away from the magnetopause, along with the underlying upstream solar wind conditions of strong northward IMF and supersonic flow exceeding 640 km/s, solidly point to a KHI generated surface mode as a sole mechanism driving the observed global ULF wave event. The fact that we have observed a relatively small azimuthal wavenumber, $m = 10$, with anti-sunward phase propagation in both dusk and dawn sectors, along with the absence of monochromatic dynamic pressure variations or solar wind buffeting, is further evidence to support the hypothesis of a KHI generated surface mode as a source mechanism. This demonstrates a well-defined path of energy transfer from the magnetopause into the inner magnetosphere and ionosphere and is reliable evidence for magnetosphere-ionosphere coupling.

Chapter 4

A Field Line Resonance Excited by a Solar Wind-Driven Magnetopause Oscillation

4.A Introduction

In this chapter, CLUSTER is used to study a discrete oscillation at the bow shock, which propagates into the dusk flank. The spacecraft data is compared with observations of the wave in the ionosphere made by the Saskatoon HF-radar. We present magnetic field and Poynting flux structures [e.g., *Junginger*, 1985; *Kouznetsov and Lotko*, 1995] in the radial direction in a Field Aligned Coordinate (FAC) system [*Baker and Wing*, 1989] and [*Gustafsson et al.*, 1992] discuss how the driver wave behaves at the magnetopause. We attempt to provide an explanation of the most probable source mechanism. This is a unique measurement provided by the CLUSTER multi-spacecraft mission which otherwise could not have been fulfilled by a single spacecraft mission.

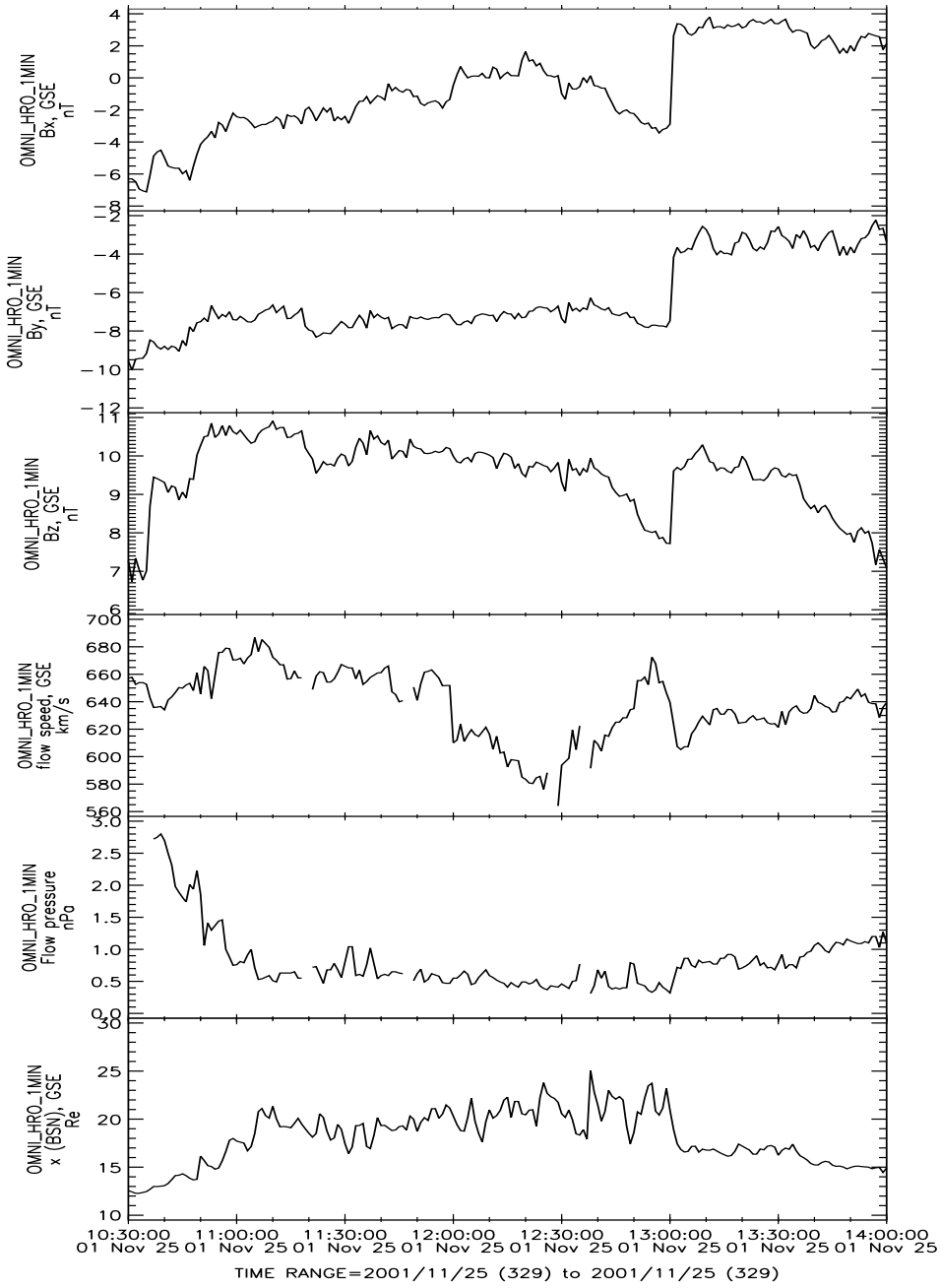

Figure 4.1: Panel of OMNI HRO 1MIN: (a)-(c) magnetic field (d) flow speed (e) flow pressure and (f) estimate of bow shock nose location in the X GSE direction for 1100 - 1400 UT on November 25, 2001.

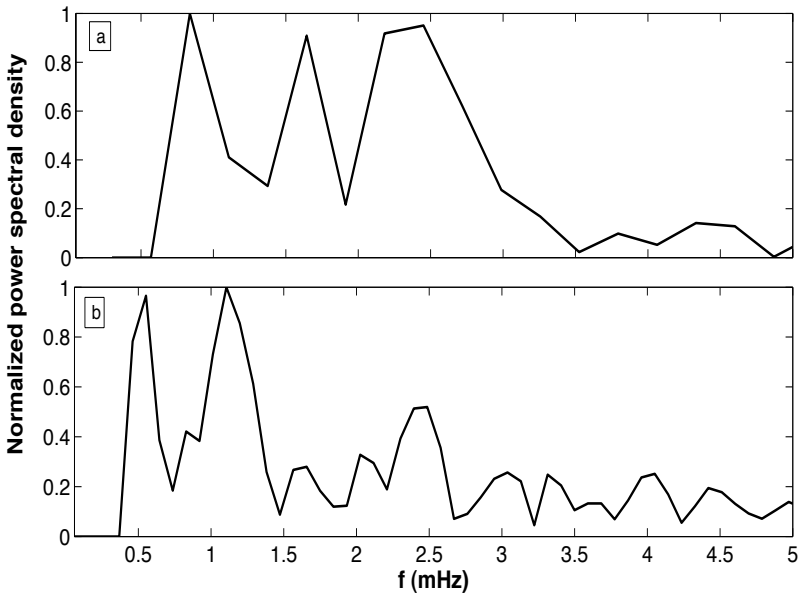

Figure 4.2: FFT panel of(a) OMNI B_y and (b) OMNI's estimate of bow shock nose location in the X GSE direction on November 25, 2001. It can be seen that both the B_y and the X location of the bow shock data have a 2.5 mHz frequency wave presence. The frequency resolution is 0.28 mHz.

4.A.1 In situ spacecraft Observation

The event presented in this chapter is chosen based on a visual inspection of oscillations in magnetic field and plasma flow measurements at the location of the bow shock and the magnetopause. Enhanced wave activity is found to occur at 1100-1300 UT on November 25, 2001, which is 2.5 hours after the event studied in chapter 3. Figure 4.1 shows a 3-hour interval of OMNI magnetic field data, flow data and, an estimate of the bow shock nose X location from OMNI HRO 1MIN. The FFT of these is shown in Figure 4.2. Note that in the interval 1100 - 1400 UT there is a quasi-periodic 2.5 mHz wave present in the OMNI B_y measurement and bow-shock location data; however, there is no signature of this wave in the flow pressure. This excludes a dynamic pressure source mechanism for the 2.5 mHz wave. We do not at this point have an

estimate of how many solar wind driven ULF pulsations have quasi-periodic bow shock oscillations such as the one we present in this section. More work needs to be done to quantify how many solar wind driven ULF pulsations have quasi-periodic bow shock oscillations.

The CLUSTER Spacecraft FluxGate Magnetometer (FGM) provides three dimensional magnetic field measurements. Figure 4.3 is a plot of CLUSTER C3 FGM raw magnetic field and C3-PP-CIS proton bulk velocity data in GSE coordinates for 25 November 2001, in the time interval from 1030 - 1400 UT. The time period 1030-1100 UT corresponds to CLUSTER skimming the magnetosheath, which can be seen from the V_x component, which is on average -500 km/s during this interval, as is consistent with magnetosheath flows. From 1100-1130 UT or so, the magnetopause moves outward over CLUSTER (because of a change in flow pressure from $\sim$ 1.5 nPa to $\sim$ 0.5 nPa that uncompressed the magnetosphere, see Figure 4.1), leaving CLUSTER at the inner edge of the magnetopause boundary layer from 1130-1310 UT at which point the magnetopause again moves inward over CLUSTER, putting it back in the magnetosheath after 1310 UT (because of a change in flow pressure from $\sim$ 0.5 nPa to $\sim$ 1.0 nPa that compressed the magnetosphere). In these time periods, inward-outward motion would correspond to velocity oscillations predominantly in the Y-GSE direction (dawn to dusk direction). However, the flow data shows similar amplitude oscillations in all three directions on the order of 200 km/s peak to peak between 1130 and 1300 UT when the 2.5 mHz wave is observed. This means the spacecraft is moving outward and the magnetopause is moving over it periodically. There is some sampling of both the magnetosheath and boundary layer between 1100 and 1130 UT; however after 1130 UT when CLUSTER sees the 2.5 mHz wave we don't see

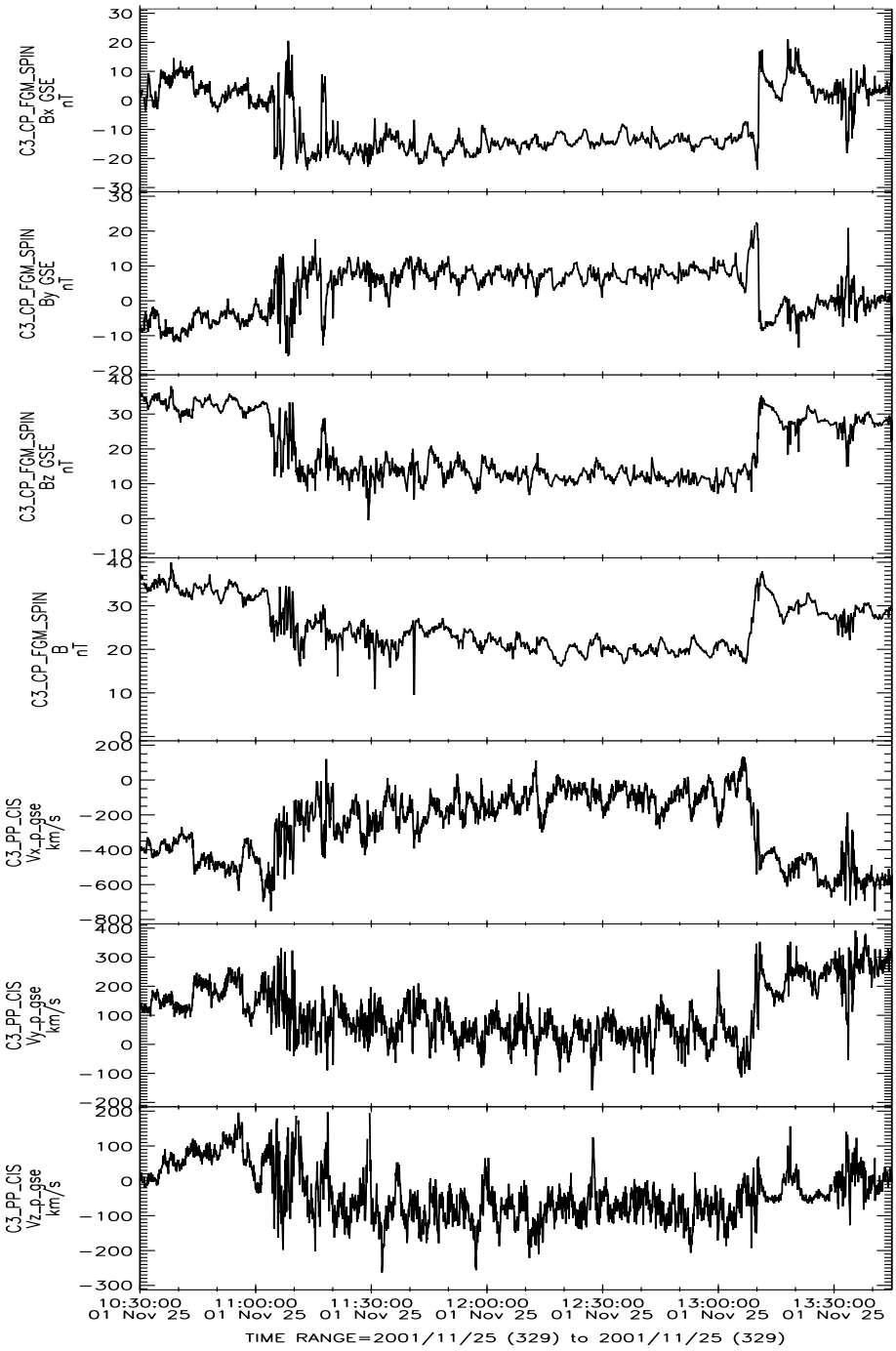

Figure 4.3: CLUSTER Spacecraft C3 CP-FGM SPIN FluxGate Magnetometer (FGM) raw magnetic field and C3-PP-CIS proton bulk velocity data from 1030 - 1345 UT on November 25, 2001.

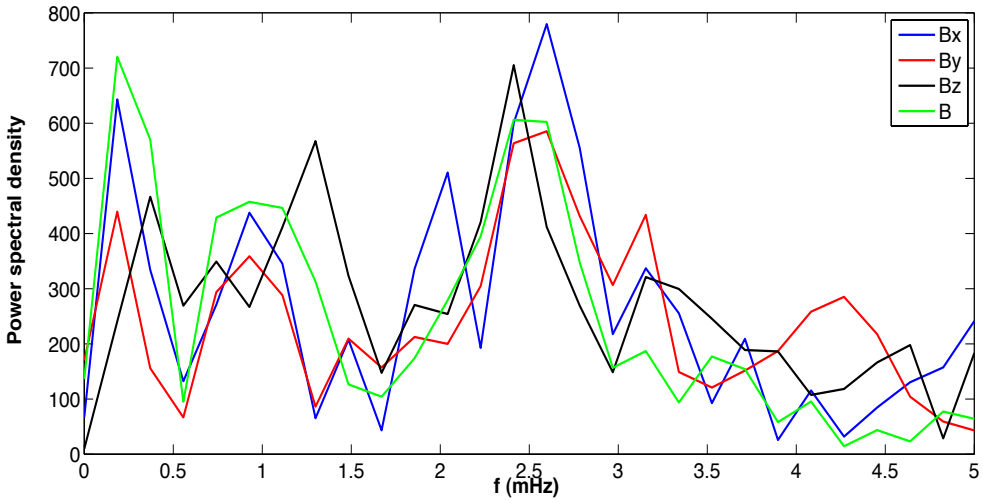

Figure 4.4: FFT of CLUSTER C3 CP-FGM SPIN FluxGate raw magnetic field data from 1100 - 1300 UT on November 25, 2001 of Figure 4.3. The 1.7 mHz wave in Bx is seen to be dominant over the others and this is found to be true for all of the CLUSTER spacecrafts. Notable also is the presence of this wave in the estimate of the bow shock nose location in the X GSE direction.

a sampling of magnetosheath conditions, i.e. parameters such as Vx and Bx don't reach values seen in the magnetosheath prior to 1100 and post 1330 UT. This is a clear indication of a quasi-periodic oscillation of the magnetopause and magnetospheric boundary layer between 1100-1130 UT. This could give an indication of the magnitude of the magnetopause oscillations. 1310-1345 UT is an interval where CLUSTER has found itself outside the boundary layer and inside the magnetosheath, because during this interval it can be clearly seen that the plasma flow data takes magnetosheath values ($\sim 400\ km/s$) followed by solar wind values ($\sim 600\ km/s$).

Focus on the second time interval from 1100-1310 UT when CLUSTER appears to be inside the boundary layer. Figures 4.4 and 4.5 show the FFT of the magnetic field data and the bulk plasma flow data V_y of Figure 4.3, and

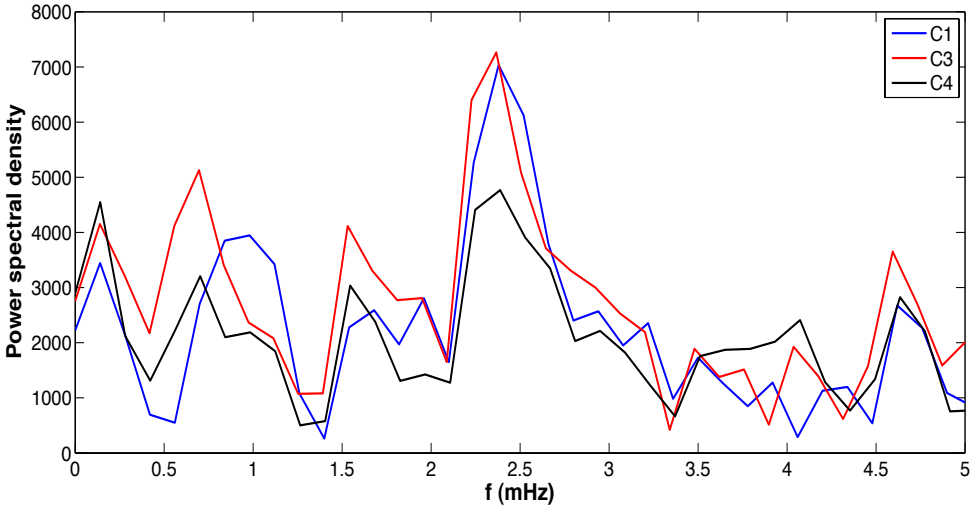

Figure 4.5: FFT of CLUSTER C-PP-CIS proton bulk velocity V_y data of C1, C3, and C4 from 1100 - 1300 UT on November 25, 2001 of Figure 4.3. Although the wave is present on other components of $\vec{V}$, V_y is chosen because it is dominant over the others in all of CLUSTER.

clearly illustrate the presence of a 2.5 mHz ULF wave. It is very interesting that this wave in the magnetic field and plasma flow data at the magnetopause boundary layer is at the same frequency as the oscillations in the solar wind IMF B_y component and in the bowshock nose location shown above in Figures 4.1 an 4.2. In the following section, we will consider ionospheric echoes from the Saskatoon HF radar to diagnose the signature of this wave activity at ionospheric heights.

4.A.2 Ground-based Ionospheric Observation

Data from the SuperDARN system of radars, mainly from Saskatoon, will be used to demonstrate ionospheric signatures of a FLR during the same time period as the boundary oscillations. In addition to a 1-D time series and FFT analysis, we consider a 2-D analysis of ionospheric HF radar measurements, to

investigate the response of the ionosphere as a result of the solar wind driven magnetopause oscillation.

Observations of waveforms in the time domain and their power spectra in the frequency domain help to provide insight into the probable energy transport mechanisms. Sample raw time series from Saskatoon and their corresponding Fast Fourier Transform (FFT) are shown in Figures 4.6 and 4.7. Figure 4.6 shows a panel of Saskatoon measured line-of-sight velocity fluctuations along beam 9 (range gates 27-30) which show similar oscillations to those seen at the magnetopause. Figure 4.7 presents the FFT of the Doppler line-of-sight velocity shown in Figure 4.6. The FFT spectra indicate a clear 2.5 mHz wave in response to the driver observed at the location of the bowshock and the magnetopause. The observation of wave power at a discrete frequency suggests that there is a direct link between the coherent oscillation of the field lines within the Saskatoon field of view and the discrete frequency magnetopause oscillation. If the signature of magnetopause disturbance is related to the F-region plasma oscillation in the ionosphere, then this provides evidence of a well defined path of energy transport from the magnetopause to the ionosphere.

Figure 4.8 shows the 2-D power spectral density and phase of a 2.5 mHz field line resonance observed by the Saskatoon HF radar located in the predawn sector. In this figure, Saskatoon observes enhanced wave activity in it's field of view from 71.5 to 75^o latitudes in AACGM. We note from this 2-D plot that the latitudinally localized power enhancement, and the decrease in phase with latitude, are signatures of a FLR. The m value of this wave activity is found to be $m \sim 12$ with anti-sunward phase propagation. It is important to

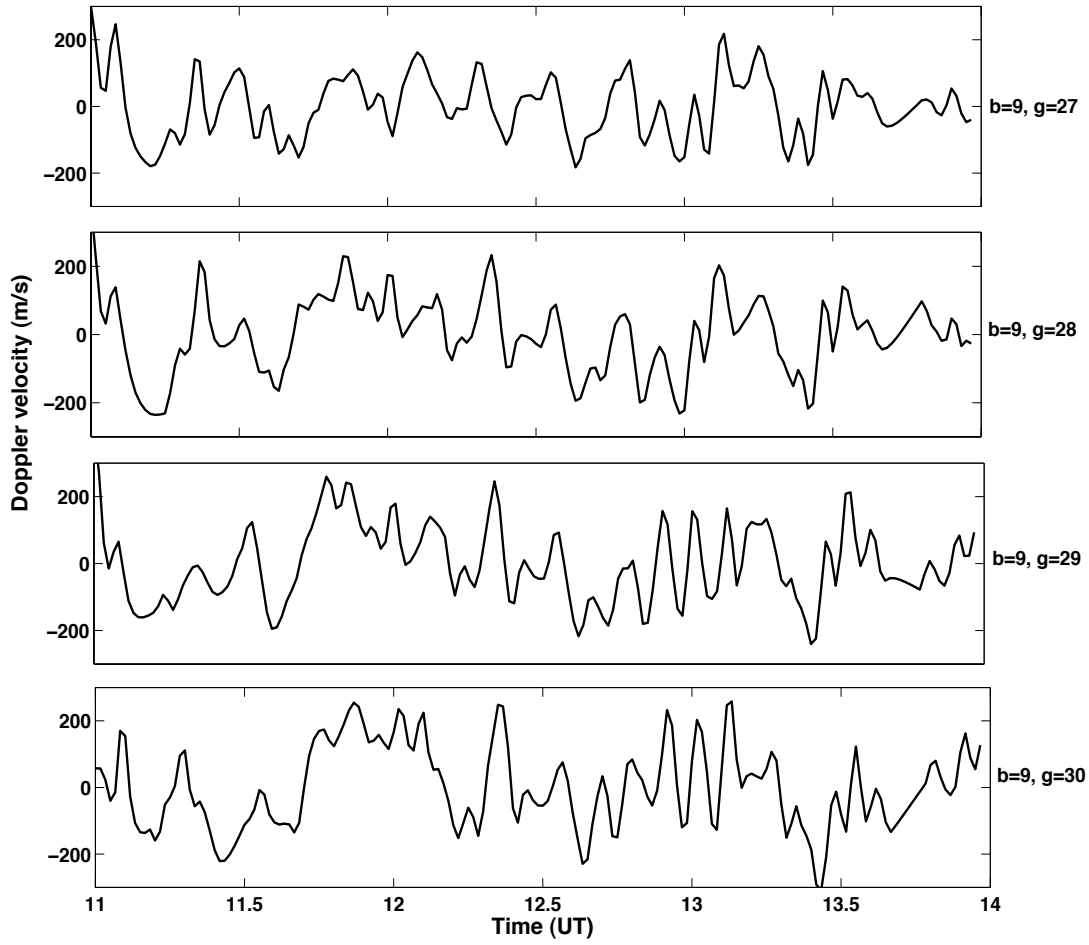

Figure 4.6: De-trended radar Doppler line-of-sight velocity from Saskatoon HF radar in the time interval 1100-1400 UT on November 25, 2001. Note that beam 9 and range gates from 27 - 30 are used in this plot.

note that Saskatoon observed this wave activity in the pre-dawn sector while the magnetopause oscillation is observed at the dusk flank. However, the original wave source is in the solar wind and thus could be causing oscillations of the dawn flank as well.

It is worth mentioning that there were other less dominant frequencies in the range 0.6-0.7, 1.0-1.1 and 1.6-1.7 mHz in OMNI B_y, in CLUSTER magnetic fields and flows, and in the SuperDARN Doppler l-o-s velocity data. The

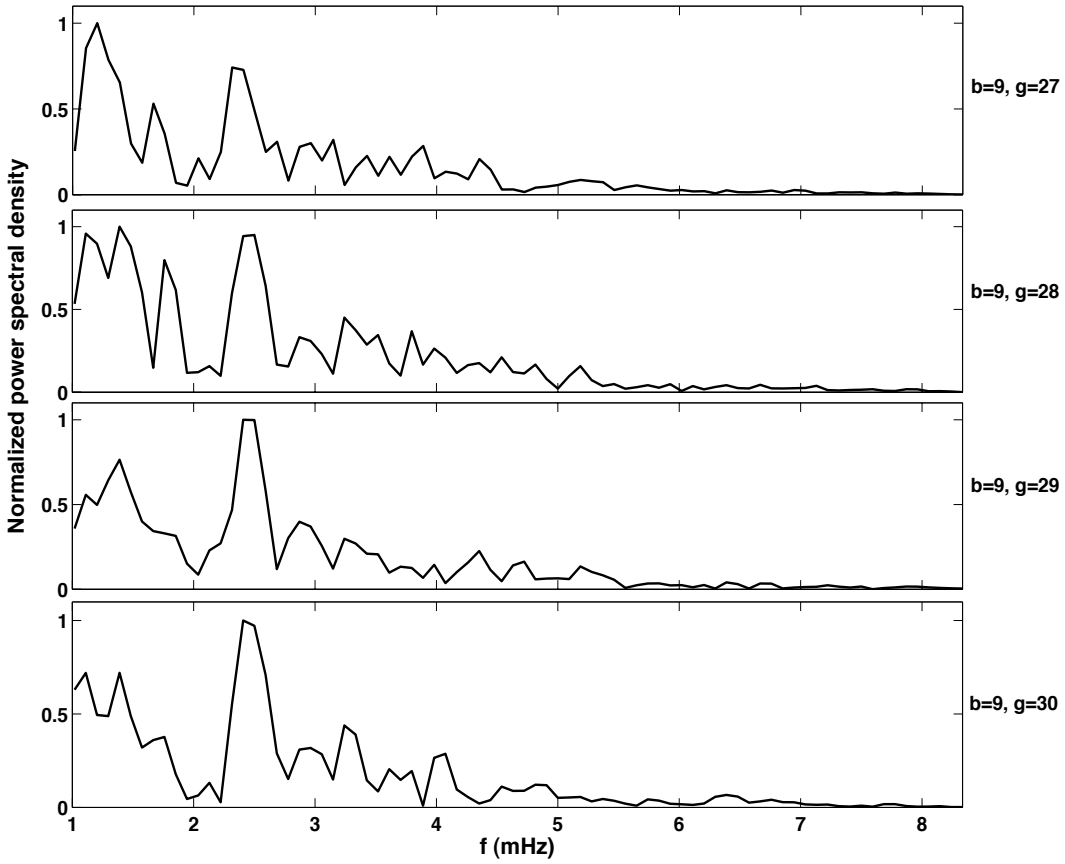

Figure 4.7: The FFT of de-trended radar Doppler line-of-sight velocity from Saskatoon HF radar in the time interval 1100-1400 UT on November 25, 2001 showing sharply peaked structure at 2.5 mHz. Note that beam 9 and range gates from 27 - 30 are used in this plot.

spectral resolution in the observed frequencies is $\sim \pm 0.1$ mHz. Considering the fact that these oscillations are observed at nearly the same time and location, with similar phase variation as the 2.5 mHz oscillation, we believe that they are driven by the same source mechanism that is driving the 2.5 mHz oscillation. The reason why we have placed emphasis on the 2.5 mHz wave is because in the time period we have chosen to study this event, the 2.5 mHz wave is dominant and clear at the location of the bow shock, magnetopause and the Saskatoon HF radar field of view.

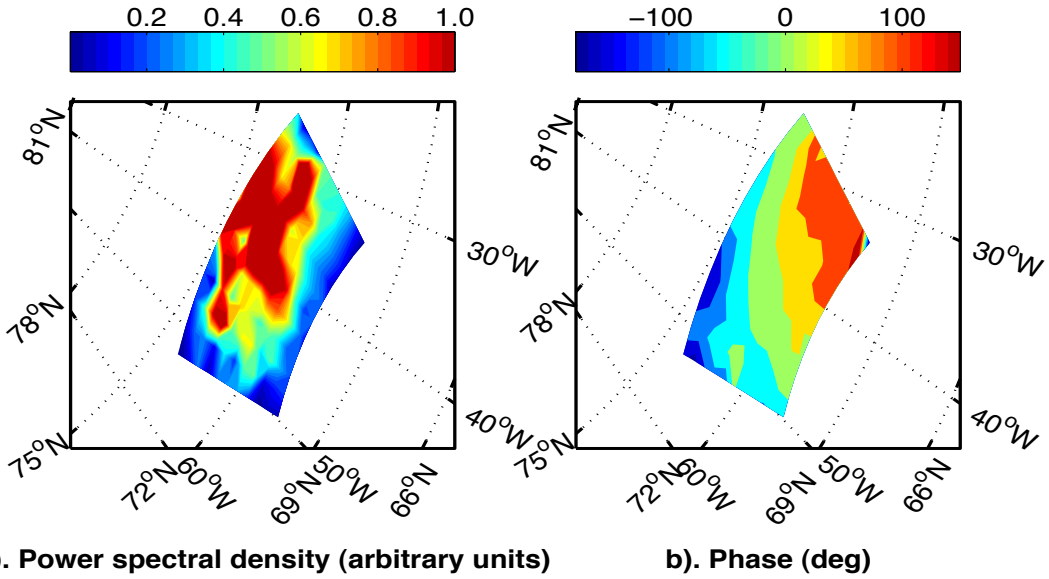

Figure 4.8: a) Contour plot of the spectral power and b) phase at at 2.5 mHz from the Saskatoon HF radar in the time interval 1223-1323 UT on November 25, 2001. Note that beams 0-10 and range gates from 23-33 which have good radar echo were only used to make this 2-D contour plot. The latitudes and longitudes shown are AACGM coordinates.

4.B Results and Discussion

This work has used measurements from several instruments to characterize a 2.5 mHz ULF wave event. The present observations provide evidence that appears to support the hypothesis of a solar wind driven magnetopause oscillation exciting an FLR. The details of how energy is transported from the solar wind driven magnetopause oscillation to the ionosphere will be discussed below.

In the time period 1100 - 1310 UT, the multi-satellite CLUSTER spacecraft were seen to skim through the boundary layer between the magnetosphere and magnetosheath. The exact sequence of their radial location is found to be C4,

C2, C3, and C1 as one moves Earthward from the magnetosheath. A schematic of the CLUSTER location is shown in Figure 4.9. Figure 4.10 shows a color-coded overlay of the filtered B_x at 2.5 mHz in field aligned coordinates (FAC) of the CLUSTER measurement in this time period. The field components are band pass filtered in the 2.3-2.7 mHz frequency band. From Figure 4.10, it is evident that the wave peaks nearly at the same time at all four spacecraft. The FAC system is discussed in Chapter 3, which also states the direction of X_{FAC} to be away from Earth. The particular merit of this technique, when used in a FAC, is that it provides information on the radial profile of energy and field measurements.

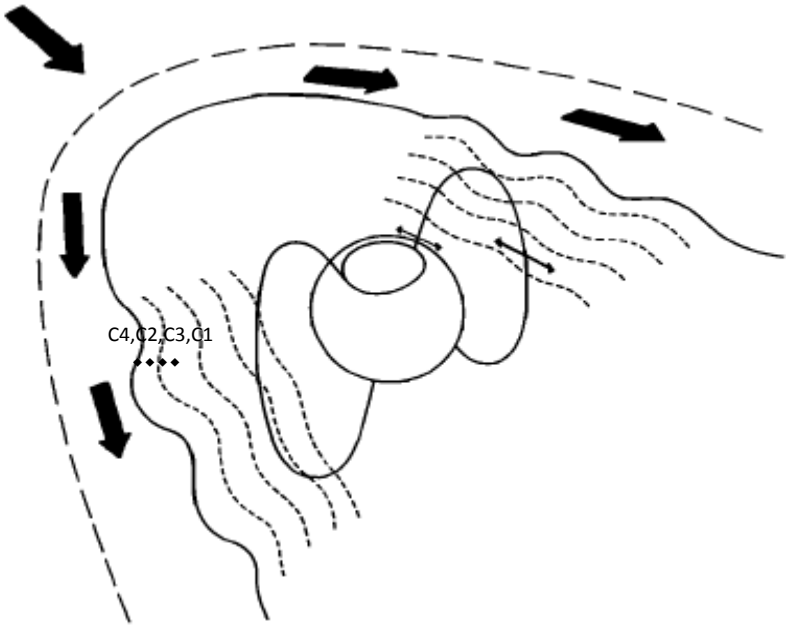

Figure 4.9: A schematic of X-position of CLUSTER in FAC (X_{FAC}) on November 2001 between 1100-1300 UT. The dots are locations where the spacecraft are situated. Positive X_{FAC} is directed radially away from the Earth and is perpendicular to the dusk flank magnetopause. Note: CLUSTER locations are not to scale. Adopted from *Poulter* [1982].

Figure 4.11 depicts a panel of the radial Poynting flux vector from C1 in

the FAC system. Components of the radial Poynting flux vector from C3 and C4 also show similar features. This feature can't be checked for C2 for there was no plasma flow data. The field components used to calculate the Poynting flux are again band pass filtered in the 2.3-2.7 mHz frequency range. Panel (a) of Figure 4.11 shows that the time averaged radial energy flux S_x is outwards pointing away from the boundary. Given that the source of the wave is in the solar wind, a positive X directed energy flux is unexpected. This can be explained in terms of the wave fields that are used to calculate this component of the Poynting flux. From $S_x = E_y B_z - E_z B_y$, since E_z is negligible, S_x can be approximated by $S_x \approx E_y B_z$, implying that the sign of S_x is dependent on the phases of E_y and B_z. If E_y and B_z are in phase, S_x becomes positive, leading to a net outward energy propagation. However, if E_y and B_z are out of phase, S_x becomes negative, leading to a net inward energy propagation. In our case, in the interval 1100-1300 UT, E_y and B_z are found to be more in phase than out of phase. This allows the net time averaged radial energy flux S_x to point outwards from the boundary.

According to the FAC definition of Chapter 3, positive Y is downtail and positive Z is along the direction of the ambient magnetic field (however here inside the boundary layer the background field is dominant in the negative x-gse direction). Panel (b) of Figure 4.11 shows a down-tail energy propagation, S_y supporting our interpretation of a source located in the solar wind. Panel (c) of Figure 4.11 shows the Z-component of the wave Poynting vector, S_z. The net S_z is in the negative Z-FAC direction, i.e, directed away from the equatorial plane and toward the southern hemisphere. Given that during this time CLUSTER is located between Z_{GSM} of $-6R_e$ and $-7R_e$, a net negative S_z is expected. Considering the fact that the Z-component of the Poynting

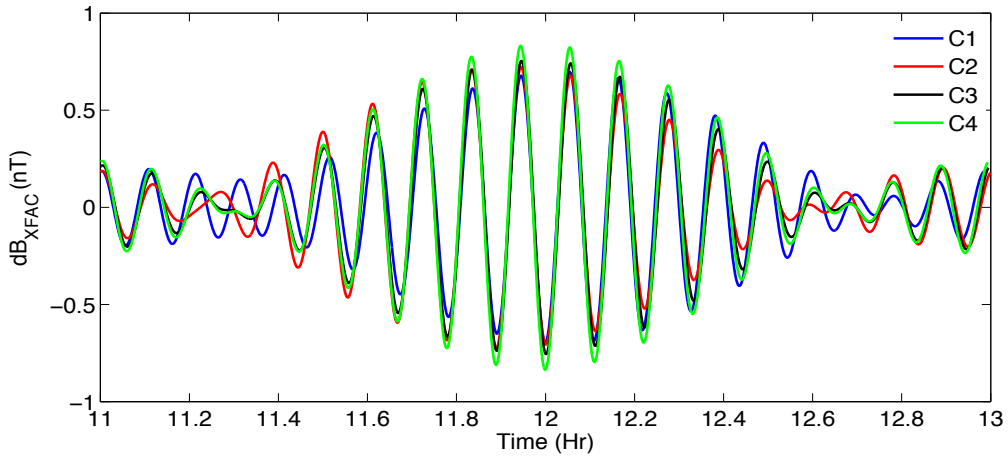

Figure 4.10: 2.5 mHz band passed filtered x-component of the CLUSTER magnetic field data in FAC on November 25, 2001 between 1100-1300 UT.

vector is the dominant one, this suggests standing Alfvén waves at the magnetopause [*Plaschke et al.*, 2009].

The above observations can be summarized as follows: discrete B_y fluctuations observed in the solar wind at ACE directly trigger a magnetopause oscillation at exactly the same discrete frequency, which in turn excites a FLR resulting in the spatial and temporal behaviour of the observed oscillations by the Saskatoon HF radar.

The pulsation observed in this work is very close to one of the frequencies (2.6 mHz) reported by *Samson et al.* [1991]. It's discrete spectrum and stable nature have led them to suggest a global waveguide/cavity mode interpretation[e.g., *Samson et al.*, 1992; *Michael et al.*, 2011]. In a cavity mode, however, the frequency is determined by the conditions in the cavity and it requires the magnetopause boundary to grow. In this event, given that the wave frequency is present in the solar wind and the magnetopause is oscillating, a

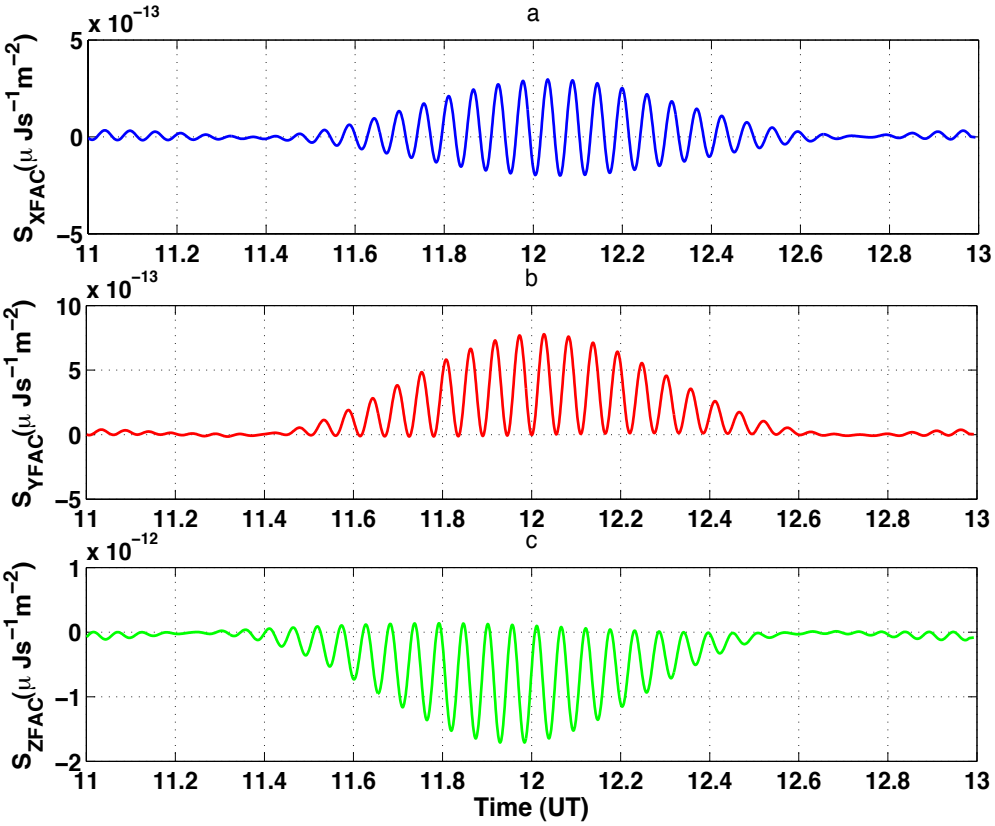

Figure 4.11: Components of the wave Poynting flux vector S of CLUSTER C1 in FAC on November 25, 2001 between 1100-1300 UT.

waveguide/cavity mode interpretation is ruled out.

Although we have identified that there is a direct link between solar wind and magnetospheric wave activities, what ultimately determines the frequency of the solar wind oscillation remains unexplained. According to *Kepko et al.* [2002] and the references therein, one possibility for the discrete, stable, and reproducible nature of the spectrum is an instability generated in the solar wind

during it's passage through the interplanetary space. Another possibility is the discrete frequency ULF oscillation of waves in the solar wind is related to solar oscillations. The discrete frequency oscillation of solar wind particles and magnetic fields observed by Ulysses spacecraft were found to closely match pressure (p) and gravity (g) mode frequencies of the Sun *Thomson et al.* [1995].

During times of northward IMF B_z and very large flow speed, such as in the event at hand, where $B_z > 9nT$ and $V_{sw} \sim 630\ km/s$, is observed in the absence of dynamic pressure oscillations, the Kelvin Helmholtz instability in particular is believed to be operative preferentially at the flanks. This may be the source generating periodic magnetopause surface modes and eventually resulting FLR observations inside the magnetosphere. The results of this observational work however show that this is not the case, as solar wind driven magnetopause and bow shock oscillations could also be responsible for such magnetopause oscillations under similar solar wind conditions. So, a careful analysis needs to be done before such a conclusion is drawn.

4.C Summary

Understanding how the solar wind interacts with the magnetopause and how energy is transported across this boundary is an important question in magnetospheric physics. In this chapter, a 2.5 mHz ULF quasi-monochromatic wave in IMF B_y is observed in the OMNI database and is subsequently observed at the magnetopause with CLUSTER and at ionospheric altitudes with SuperDARN. A FAC system at the location of CLUSTER is used to examine the radial Poynting flux and the components of the measured $\vec{B}$ profile. It is

found that the wave peaks at nearly the same time on the different spacecraft, accounting for the very close proximity of the spacecrafts. The outward propagation direction of S_x is explained in terms of the relative phase difference of E_y and B_z. Furthermore, the fact that the Z-component of the Poynting vector is dominant is suggestive of a standing Alfvén wave driven at the magnetopause. Plasma and field measurements at the boundary have shown an unambiguous signature of magnetopause oscillations at a 2.5 mHz discrete frequency.

A 2-D analysis of spectral power density and phase measurements was also done with the SuperDARN Saskatoon radar in the pre-dawn sector and is found to demonstrate the classical characteristic signature of a FLR structure, with anti-sunward phase propagation. The anti-sunward phase propagation, along with the estimated relatively small m-value ($m \sim 12$), supports interpretation of an external driver as a source mechanism. One possible explanation is that the solar wind wave enters the magnetosphere on the dayside and propagates globally through the magnetosphere, possibly causing oscillations on the dawn flank as well. This is the first work in which an FLR oscillation has been shown to have been excited by a solar wind driven magnetopause oscillation at exactly the same discrete frequency. The result of this work sheds new light on our understanding of how the solar wind interacts with the magnetopause and how energy is transported across this boundary to produce FLRs deep inside the magnetosphere.

Chapter 5

A 2D ideal MHD model for ULF waves

5.A Equatorial MHD ULF wave model

This chapter presents results of a linear model for global scale MHD waves that is based on the set of linearized ideal MHD equations in a collisionless plasma [*Degeling et al.*, 2011]. The MHD model incorporates a background magnetic field model with the inclusion of day/night asymmetry and a parabolic magnetopause boundary. The rationale and motive for using the wave model is to diagnose whether the spatio-temporal analysis of the observations made in chapters 3 and 4 can be qualitatively reproduced. In order to do that, we consider two distinct cases: 1) where a localized monochromatic source along the model magnetopause boundary launches fast compressional waves mimicking a KH source mechanism scenario. 2) where a driver is applied at the day side noon-magnetopause that represents a direct source inherent in the solar wind. The objective is to investigate whether the observed ULF source mech-

anism and the resulting FLR structure can persist under a realistic magnetic field geometry and source location imposed by the model. In addition, this will provide an opportunity to qualitatively examine the difference in wave propagation behaviour inside the magnetosphere of a fast compressional wave launched from the magnetopause flanks, against those launched from within the solar wind region.

Comparison of perturbation amplitudes of waves with the background plasma and field parameters of CLUSTER measurements of Chapters 3 and 4 revealed that amplitudes are much less than the background values. Thus, waves can be considered as small perturbations and the linear MHD model approximation is justifiable; higher order terms can be dropped to a good approximation.

The modelling framework of *Degeling et al.* [2011] upon which this section is based, starts with linearized ideal MHD equations. In this regime, low frequency waves are describable by equations

$$\frac{\partial \vec{b}}{\partial t} = -\nabla \times \vec{E}, \tag{5.1}$$

$$\frac{1}{V_A^2}\frac{\partial \vec{E}}{\partial t} = (\nabla \times \vec{b})_\perp - \frac{\mu_o(\vec{J} \times \vec{b}) \times \vec{B}}{B^2} + \mu_o \vec{J}^{ext} \tag{5.2}$$

where $\vec{b}$ and $\vec{E}$ are first order perturbations in magnetic and electric field respectively, $\vec{J}$ is the background current density eminent in Ampere's law, V_A is the Alfvén speed of the plasma medium, and $\vec{J}^{ext}$ is a perpendicular current source term for launching monochromatic waves in the model.

In *Degeling et al.* [2011], the authors used the "box model" magnetic field geometry of *Zhu and Kivelson* [1988] to help them simplify the model. In other words, the treatment of the complexity in the shear Alfvén wave eigenfunctions along the magnetic field lines (equatorial polarizations) is simplified. That is, straight and constant magnitude magnetic field lines terminating at the conducting ionospheres are used everywhere in the wave model. The *Stern* [1985] model that is used allows gradients in $\vec{B}$ perpendicular to $\vec{B}$, such that $\vec{B_o} = B_o(x, y)\hat{z}$. This is an approximation of the equatorial magnetic field inside the magnetosphere, but gradients in the Alfvén speed perpendicular to the magnetic field facilitate energy transfer from the fast compressional mode into the field aligned shear Alfvén mode as in the linear theory of mode coupling. As the Alfvén wave is mainly influenced by the density and magnetic field in the vicinity of the equatorial plane, the model captures enough physics to allow a qualitative comparison with observations.

Employing a rectangular system of coordinates (x,y,z), and also assuming a magnetic field parallel to z and normal to the equator, with $\vec{B_o} = B_o(x, y)\hat{z}$ (*Stern* [1985] magnetic field model in the equatorial plane is used here), equations 5.1 and 5.2 in component form reduce to

$$\left(\frac{\partial^2}{\partial z^2} - \frac{1}{V_A^2}\frac{\partial^2}{\partial t^2}\right)\begin{pmatrix} E_x \\ E_y \end{pmatrix} = \frac{1}{B_o}\begin{pmatrix} -\partial/\partial y \\ \partial/\partial x \end{pmatrix}\left[B_o\left(\frac{\partial E_x}{\partial y} - \frac{\partial E_y}{\partial x}\right)\right] + \mu_o\frac{\partial}{\partial t}\begin{pmatrix} J_x^{ext} \\ J_y^{ext} \end{pmatrix} \tag{5.3}$$

Within the framework of the box model, all field aligned eigenfunctions

are decoupled, leading to linearly independent solutions, which along with conducting ionospheric boundary conditions, express the electric field, $\vec{E}$ as

$$\vec{E} = \vec{E}_n(x, y)cos(k_n z)e^{-i\omega t}, \tag{5.4}$$

where $k_n = n\pi/z_{fl}$, (n=1, 2,...) and z_{fl} is the field line length between the flat conducting surfaces (representing the north and south ionospheres). This description of the electric field reduces equation 5.4 to a pair of coupled elliptical partial differential equations for E_{nx} and E_{ny} which are solved by using the MATLAB two dimensional finite element method (FEM) solver of the Partial Differential Equation (PDE) toolbox. The FEM solver uses an adaptive mesh refinement technique. In regions where the source is located and the FLR is localized, the grids have been refined to scale sizes of about $0.03R_e$. In regions of no interest the the scale size is course and has a grid scale close to $1.2R_e$.

The singularity in the linear MHD equations in the simulation is avoided by assuming that ω of the driver frequency ($\omega = \omega_r - i\omega_i$) has small imaginary part with a sign that allows a solution that damps with time. The sign of ω_i is made negative such as to ensure energy transfer irreversibly. In regions of interest, this can be done by setting $\omega_i/\omega_r = 0.1$, which ensures damping in the form of finite ionospheric Pederson conductivity. Outside regions of interest, strong damping is introduced by setting $\omega_i/\omega_r >> 1$.

The details of the source of waves in the model is described as follows. The external current, $\vec{J}^{ext}$ (perpendicular to $\vec{B}$) that gives rise to ULF waves in

the model has the following functional form:

$$\vec{J}^{ext}(\vec{r},t) = A(t)Q(\vec{r})e^{-i(\vec{k}.\vec{r}-\omega t)}\hat{N}(\vec{r}) \tag{5.5}$$

where:

- $\vec{r}$ is the 2D position vector in the equatorial plane
- A(t) (scalar) is a time-dependent envelope amplitude
- Q($\vec{r}$) (scalar) describes the amplitude and spatial extent of the ULF wave source
- $\vec{k}$ is a wave vector for specifying any phase propagation in the source
- ω (scalar) is the wave frequency
- $\hat{N}$ is a unit vector specifying the direction of the source current

with A(t) and Q($\vec{r}$) defined by

$$A(t) = e^{-t/\tau_d}\left(1 - e^{-t/\tau_r}\right), \tag{5.6}$$

$$Q(\vec{r}) = Q(\lambda,\mu) = e^{-}\left(\left[\frac{\lambda^2 - {\lambda_o}^2}{(\Delta\lambda)^2}\right]^2 + \left[\frac{\mu^2 - {\mu_o}^2}{(\Delta\mu)^2}\right]^2\right), \tag{5.7}$$

where τ_d and τ_r are rise and decay time constants of the envelope function, and λ and μ are the coordinates defining the parabolic system as in *Stern* [1985]. With L being the length scale measured in Earth radii of the equatorial plane, note that (λ, μ) have dimensions of $L^{1/2}$. Defining x_o to be the locus of all the parabolas in this coordinate system, a point in the equatorial plane can

be described in rectangular coordinates (x, y) by $x - x_o = (\lambda^2 - \mu^2)/2$ and $y = \lambda\mu$. Here, $r^2 = x^2 + y^2$ defines distance to the center of the Earth from the origin, λ_o describes the magnetopause boundary in this paraboloid coordinate system, and μ_o is invoked for the purpose of defining the source parametrized by this system of coordinate, i.e., (λ_o, μ_o) is a point where the source of the wave is located.

The functional form of the terms in equation 5.5 depends on the specific scenario that is chosen. For example, for a magnetopause source, Q($\vec{r}$) has a 2D Gaussian profile described in the parabolic coordinate system used to define the magnetopause, such that the source is draped in a crescent shape following the magnetopause boundary (and has a defined thickness across the boundary). The unit vector $\hat{N}$ specifies the direction tangent to the magnetopause boundary in this case, and the wave vector is directed in the -x (anti-sunward) direction.

In mapping the ionosphere into the equatorial magnetospheric region, the magnetic field model of *Stern* [1985] is used. This model assumes a conducting paraboloid magnetopause and attempts to solve Laplace's equation in parabolic coordinates for a zero curl magnetic field corresponding to $\vec{B} = -\nabla\gamma$. The location and shape of the the model magnetopause boundary is approximated using typical values of the noon and the dawn/dusk meridian and are set to 10 R_e and 15 R_e, respectively.

Figure 5.1a shows the the equatorial magnetic field profile used in the model. The equatorial plasma density inside and outside the plasmapause is based on a parametric model where a power law scaling with L-shells is

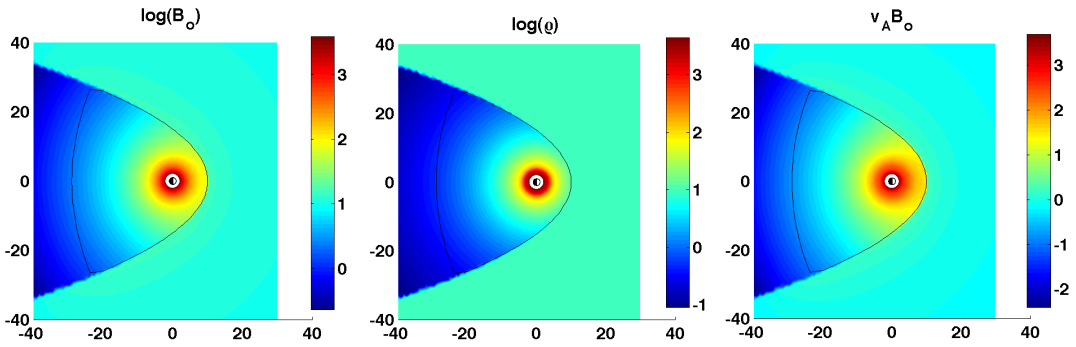

Figure 5.1: The equatorial plane view of the ULF wave model and input parameter profiles of: a) magnetic field strength; b) plasma density; c) Alfvén speed times B_o. Here the solid parabolic line signifies the model magnetopause.

employed as in *Degeling et al.* [2011]. The density across the width of the plasmapause or transition region is specified by smoothly joining the model solutions from inside to outside the plasmapause. In this study, we considered inner and outer edges of the plasmapause to be located at L-shells of $L = 3$ and $L = 6$, with plasma density $\rho = 1200$ and $\rho = 20$ amu/cm^3 where scaling powers of $n = -2$ and $n = -1$ respectively are used at these edges. Figures 5.1b and 5.1c also show the equatorial plasma density and Alfvén velocity profiles used in this model. Because of the fact that the density gradient across the plasmapause is weak, the radial profile in the Alfvén speed lacks the expected bump across the transition region. This results in a decrease in the radial profile of the local Alfvén frequency gradient with radial distance. Subsequently, for a monochromatic MHD fast wave driver launched from outside the magnetosphere, coupling with the standing shear Alfvén mode to produce a FLR is

the ultimate expectation. The strongest coupling occurs when the frequency of the fast mode matches the standing shear Alfvén wave frequency. In the following two sections, the linear and ideal 2D model for global scale MHD waves in the equatorial plane will be studied by constraining the characteristics of the ULF wave source mechanisms.

5.B FLRs driven by a dawn-dusk flank magnetopause source

In this section, a localized MHD fast compressional wave with a frequency of 1.7 mHz that mimics a KH wave source scenario is launched along the magnetopause boundary. The driver frequency is imposed on an external oscillating current directed along the flank magnetopause and perpendicular to the meridional plane containing the magnetic field. Defining the external current in this way introduces displacement in the meridional plane which is the characteristic feature of a MHD fast wave mode propagating both inward and outward from the magnetopause. A driver defined in such a manner helps to reasonably model a source launched from the dayside flank magnetopause in characterizing FLR wave structures such as those observed by the Kodiak and Goose Bay HF radars in Chapter 3.

Figures 5.2 and 5.3 show the ULF wave model outputs of the ratio of the wave magnetic field to the background field, the radial and azimuthal electric fields for a source located at the flank magnetopause to make model predictions for the areas where pulsations could have been observed by the Kodiak

and Goose Bay radars. In this scenario, $b_z/B_o \approx 0.3$ is considered because we are working on the linear MHD regime where small scale perturbations are assumed from the outset. The white dashed lines are the traces of the field line mapping from the ionosphere (Kodiak's and Goose Bay's field of views in the dusk and the morning sectors, respectively) to the outer parts of magnetosphere. Notable in both figures is the down-tail propagation direction of the wave phase as indicated by the direction of the change in phase from positive to negative, radially localized large amplitude wave power along with a phase change (decreasing radially outward) of close to π radians across the peak in E_r, and the absence of azimuthally localized large amplitude wave power in E_ϕ. These interesting features will be explained in detail in section 5.E.

5.C FLRs driven by a source placed on the dayside noon-magnetopause

In this section, we consider the effect of exciting a wave that decays evanescently from the dayside noon-magnetopause. Once again, a monochromatic source is defined in a manner similar to the previous section, but placed on the dayside noon-magnetopause. The frequency of the MHD fast mode driver is taken to be 2.5 mHz to mimic our observation of the Saskatoon HF radar in Chapter 4. The objective here is to compare the effect of exciting an evanescent wave from the dayside noon-magnetopause with the spatio-temporal FLR structures observed by the Saskatoon HF radar that resulted from a solar wind driven magnetopause oscillation in Chapter 4.

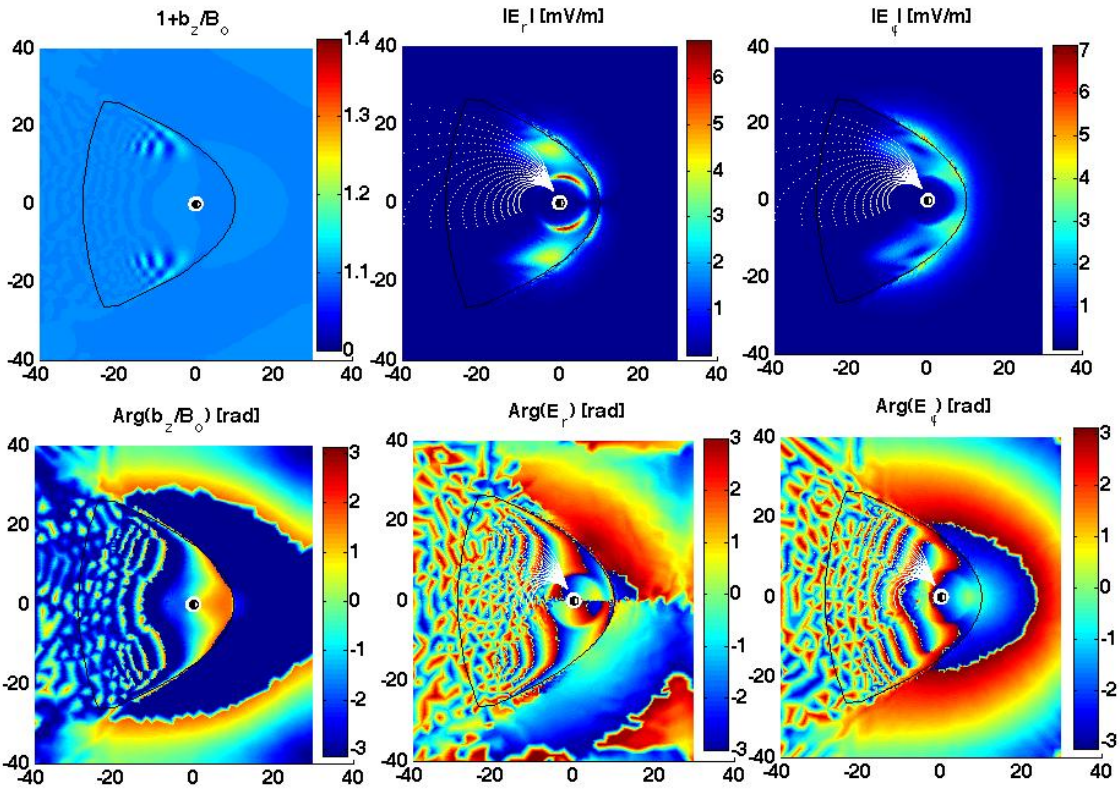

Figure 5.2: The amplitude (top) and phase (bottom) of ULF wave model outputs for a 1.7 mHz wave source launched from the dawn-dusk flanks. a) the ratio of the wave magnetic field to the background field, $1 + b_z/B_o$ b) radial, E_r and c) azimuthal, E_ϕ electric fields in mV/m. The white dashed lines represent the field line mapping from Kodiak's field of view in the dusk sector to the equatorial magnetosphere. Note: The X- and Y- axes are in units of R_e.

Figure 5.4 shows the ULF wave model outputs of the ratio of the wave magnetic field to the background field, the radial and azimuthal electric fields for a source placed on the noon-magnetopause. In this situation, $b_z/B_o \approx 0.3$ is again considered. The white dashed lines are traces of the field line mapping from the ionosphere (Saskatoon's field of view between dawn and midnight) to the equatorial magnetosphere.

Notable from Figure 5.4 is the down-tail propagation of the phase of the

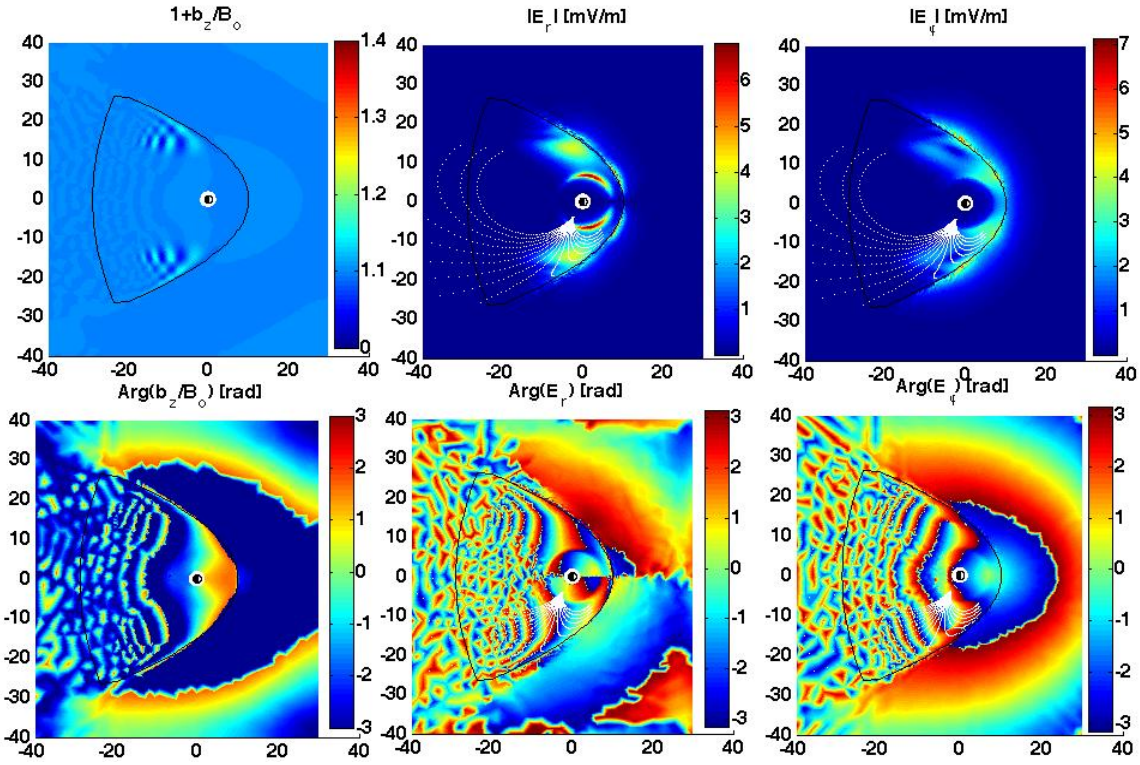

Figure 5.3: The amplitude (top) and phase (bottom) of ULF wave model outputs for a 1.7 mHz wave source launched from the dawn-dusk flanks. a) the ratio of the wave magnetic field to the background field, $1 + b_z/B_o$ b) radial, E_r and c) azimuthal, E_ϕ electric fields in mV/m. The white dashed lines represent the field line mapping from Goose Bay's field of view in the dawn sector to the equatorial magnetosphere. Note: The X- and Y- axes are in units of R_e.

driver wave, the penetration of wave power across the dayside magnetopause, a radially localized large amplitude wave power in E_r, and the absence of radially localized wave power along with a phase change of close to π radians across the peak in E_r. Direction of propagation of the phase of the driver wave is also shown to be down-tail in Figure 5.4. These interesting features will also be discussed in detail in section 5.E.

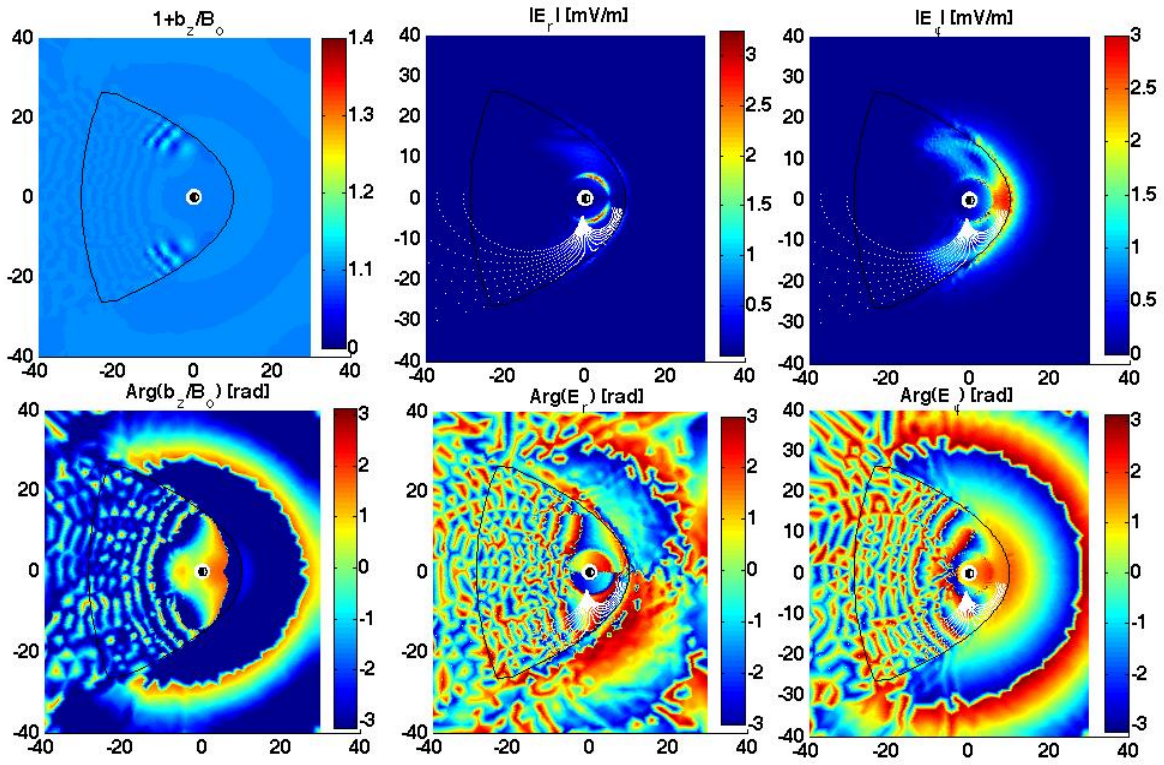

Figure 5.4: The amplitude (top) and phase (bottom) of ULF wave model outputs for a 2.5 mHz wave source launched from the dayside noon magnetopause. a) the ratio of the wave magnetic field to the background field, $1 + b_z/B_o$ b) radial, E_r and c) azimuthal, E_ϕ electric fields in mV/m. The white dashed lines represent the field line mapping from Saskatoon's field of view in the morning sector to the equatorial magnetosphere. Note: The X- and Y- axes are in units of R_e.

5.D Spatial and Temporal Characteristics of a ULF wave Source

Depending on the source a fast compressional wave mode might decay spatially inwards from the magnetopause or propagate radially into the magnetosphere. This section investigates this subject from the stand point of an MHD model for ULF waves. For both source mechanisms, once the compressional wave

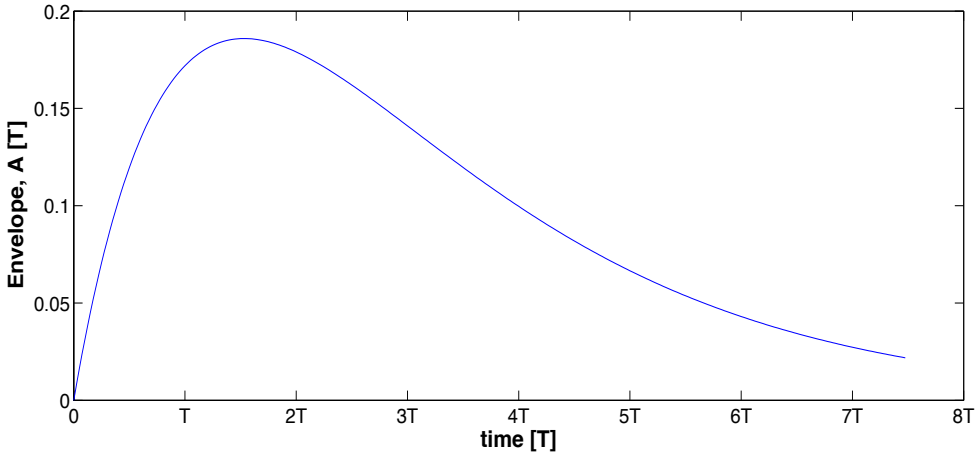

Figure 5.5: The temporal evolution of a time-dependent envelope amplitude as a function of wave period (T = 9.8 min) for a source launched from the flank magnetopause.

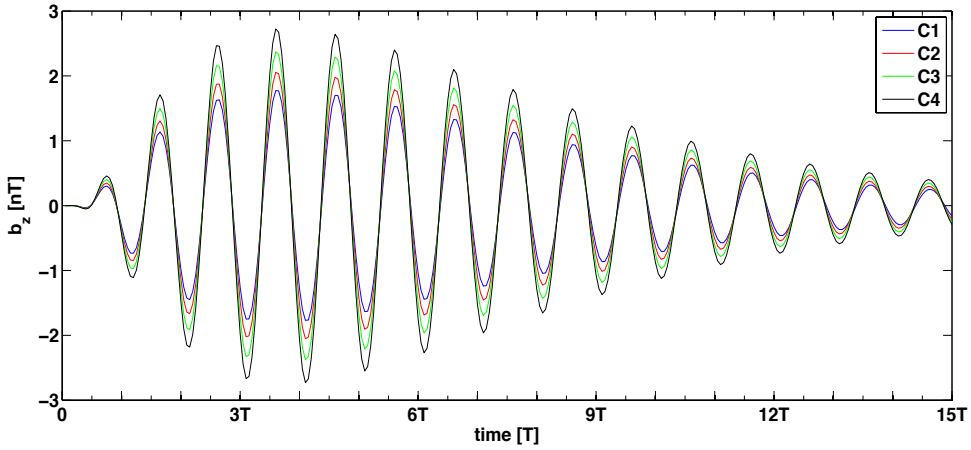

Figure 5.6: The spatial and temporal evolution of a model ULF wave source magnetic field b_z inside the magnetosphere for the case where the source is located at the magnetopause flank. Points C1 through C4 represent multi-point measurements from stationary synthetic spacecrafts. Note that C4 is the closest to the magnetopause while C1 is the furthest away from the magnetopause (closest to the Earth) in the radial direction to the flank magnetopause. Notable here is the spatial evanescent penetration of the fast compressional mode.

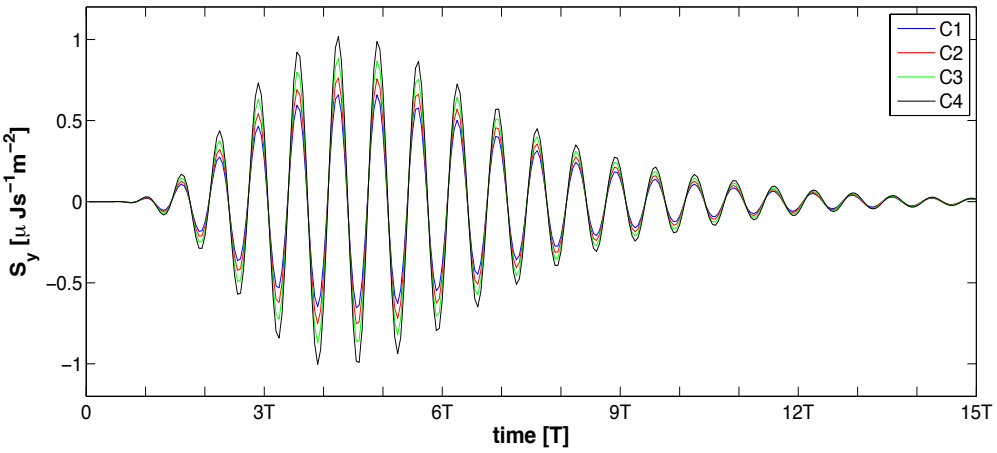

Figure 5.7: The spatial and temporal evolution of a model fast compressional wave radial energy transport S_y through the magnetosphere for the case where the source is located at the magnetopause flank. The points C1 through C4 represent multi-point measurements from stationary synthetic spacecrafts. Notable here is the radial evanescent penetration of the driver wave.

has made its way into the magnetosphere, we will try to distinguish between KHI generated and noon-magnetopause evanescent waves by using stationary multi-point measurements representing synthetic spacecrafts. Then, comparisons will be made between the results of the model and the observations made in Chapters 3 and 4.

In examining the spatial and temporal characteristics of compressional ULF wave power using the ULF wave model, we placed 4 probes into the simulation at various positions. Placing these probes at the radial locations C1 (farthest from the flank magnetopause, and nearest to the Earth) through C4 (nearest to the magnetopause, and farthest from the Earth) across the magnetopause flank provides an opportunity to examine the propagation time delay in the wave phase and the radial Poynting flux profile. The probes C1 through C4

are placed at (8.25, 8.5, 8.75, 9)R_e along the line joining the center of the Earth to the dusk flank magnetopause.

Figure 5.5 shows the temporal evolution of the time-dependent amplitude (equation 5.6) of a wave that is launched in the vicinity of the flank magnetopause. The horizontal axis is in units of the wave period. Figure 5.6 shows the wave signature of a 1.7 mHz driver wave launched from the dusk flank magnetopause as measured from the location of the probes. As can be seen from the color-coded overlay of Figure 5.6, the evanescence of the wave's parallel magnetic field b_z is seen in traversing from C4 (closest to the magnetopause) to C1 (farthest to the magnetopause). Figure 5.7 also shows a color-coded overlay of the radial Poynting flux profile, S_y. Notable is the evanescent barrier penetration of the 1.7 mHz (flank magnetopause driver) wave energy in the radial direction, i.e. the amplitude is decreasing as one moves away from the magnetopause. This characteristic feature of decay in the radial Poynting flux profile is the feature that we observed for a flank magnetopause driver in Chapter 3. It is also interesting to note that b_z, S_y inside the magnetosphere, and S_y at the location of the resonance (Figure 5.8) almost follow the time evolution of the envelope profile of Figure 5.5. This implies that the resonance is driven only when the source exists. Similar results are found when the source is launched from the dayside-noon magnetopause.

In this study, it has been found that once the source has made its way into the magnetosphere, analysis did not distinguish between KHI-like and dayside noon-magnetopause drivers (figure not shown). This conclusion is drawn due to the fact that the wave amplitudes from the model in both cases were found to decay spatially as one traverses earthward from the magnetopause flank. This

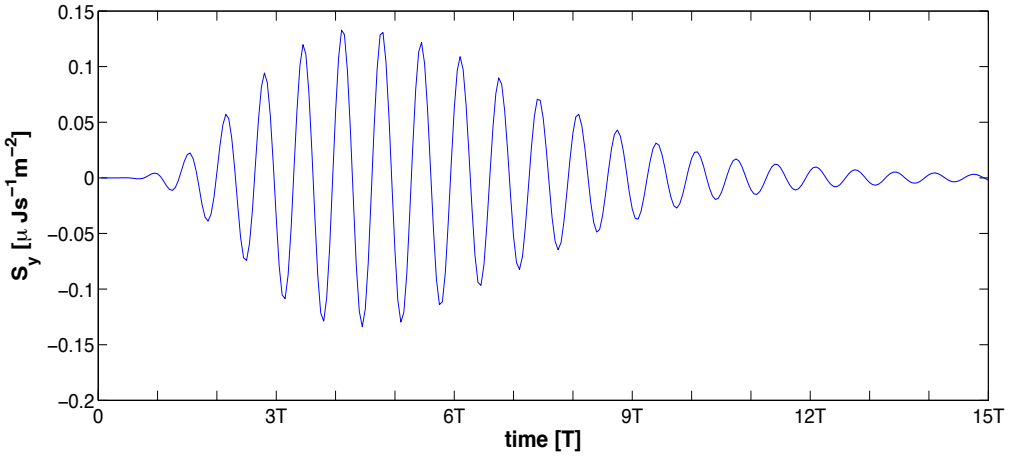

Figure 5.8: The temporal evolution of the component of the Poynting flux along y (S_y) as a function of wave period ($T = 9.8$ min) for a source launched from the flank magnetopause at the location of the resonance, $y \sim 6.2R_e$.

is not surprising since in both cases the same source generation method was used in the model. Although evanescence is found to be observationally true for a KH driven surface mode (on the magnetosheath side of the boundary), it was not possible to examine this scenario experimentally in the magnetospheric side of the boundary for the spacecraft were located outside the boundary in the time interval considered.

5.E Discussion of the ULF Wave Model

Evident from Figures 5.2, 5.3 and 5.4 are the down-tail (anti-sunward) propagation of an oscillatory driver wave towards the nightside and the radial evanescent plasma penetration of the driver wave electric field. The direction of propagation of the driver wave is consistent with the Kodiak and Goose Bay HF radar observations and the evanescent barrier penetration is in agreement with CLUSTER observation of Chapter 3. Figure 5.4 also shows the evanes-

cent penetration of the wave electric field through the dayside magnetopause for a solar wind like driver.

The FLR structures which are characteristic signatures of mode coupling between the fast compressional driver wave and the shear Alfvén mode are also clearly discernible in both cases. As expected, the FLRs from both source mechanisms are localized at constant L shells and are evident from the enhancement of the radial electric field along with a phase change of π radians across the peak in electric field. The lack or weak FLR signatures in the azimuthal component of the electric fields suggest a relatively small-m toroidal FLR event where the driver could be located from external to the magnetosphere, which actually is the situation for both cases at hand (from our observations of Chapters 3 and 4, m $\sim$10 and 12, respectively). The ULF wave model employed here has qualitatively reproduced the spatio-temporal features of the observations made by the Kodiak and Goose Bay HF radars in Chapter 3 and the Saskatoon HF radar in Chapter 4. Comparison of the FLR structures from both cases clearly demonstrate that when the source is located on the dayside noon-magnetopause, the FLR peak location tends to move towards the local noon as expected than when the source is located at the magnetopause flank. This is strong evidence that the accessibility of the driver wave power at a given frequency inside the magnetosphere is dependent on the Magnetic Local Time (MLT) location of the driver wave, which in turn determines the location of the FLR mode coupling.

The localization of the source mechanisms in the model representing a source along the flank magnetopause (section 5.B) and a dayside noon mag-

netopause (section 5.C) appeared to have qualitatively reproduced the FLR structures in Chapters 3 and 4, respectively. The one case (section 5.B) corresponds to the observation in Chapter 3, the other case (section 5.C) corresponds to a scenario where the solar wind driven magnetopause oscillation is replicated by a dayside noon-magnetopause evanescent driver in Chapter 4. In addition to that, the spatio-temporal characteristics of the model FLRs are found to be in good agreement with the observed FLRs and their suggested source mechanisms. Given that the model does not have a solar wind in it, it does not provide an understanding of how the solar wind interacts with the magnetopause. It also does not deal with energy transport across the boundary. It however provides information on how the wave behaves once inside the magnetosphere when generated at different locations on the magnetopause.

Chapter 6

Conclusions

ULF waves in the Earth's magnetosphere are considered to be electromagnetic (em) wave disturbances with frequencies in the mHz range. Particularly, those wave processes in the range between the lowest a magnetospheric cavity mode oscillation can support (the scale size of the magnetosphere $\sim$ 1 mHz) to the natural plasma frequency and the ion gyro-frequency ($\sim$ 1 Hz) are of interest to magnetospheric physics. Much of our focus in this thesis was on the so-called Magneto-hydro-dynamic (MHD) waves, and also on the special class of them referred to as geomagnetic pulsations. In contrast to MHD waves, the term "ULF waves" is broader and should be used with caution since it refers to all electromagnetic disturbances in the same frequency range. ULF also includes waves of non-MHD origin such as magnetic signals in the ionosphere generated by acoustic processes and atmospheric electromagnetic waves *Pilipenko* [1990].

The mechanism of how standing MHD Alfvén waves are excited has been a subject of much study for decades. Despite decades of intense work on theory, numerical modelling and data analysis from coordinated ground and in-situ

space-based instrumentation, the discrete nature of the source of oscillations driving these FLRs remains unexplained. Potential driving mechanisms include: Kelvin Helmholtz Instability (KHI) surface waves on the magnetopause, magnetospheric waveguide/cavity modes driven by a pressure pulse in the solar wind and a direct driving via entry of the solar wind MHD waves across the magnetopause.

Although there is observational evidence in support of the hypothesis that both pressure pulses in the solar wind and direct entry of MHD waves driving FLRs across the magnetopause, to date no solid observational evidence has been presented to prove or disprove the existence of KHI generated surface waves and/or magnetospheric boundary perturbations/oscillations as drivers of FLRs. Previous work suggests a KHI generated surface wave as a source mechanism based on upstream solar wind conditions such as: very high flow speed, direction of the IMF Bz (positive) and absence of monochromatic and quasi-periodic oscillations in the solar wind. These conditions are insufficient to be presented as compelling evidence for a KHI source. An in-depth investigation of ULF wave activity near the magnetopause is therefore imperative to improve our understanding of magnetopause generated waves as drivers of standing geomagnetic Alfvén waves and the physical interrelationships between them. It was the very objective of this thesis to regard or disregard these boundary instabilities/oscillations as drivers based upon substantial multi-point observations of ULF waves near the magnetopause and deep inside the magnetosphere using data from both ground and space-based instrumentation. Results from observations were then compared with a 2D ideal MHD model for ULF waves to see if the spatio-temporal features of the observations can

be qualitatively reproduced.

Given proper spacecraft orientation and trajectories, the CLUSTER multi-satellite mission offered opportunities to observe plasma boundary instabilities/oscillations. This allowed a much better characterization of magnetopause instability and/or oscillation. This mission provided a direct means to accurately measure magnetic field and plasma velocity that was used to investigate the radial energy profile of a KHI generated magnetopause surface wave or boundary oscillation. This provided a reliable means of identifying time varying boundary wave processes such as magnetopause instability and oscillation.

Publicly available data from solar wind monitors such as ACE, WIND, OMNI and GEOTAIL were also used to characterize upstream solar wind conditions. Multi-point observation of ULF waves were important and fundamental to fully diagnose magnetospheric ULF waves excited during times of magnetopause oscillation and instability. Ground-based SuperDARN observations were substantially used in conjunction with the CLUSTER multi-satellite mission and were found to be ideally suited to monitor the spatio-temporal evolution of the ionospheric signatures of these wave activities. The studies that were undertaken in this thesis were also augmented by analysis of data from other satellite missions such as POLAR, GOES and GEOTAIL whenever appropriate and possible. Data from the array of ground-based magnetometers such as CARISMA, CANOPUS and IMAGE were an integral part of this study too.

In this thesis, three different ULF wave events were analyzed and char-

acterization of the wave process was made. Analysis was made using data from coordinated and simultaneous measurements from HF radars, optical instrumentation, ground-based magnetometers and in-situ satellite-based instrumentation. A global ULF wave model was also used to qualitatively reproduce the spatio-temporal features of the FLRs in response to a KHI-like driver and a solar wind driven magnetopause oscillation.

Chapter 2 presented a unique event where a completely new feature of phase coherence on open field lines at exactly the observed resonant frequency (0.8 mHz) was exhibited. There are a number of key results presented in chapter 2 which justify novelty. First, this is one of the few observations of MHD driver wave on open field lines by SuperDARN. MHD waves in the outer magnetosphere which couple to FLRs are seldom observed and this is one of only a few ground based observations of the driver wave. Second, the observation demonstrates that SuperDARN has the capability to monitor MHD wave transmission across the magnetopause and through the outer regions of the magnetosphere. Third, the observation that the FLR and driver wave on open field lines are directly driven by a discrete oscillation in the solar wind is important. Discrete ULF oscillations in the solar wind as direct drivers of ULF waves in the magnetosphere is a controversial topic. These results add to the growing body of evidence in support of direct solar wind drivers of ULF waves. Finally, the observation of first and second order harmonic FLRs in SuperDARN data is a unique observation. The observation of first and second order harmonic FLRs in SuperDARN data supports the theoretical body of work on expected behaviour of FLRs, and their potential use in estimating magnetospheric properties such as density and magnetic topology.

The observation in Chapter 3 focused on the characterization of magnetopause boundary instability and a global ULF wave mode in the magnetosphere, with the ultimate goal of elucidating the causal relationship between the two. In this study, we analyzed a ULF wave event and characterized the observations with simultaneously coordinated measurements from HF radars, multi-satellite-borne instrumentation and ground-based magnetometers. The simultaneous presence of data from various instrumentation offered a unique opportunity to diagnose the properties of the observed ULF wave in different parts of the magnetosphere and identify a plausible source mechanism at the boundary. In this event, we observed a clear wave activity in electric, magnetic, density and plasma flow data outside the magnetopause using CLUSTER data and compared it with fluctuations inside the magnetosphere, at ionospheric altitudes and on the ground. Comparisons clearly revealed that ULF fluctuations at the magnetopause coincide with the discrete frequency oscillations observed by HF radars, magnetometers and spacecrafts inside the magnetosphere.

The decay in the outward-directed electromagnetic Poynting vector and the propagation time delay in the phase of the driver wave radially outward from the magnetopause along with the underlying upstream solar wind conditions of strong northward IMF and supersonic flow exceeding 640 km/s, solidly point to a KHI generated surface mode as a sole mechanism driving the observed global ULF wave activity. The fact that we have observed a relatively small azimuthal wavenumber, $m = 10$, with anti-sunward phase propagation in both dusk and dawn sectors along with the absence of monochromatic dy-

namic pressure variations or solar wind buffeting is further evidence to support the hypothesis of a KHI generated surface mode as a source mechanism. The result of this work demonstrates a well-defined path of energy transfer from the magnetopause into the inner magnetosphere, and ionosphere, and is reliable evidence for magnetosphere-ionosphere coupling. Analysis showed that the observation is consistent with the theory of a KHI driven FLR. This observation provided evidence on how the global nature of MHD waves combines two areas of study: magnetopause instability and magnetosphere-ionosphere coupling.

Chapter 4 presents another case study where a solar wind driven magnetopause oscillation is found to excite an FLR at 2.5 mHz deep inside the magnetosphere. In this chapter, a quasi-periodic 2.5 mHz discrete wave oscillations in B_y is observed in the solar wind and the multi-spacecraft CLUSTER mission at the dusk flank magnetopause is used to fully characterize the wave's imprint near the dusk-sector magnetopause. Interestingly, the OMNI derived bow shock location was found to have a discrete frequency oscillation of 2.5 mHz along the sun-earth line. A detailed analysis of this wave at the dusk flank magnetopause has been carried out and showed an intriguing feature in the radial energy profile. The outward propagation direction of the Poynting flux, S_x, is explained in terms of the relative phase difference of E_y and B_z. Furthermore, the fact that the Z-component of the Poynting vector is dominant is suggestive of a standing Alfvén wave driven at the magnetopause. Plasma and field measurements at the boundary have shown unambiguous signatures of magnetopause oscillation at a 2.5 mHz discrete frequency.

Also worth discussing from the event in Chapter 4 is, the fact that the SuperDARN Saskatoon radar located in pre-dawn sector demonstrated a very clear and unambiguous characteristic footprint of an FLR oscillation at the same discrete frequency, 2.5 mHz. The observed anti-sunward phase propagation within the field of view of Saskatoon is consistent with an external source mechanism, the solar wind-driven magnetopause oscillation in this case. With the help of coordinated multi-instrumentation inside and outside magnetosphere, the following conclusion can be drawn. A discrete frequency oscillation in the solar wind B_y is found to drive a magnetopause oscillation resulting in the spatio-temporal features of the observed discrete frequency FLR at 2.5 mHz by the Saskatoon HF radar. This is the first observational work that has shown an FLR oscillation be excited by a solar wind driven magnetopause oscillation.

Furthermore, the success of the *Degeling et al.* [2011] ideal MHD model for ULF waves used in this thesis was fairly successful in explaining the ground-based FLR observations. The main aim of the model was to qualitatively reproduce the the spatio-temporal structures of the observations made in Chapters 3 and 4. The model used was a 2D ideal MHD numerical model for ULF waves in the equatorial plane intended to mimic a monochromatic wave source launched at the flanks of the magnetopause for the observation in Chapter 3. For Chapter 4, the model was run in such a way that a monochromatic driver wave was launched from the dayside noon magnetopause and comparison was made with the solar wind-driven magnetopause oscillation. Interestingly, in both cases, the ULF wave model qualitatively reproduced the spatio-temporal structures of observations made by the SuperDARN HF radars. That is, the

detected radial and azimuthal structure of the FLR wave activities of both the observations and the model have been found to be localized in L-shells and exhibit the theoretically expected structures in the FLR regions. This implies the source parameters represented in the model can approximately mimic the sources represented and are in agreement with the hypothesis that the observed FLRs may be driven by a KH instability and a solar wind driven magnetopause oscillation for Chapter 3 and 4, respectively.

In employing the ideal 2D model for ULF waves, comparison of the FLR structures from both source locations clearly demonstrated that when the source is located at the dayside noon-magnetopause, the FLR location moved slightly towards the local noon compared to when the source is located at the flank magnetopause. This demonstrates that the accessibility of the driver wave power at a given frequency inside the magnetosphere is dependent on the MLT location of the driver, which in turn determines the ultimate location of the FLR.

Insight into how a fast compressional wave behaves inside the magnetosphere can be found from the results of the ULF wave model in this thesis. Depending on the source the fast compressional driver wave may decay spatially earthward from the magnetopause or propagates radially into the magnetosphere. The ULF wave model has shown that once the source has crossed the magnetopause, analysis was incapable of distinguishing between a KHI-like driver and a noon-magnetopause driver (proxy to a solar wind driver). It has been found that the model wave amplitudes for both cases were found to decay spatially as one moves earthward from the magnetopause. This is proven to

be observationally true in this case study for a KHI driven surface mode (on the magnetosheath side of the boundary). It however was impossible to examine this scenario experimentally for a solar wind driven source mechanism, because during the time period of interest the spacecrafts were located inside the magnetopause boundary.

The primary goals of this thesis have been achieved. Observational evidence consistent with a 2D global ULF wave model is found to be in good agreement with the main features of the theory for drivers launched from the boundary. This study has demonstrated how the global nature of MHD waves combines two areas of study: magnetopause instability/oscillation and magnetosphere-ionosphere coupling. The results of this thesis help to clarify and extend our understanding of the ULF wave source mechanism, propagation and coupling in the terrestrial magnetosphere. It has provided a better understanding of a KHI-like source mechanism, a source inherent in the solar wind, and a solar wind driven magnetopause oscillation, in the excitation of FLRs. This gets us one step closer to fully understanding the dynamics of the magnetosphere and the physical interrelationship between the magnetosphere and ULF waves.

Future studies are encouraged as a continuation of this work to investigate wave transmission across the magnetopause boundary using SuperDARN, in order to examine whether the event reported in Chapter 1 is a common occurrence in the magnetosphere.

Bibliography

Allan, W., and F. B. Knox (1978), A dipole field model for axissymmetric Alfven waves with finite ionosphere conductivities, *Planet. Space Sci.,* (27), 79-85.

Allan, W., and E. M. Poulter (1992), ULF waves-their relationship to the structure of the Earth's magnetosphere, *Rep. Prog. Phys.,* (55), 533-598.

Baker, K. B., and S. Wing (1989), A New Magnetic Coordinate System for Conjugate Studies at High Latitudes, J. Geophys. Res., (94), 9139-9143.

Baker, K. B. (1995), HF radar signatures of the cusp and low-latitude boundary layer, *J. Geophys. Res.,* (100), 7671-7695.

Baker, D. N. (1998), Coronal mass ejections, magnetic clouds, and relativistic magnetospheric electron events: ISTP, *J. Geophys. Res.,* (103), 17279-17291.

Blanchard, G. T, L. R. Lyons, and J. C. Samson (1997), Accuracy of using 6300 A^o auroral emission to identify the magnetic separatrix on the night side of the Earth, *J. Geophys. Res.,* 102, 9697-9703.

Boakes, P. D. (2008), On the use of IMAGE FUV for estimating the latitude of the open/closed magnetic field line boundary in the ionosphere, *Ann. Geophys.,* (26), 2759-2760.

Brittnacher, M., M. Fillingim, M. Parks and J. Spann (1999), Polar cap area and boundary motion during substorms, *J. Geophys. Res.,* (104), 12251-12262.

Buneman, O. (1963), Excitation of field aligned sound waves by electron streams, *Phys. Rev. Letts.*, (10), 285-287.

Chapman, S., and V. C. A. Ferraro (1931), A new theory of magnetic storms, *Nature,* (126), 129-130.

Chen, L., and A. Hasegawa (1974), A theory of long-period magnetic pulsations, 1, Steady excitation of field line resonances, *J. Geophys. Res.,* (79), 1024-1032.

Chisham, G., and M. P. Freeman (2004), A statistical comparison of SuperDARN spectral width boundaries and DMSP particle precipitation boundaries in the nightside ionosphere, *Geophys. Res. Lett.,* (31), L02804, doi:10.1029/2003GL019074.

Claudepierre, S. G., S. R. Elkington, and M., Wiltberger (2008), Solar wind driving of magnetospheric ULF waves: Pulsations driven by velocity shear at the magnetopause, *J. Geophys. Res.,* (113), 6343-6353.

Couzens, D. (1985), ISEE Particle Observations of Surface Waves at the Magnetopause Boundary Layer, *J. Geophys. Res.,* (90), 6343-6353.

Degeling, A. W. (2008), Drift resonant generation of peaked relativistic electron distributions by Pc 5 ULF waves, *J. Geophys. Res.,* (113), A02208, doi:10.1029/2007JA012411.

Degeling, A. W., R. Rankin, and S. R. Elkington (2011), Convective and diffusive ULF wave driven radiation belt electron transport, *J. Geophys. Res.,* (116), A12217, doi:10.1029/2011JA016896 .

De Keyser, J. (2002), Trying to bring the magnetopause to a standstill, *Geophys. Res. Lett.,* 29, doi:10.1029/2002GL015001.

De Keyser, J., and M. Roth (2003), Structural analysis of periodic surface waves on the magnetosphere boundary, *Planet. Space. Sci.,* 51, 757-768.

De Pontieu, B. (2007), Chromospheric alfvnic waves strong enough to power the solar wind, *Science,* 318, 5886, 1574-1577.

Dobias, P., I. O. Voronkov, and J. C. Samson (2004), On nonlinear plasma instabilities during the substorm expansive phase onset, *Phys. Plasmas,* 11, 2046-2053, doi: 10.1063/1.1695357.

Dungey, J. W. (1956), Convective diffusion in the equatorial F region, *J. Atmos. Terr. Res.,* (9), 304-310.

Dungey, J. W. (1954), *Ionosphere Research Laboratory Report*, (69) (Pennsylvania State University).

Dungey, J. W. (1967), Hydromagnetic waves, *in Physics of Geomagnetic Phenomena*, vol. 2, edited by S. Matsushita and W. H. Campbell, pp. 913-934, Academic, San Diego, Calif.

Eastman, T. E. (1976), The magnetopsheric boundary layer - Site of Plasma, momentum and energy transfer from the magnetosheath into the magnetosphere, *Geophys. Res. Lett.,* 3, 685-688.

Eastman, T. E, B. Popielawska, and L. A. Frank (1985), Three-dimensional plasma observations near the outer magnetopsheric boundary, *J. Geophys. Res.,* (90), 9519-9539.

Elkington, S. R, M. K. Hudson, and A. Chan (1999), Acceleration of relativistic electrons via drift-resonance interaction with toroidal-mode Pc-5 ULF oscillations, *Geophys. Res. Lett.,* 26, 3273, doi:10.1029/1999GL003659.

Elkington, S. (2006), A review of ULF interactions with radiation belt electrons, in Magnetospheric ULF Waves: Synthesis and New Directions, *Geophys. Monogr. Ser., vol. 169, AGU, Washington, D. C.*

Eriksson, S. (2005),On the generation of enhanced sunward convection and transpolar aurora in the high-latitude ionosphere by magnetic merging, *J. Geophys. Res.,* (110), A11218, 27, doi:10.1029/2005JA011149.

Fairfield, D. H. (2000), Geotail observations of the Kelvin-Helmholtz instability at the equatorial magnetotail boundary for parallel northward fields, *J. Atmos. Terr. Phys.,* (71), 1677-1680.

Farley, D. T. (1963), A plasma instability resulting in field-aligned irregularities in the ionosphere, *J. Geophys. Res.*, (68), 6083-6097.

Farrugia, C. J., F. T. Gratton, J., Contin,C. C. Cocheci, R. L. Arnoldy, K. W. Ogilvie, R. P. Lepping, G. N. Zastenker, M. N. Nozdrachev, A. Fedorov, J. A. Sauvaud, J. T. Steinberg, G. Rostoker (2000), Coordinated

wind: Interball-Tail, and ground observations of Kelvin Helmholtz waves at the near tail, equatorial magnetopause at dusk: January 1997, *J. Geophys. Res.,* (105), 7639-7667.

Fejer, J. A. (1964), Hydromagnetic stability at a fluid velocity discontinuity between compressible fluids, *Phys. Fluids* (7), 499-503.

Fejer, B. G., R. W. Reed, D. T. Farley, W. E. Swart and M. C. Kelley (1984), Ion Cyclotron Waves as a Possible Source of Resonant Auroral Radar Echoes, *J. Geophys. Res.* (89), 187-194.

Fejer, B. G., and M. C. Kelley (1980), Ionospheric irregularities, *Reviews of Geophysics and Space Physics,* (18), 401-454.

Fenrich, F. R., and J. C. Samson (1997), Growth and decay of field line resonances, *J. Geophys. Res.,* (102), 20031-20039.

Fenrich, F. R. (1997), *The field line resonance: Observation and Theory*, PhD. Thesis.

Fenrich, F. R., and C. L. Waters (2008), Phase coherence analysis of a field line resonance and solar wind oscillation, *Geophys. Res. Lett.,* (35), L20102, doi:10.1029/2008GL035430.

Fenrich, F. R., J. C. Samson, G. Sofko, and R. A., Greenwald (1995), ULF high- and low- m field line resonances observed with Super Dual Auroral Radar Network, *J. Geophys. Res.,* (105), 21159-21173.

Ferraro, V. C. A. (1960), The theory of magnetic storms and auroras, *Nature,* (167), 92-94.

Greenwald, R. A. (1985), An HF phased-array radar for studying small scale structure in the high-latitude ionosphere, *Radio science,* (20), 63-79.

Greenwald, R. A. (1995), DARN/ SuperDARN A global view of the dynamics of high-latitude convection, *Space Sci. Rev.,* (71), 773-795.

Gurnett, D., and A. Bhattachajee(2005), *Introduction to Plasma Physics With Space and Laboratory Applications*, Cambridge University Press, Cambridge.

Gustafsson, G. (1992), A revised corrected geomagnetic coordinate system for Epochs 1985 and 1990, *J. Atmos. Terr. Phys.,* (54), 1609-1631.

Hasegawa, A. (1969), Drift Mirror Instability in the Magnetosphere, *Phys. Fluids,* (12), 2642-2650.

Hasegawa, A. (1975), *Plasma Instabilities and Nonlinear Effects*, Springer, New York.

Hasegawa, H. (2004), Transport of solar wind into Earth's magnetosphere through rolled-up Kelvin-Helmholtz vortices, *Nature* (430), 755-757.

Hollweg, J. V., and P. A. Isenberg (2003), Generation of the fast solar wind: A review with emphasis on the resonant cyclotron interaction, *J. Geophys. Res.,* 107, 1147, doi:10.1029/2001JA000270.

Hones, E. W. (1972), Measurements of magnetotail plasma flow made with Vela 4B, *J. Geophys. Res.,* (77), 5503-5522.

Hosokawa, K. (2010), Reorganization of polar cap patches through shears in the background plasma convection, *J. Geophys. Res.* (115), A01303, doi:10.1029/2009JA014599.

Hughes, W. J. (1983), Hydromagnetic waves in the magnetosphere. In: Carovillano, R. L., Forbes, J. M. (Eds.). *Solar Terr. Phys.,* Reidel, Dordrecht.

Hughes, W. J. (1994), Magnetospheric ULF waves: A tutorial with a historic perspective, in, *Solar Wind Sources of Magnetospheric Ultra-Low-Frequency Waves, Geophys. Monogr. ser.,* vol. 81, edited by M. J. Engebretson, K. Takahashi, and M. Scholer, p.1, AGU, Washington, D. C.

Joseph, E. B., F. T. Michelle, J. M. David (1997), The superdense plasma sheet: Plasmaspheric origin, solar wind origin, or ionospheric origin?, *J. Geophys. Res.,* (102), 22089-22097.

Junginger, H. (1985), Poynting vector as a diagnostic of hydromagnetic wave structure, *J. Geophys. Res.,* (90), 4155-4163.

Kauristie, K., J. Pulkkinen, T. I. Murphree, J. S. Murphree, and P. T. Newell (1999), Size of the auroral oval: UV ovals and preciptation boundaries compared, *J. Geophys. Res.,* (104), 2321-2331.

Kepko, L., H. E. Spence, H. J. Singer (2002), ULF waves in the solar wind as direct drivers of magnetospheric pulsations, *J. Geophys. Res.,* 29, 1197, doi:10.1029/2001GL014405.

Keskinen, M. J. (1988), Nonlinear evolution of the Kelvin-Helmholtz instability in the high-latitude ionosphere, *J. Geophys. Res.,* (93), 137-152.

Kivelson, M. G., and Z. Pu (1984), The Kelvin-Helmholtz instability on the magnetopause, *Planet. Space. Sci.,* (32), 1335-1341.

Kivelson, M. G., and D. J. Southwood (1985), Resonant ULF waves: A new interpretation, *Geophys. Res. Lett.,* (12), 49-52.

Kivelson, M. G., and D. J. Southwood (1988), Hydromagnetic waves and the ionosphere. *Geophys. Res. Lett.,* (15), 1271-1274.

Kivelson, M. G., J. Etcheto, and J. G. Trotingnon (1984), Global compressional oscillations of the Terrestrial magnetosphere: The evidence and a model, *J. Geophys. Res.,* (89), 9851-1984.

Kivelson, M. G., and S. H. Chen (1995), The magnetopause: Surface waves and instabilities and their possible dynamical consequences, in *Physics of the Magnetopause, Geophys. Monogr. Ser.,* vol.(90), edited by P. Song, B. U. O, Sonnerup, and M. F. Thomsen, pp. 257-268, AGU, Washington, D.C.

Kivelson, M. G., and C. T. Russel (1995), Eds., *Introduction to Space Physics*, Cambridge University Press, New York.

Knox, F. B. (1964), A contribution to the theory of the production of field-aligned ionization irregularities in the equatorial electrojet, *J. Atmos. Terr. Phys.,* (26), 239-249.

Kouznetsov, I., and W. Lotko (1995), Radial energy transport by magnetospheric ULF waves: Effects of magnetic curvature and plasma pressure, *J. Geophys. Res.,* (100), 75997612, doi:10.1029/94JA02293.

Kronberg, E. A. (2011), On the origin of the energetic ion events measured upstream of the Earth's bow shock by STEREO, Cluster, and Geotail, *J. Geophys. Res.,* (116), doi:10.1029/2010JA015561.

Ledley, B. G. (1971), Magnetopause attitudes during OGO 5 crossings, *J. Geophys. Res.,* (76), 6736-6742.

Lee, L. C, R. K. Albano, and J. R. Kan (1981), Kelvin-Helmholtz instability in the magnetopause-boundary layer region, *J. Geophys. Res.,* (86), 54-58.

Liu, W. W, G. Rostoker, and D. N. Baker (1999), Internal acceleration of relativistic electrons by large-amplitude ULF pulsations, *J. Geophys. Res.,* (104), 17391-17407.

Lotko, W. A, V. Streltsov, and C. W. Carlson (1998), Discrete auroral arc, electrostatic shock and suprathermal electrons powered by dispersive, anomalously resistive field line resonance, *Geophys. Res. Lett.,* (25), 4449-4452.

Mager, P. N., D. Yu. Klimushkin, and N. Ivchenko (2009), On the equatorward phase propagation of high-m ULF pulsations observed by radars, *J. Atmos. Terr. Phys.,* (71), 1677-1680.

Mann, I. R., A. N. Wright, K., J. Mills, and V. M. Nakariakov (1999), Excitation of magnetospheric waveguide modes by magnetosheath flows, *J. Geophys. Res.,* (104), 333-353.

Mann, I. R. (2002), Coordinated ground-based and Cluster observations of large amplitude global magnetospheric oscillations during a fast solar wind speed interval, *Ann. Geophys.,* (20), 405-426.

Marcucci, M. F. (2006), Ionospheric convection observed by SuperDARN during ongoing lobe reconnection revealed by Cluster, *Societa Astronomica Italiana,* (9), 114-116.

Martyn, D. F. (1951), The theory of magnetic storms and auroras, *Nature,* (167), 92-94.

Mathie, R. A., F. W. Menk, and I. R., Mann, and D. Orr (1999), Discrete field line resonances and the Alfven continuum in the outer magnetosphere, *Geophys. Res. Lett.,* (26), 659-662.

Mathie, R. A., and I. R. Mann (2000), Observations of Pc5 field line resonance azimuthal phase speeds: A diagnostic of their excitation mechanism, *J. Geophys. Res.,* (105), 10713-10728.

Menk, F. W. (2003), High latitude observations of impulsive-driven ULF pulsations in the ionosphere and on the ground, *Ann. Geophys.,* (21), 559-576.

Michael, H. (2011), Golabl energy transfer during a magnetospheric field line resonance, *Geophys. Res. Lett.,* (38), doi:10.1029/2011GL047846.

Milan, S. E., M. Lester, and S. W. H. Cowley, K. Oksavik, M. Brittnacher, R. A. Greenwald, G. Sofoko, J. P. Villain (2003), Variations in the polar cap area during two substorm cycles, *Ann. Geophys.,* (21), 1121-1140.

Miura, A. (1990), Kelvin-Helmholtz instability for supersonic shear flow at the magnetospheric boundary, *Geophys. Res. Lett.,* (17), 749-752.

Miura, A, and P. L. Prichett (1982), Nonlocal stability analysis of the MHD Kelvin-Helmholtz instability in a compressible plasma, *J. Geophys. Res.,* (87), 7431-7444.

Moldwin, M. B. (2002), A new model of the location of the plasmapause: CRRES results, *J. Geophys. Res.,* (107), 1339, doi:10.1029/2001JA009211.

Nedie, A. Z., R. Rankin, and F. R. Fenrich (2012), SuperDARN observations of the driver wave associated with FLRs, *J. Geophys. Res.,* (117), A06232, doi:10.1029/2011JA017387.

Newton, R. S., D. J. Southwood, and W. J. Hughes (1979), Damping of geomagnetic pulsations by the ionosphere, *Planet. Space Sci.,* (26), 201-209.

Oslon, J. V., and G. Rostoker (1978), Longitudinal phase variations of PC4-5 micropulsations, *J. Geophys. Res.,* (83), 2481-2488.

Otto, A., and D. H. Fairfield (2000), The Kelvin Helmholtz instability at the magnetotail boundary: MHD simulations and comparison with Geotail Observations, *J. Geophys. Res.,* (105), 21, 175 -21, 190.

Parks, G. K. (2004), *Physics of Space Plasmas an Introduction*, Westview Press, Boulder.

Parker, E. N. (1958), Dynamics of the interplanetary gas and magnetic fields, *Astrophys. J.,* (128), 664-676.

Pilipenko, V. A. (1990), ULF waves on the ground and in space, *J. Atmos. Terr. Phys.,* (52), 12, 1193-1209.

Plaschke, F. (2009), Standing Alfvén waves at the magnetopause, *Geophys. Res. Lett.,* (36), L02104, doi:10.1029/2008GL036411.

Poulter, E. M. (1982), Pc 5 micropulsation resonanceregions observed with the STARE radar, *J. Geophys. Res.,* (87), 8167.

Priest, E. R. (1995), The Sun and it's magnetohydrodynamics, in *Introduction to space plasma physics*, ed. M. G. Kivelson and C. T. Russel.

Prikryl, P. (1998), Observations of polar patches generated by solar wind Alfven wave coupling to the dayside magnetosphere, *Ann. Geophys. Res.,* (17), 463-489.

Prikryl, P. (1998), Solar-wind-driven pulsed magnetic reconnection at the dayside magnetopause, Pc5 compressional oscillations, and field line resonances, *J. Geophys. Res.,* (103), 17,307-17,322.

Prikryl, P. (2005), Solar wind Alfven waves: a source of pulsed ionospheric convection and atmospheric gravity waves, *Ann. Geophys. Res.,* (23), 401-417.

Pu, Z. Y, and M. G. Kivelson (1983), Kelvin-Helmholtz Instability at the Magnetopause: Energy Flux Into the Magnetosphere *J. Geophys. Res.,* (88), 841-852.

Radoski, H. R. (1967), Highly asymmetric MHD resonances: The guided poloidal mode, *J. Geophys. Res.,* (72), 4026-4027.

Rae, I. J. (2005), Evolution and Characterisitcs of global PC5 ULF waves during a high solar wind speed interval, *J. Geophys. Res.,* (110), A12211, doi:10.1029/2005JA011007.

Rae, I. J. (2007), Energy deposition in the ionosphere through a global field line resonance, *Ann. Geophys.,* (25), 2529-2539.

Rankin, R., B. G. Harrold, J. C. Samson, and P. Frycz (1993), The nonlinear evolution of field line resonances in the Earth's magnetosphere, *J. Geophys. Res.,* (98), 5839-5853.

Rankin, R., J. C. Samson, and V. T. Tikhonchuk (1999), Discrete auroral arcs and nonlinear dispersive field line resonances, *Geophys. Res. Lett.,* 26, 6 : doi: 10.1029/1999GL900058. issn: 0094-8276.

Reid, F. B. (1968), The formation of small-scale irregularities in the ionosphere, *J. Geophys. Res.,* (73), 1627-1640.

Ruohoniemi, J. M., and K. B. Baker (1998), Large-scale imaging of high-latitude convection with Super Dual Auroral Radar Network HF radar observations, in *J. Geophys. Res.,* (103), 20797-20811.

Roelof, E. C., and D. G. Sibeck (1993), Magnetopause shape as a bivariate function of interplanetary magnetic field Bz and solar wind dynamic pressure, in *J. Geophys. Res.,* (98), 21421-21450.

Rostoker, G. S. (1998), On the origin of relativistic electrons in the magnetosphere associated with some geomagnetic storms, *Geophys. Res. Lett.,* (25), 3701-3704.

Samson, J. C. (1991), Magnetometer and radar observations of magnetospheric cavity modes in the Earth's magnetosphere, *Can. J. Phys.,* (69), 929-937.

Samson, J. C. (1991b), Observations of a detatched, discrete arc in association with field line resonances, *J. Geophys. Res.,* (96), 15683-15695.

Samson, J. C., B. G. Harrold, J. M. Ruohoniemi, and A. D. M. Walker (1992), Field line resonances associated with MHD waveguides in the magnetosphere, *Geophys. Res. Lett.,* (19), 441-444.

Samson, J. C., L. L. Cogger, and Q. Pao (1996), Observations of field line resonances, auroral arcs and auroral vortex structures, *J. Geophys. Res.,* (101), 17373-17383.

Sanchez, E. R. (1997), Alfven modulation of substorm magnetotail transport, *Geophys. Res. Lett.,* (24), 979, doi:10.1029/97GL00865.

Sckopke, N. G. (1981), Structure of the low latitude boundary layer, *J. Geophys. Res.,* (86), 2099-2110.

Sen, A. (1963), Stability of Hydromagnetic Kelvin-Helmholtz discontinuity, *Phys. Fluids,* (6), 1154-1163.

Shafer, S. (2008), Spatial and temporal structure of Alfvn resonator waves at the terrestrial plasmapause, *PhD. Thesis.*

Sibeck, D. G., R. E. Lopez, and E. C. Roelof (1991), Solar wind control of the magnetopause shape, location, and motion *J. Geophys. Res.,* (96), 5489-5495.

Simon, A. (1963), Instability of a partially ionized plasma in crossed electric and magnetic fields, *Phys. Fluids,* (6), 382-388.

Song, P., R. C. Elphic, and C. T. Rusell (1988), ISEE 1 and 2 observations of the oscillating magnetopause, *Geophys. Res. Lett.,* (15), 744-747.

Southwood, D. J. (1968), The hydromagnetic stability of the magnetospheric boundary, *Planet. Space Sci.,* (16), 587-605.

Southwood, D. J., J. W. Dungey, R. J. Etherington (1969), Bounce resonant interaction between pulsations and trapped particles, *Planet. Space Sci.,* 17, 349-361.

Southwood, D. J. (1974), Some features of field line resonance in the magnetosphere, *Planet. Space Sci.,* (22), 483-491.

Southwood, D. J. (1979), Magnetopause Kelvin-Helmholtz instability. in *Proceedings of Magnetospheric Boundary Layers Conference*, ESA Scientific and Technical Publications Branch. Noordwijk, The Netherlands.

Stephenson, J. A. E, and A. D. M. Walker (2002), HF radar observations of pc5 ULF pulsations driven by the solar wind, *J. Geophys. Res.,* (108), A2, 1095, doi:10.1029/2002JA009675.

Stern, D. P. (1985), Parabolic harmonics in magnetospheric modeling - the main dipole and the ring current, *J. Geophys. Res.,* (90), 851-863.

Stewart, B. (1861), On the great magnetic disturbance which extended from August 28 to September 7, 1859, as recorded by photography at the Kew Observatory *Philos. Trans. R. Soc. London,* 151, 423-430.

Tamao, T. (1966), Transmission and coupling resonance of hydromagnetic disturbances in the non-uniform Earth's magnetosphere, *Sci. Rep. Tohoku Univ. Ser.,* (5), 17-43.

Thomson, D. J, C. G. Maclennan, and L. J. Lanzerotti (1995), Propagation of solar oscillations through the interplanetary medium, *Nature,* 376, 139-144.

Villante, U. (1975), Some remarks on the structure of distant neutral sheet, *Planet. Space. Sci.,* (28), 723-728.

Walker, A. D. M. (1981), The Kelvin-Helmholtz instability in the low-latitude boundary layer, *Planet. Space. Sci.,* (29), 1119-1120.

Walker, A. D. M. (1992), Spatial and temporal behavior of ULF pulsations observed by the Goose Bay HF radar, *J. Geophys. Res.,* (97), 12187-12202.

Walker, R., and C. Russell (1985), Solar-wind interactions with magnetized planets, in *Introduction to Space Physics*, ed. M.G. Kivelson and C.T. Russell, Cambridge University Press, Cambridge.

Walker, A. D. M. (2002), Excitation of field line resonances by MHD waves originating in the solar wind, *J. Geophys. Res.,* (107), A12, 1481, doi:10.1029/2001JA009188.

Waters, C. L., J. C. Samson, and E. F. Donovan (1996), Variation of plasmatrough density derived from magnetospheric field line resonances, *J. Geophys. Res.,* (101), 24737-24745.

Woodfield, E. E. (2002), A case study study of HF radar spectral width in the post-midnight magnetic local time sector and its relationship to the polar cap boundary, *Ann. Geophys.,* (20), 501-509.

Zhu, X., and M. G. Kivelson (1988), Analytic formulation and quantitative solutions of the coupled ULF wave problem, *J. Geophys. Res.,* (93), 8602-8612.